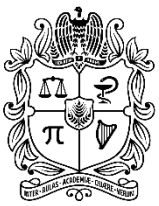

UNIVERSIDAD
NACIONAL
DE COLOMBIA

Energy generation from salinity gradients through Reverse Electrodialysis and Capacitive Reverse Electrodialysis

Sara Vallejo Castaño

Universidad Nacional de Colombia

Facultad de Minas, Departamento de Procesos y Energía

Medellín, Colombia

2016

Energy generation from salinity gradients through Reverse Electrodialysis and Capacitive Reverse Electrodialysis

Sara Vallejo Castaño

Thesis submitted as partial requirement for the degree of:

Magister en Ingeniería Química

Director:

Chemical Engineer Carlos Ignacio Sánchez Sáenz

Research line:

Marine Energy

Research group:

GRIEQUI – Research group in Electrochemical Engineering.

Universidad Nacional de Colombia

Facultad de Minas, Departamento de Procesos y Energía

Medellín, Colombia

2016

Difference is divine ~ Yemaya.

Anonymous

Acknowledgments

All my gratitude to my adviser and mentor Carlos Ignacio Sánchez Sáenz, who I admire for his intelligence, wisdom, patient and human quality. Special thanks to Oscar Andrés Álvarez Silva for involving me in the construction of a renewable energy solution for the world. I also want to express my gratitude to professor Andrés Fernando Osorio Arias, who has believed in this project from the beginning and has supported all the efforts to develop salinity gradient energy in Colombia.

Thanks to my parents for the gift of life, and for their unconditional love and support. To my brothers and to Sebastián, the engines of my life.

I want to thank the team that supported Colciencias project in 2015 – 2016. Specially Mateo and Darling for their enormous contributions to this work. I also express my gratitude to all my colleges and friends that have accompanied in somehow this process

I am especially grateful with Ph.D. Michele Tedesco for the important contribution to this work with the Collaborative project, for his patient, direction and guidance in the process.

I want to give special thanks to the research group in Oceanography and Coast Engineering OCEANICOS and research group in Electrochemical Engineering GRIEQUI.

I express my gratitude with Colciencias for the financial aid in this research with “Jóvenes Investigadores 2014” program and “Pruebas de Concepto 2014” Program. I also want to thank Universidad Nacional de Colombia for the support of the project through the “National program to support postgraduate students for strengthen of research, creation and innovation 2013 – 2015” and for the fellowship given through the “physics school academic instructors program” in 2016.

.

Resumen

El presente trabajo constituye el primer esfuerzo en Colombia y América Latina para desarrollar la tecnología de electrodiálisis inversa para obtención de energía a partir de gradiente salino. En esta tesis se utiliza un modelo en estado estacionario previamente descrito en la literatura y se desarrolla un modelo dinámico para describir el comportamiento de las tecnologías electrodiálisis inversa (RED) y electrodiálisis inversa capacitiva (CRED). Los modelos son validados experimentalmente.

Se realiza la construcción y puesta en marcha de un generador de energía funcional para RED y CRED, se estudia el efecto de espaciadores conductores con geometrías alternativas sugeridas en la literatura. Además se estudia el potencial de generación de energía en Colombia mediante la prueba de la pila construida, utilizando agua recogida en campañas de campo proveniente del río Magdalena y del mar Caribe.

La máxima densidad de potencia obtenida experimentalmente fue de 0.14 W/m^2 para una pila de RED con 10 celdas con soluciones artificiales, mientras que la máxima potencia obtenida para CRED fue de 0.035 W/m^2 para un stack con 3 celdas y espaciadores utilizando agua del río Magdalena y del mar Caribe.

Finalmente se estudia experimentalmente el efecto que tiene en la concentración en equilibrio de membranas de intercambio iónico selectivas, el uso de soluciones de NaCl en presencia de iones bivalentes. Se estudia el efecto de los iones más abundantes en el agua de mar, tales como Mg^{+2}, Ca^{+2} y SO_4^{-2}. Se observa un comportamiento de decrecimiento exponencial en la absorción de iones monovalentes en presencia de iones bivalentes, es decir, a bajas concentraciones de iones bivalentes (concentraciones similares al agua de mar), la capacidad de absorción de iones monovalentes de la membrana disminuye considerablemente.

Palabras clave: Energía de Gradiente Salino, Electrodiálisis Inversa, Electrodiálisis inversa Capacitiva, Energía renovable, Equilibrio en membranas, Membranas de intercambio iónico selectivas

Abstract

The present thesis work constitutes the first effort in Colombia and America Latina for developing Reverse Electrodialysis (RED) technology for energy recovery from salinity gradients. This thesis develops a dynamic model for RED and CRED and it also uses a stationary state model presented in literature to describe energy generation through salinity gradients. The model is experimentally validated.

A lab scale energy generator for RED and CRED is designed, constructed and operationalized. The effect of conductive spacers with an alternative geometry suggested in literature is studied. Besides, the potential of energy generation in Colombia is studied by testing the stack with waters from the Magdalena River and the Caribbean Sea.

Maximum power density obtained experimentally was 0.14 W/m^2 for a 10 cell RED stack using artificial solutions, while maximum power obtained for CRED was 0.03 W/m^2 for a stack of 3 cells with spacers and river and sea water.

Finally the effect that bivalent ion solutions have over equilibrium concentration in ion Exchange membranes (IEM) is experimentally tested. The ions studied are the most abundant in sea water: Mg^{+2}, Ca^{+2} and SO_4^{-2}. An exponential decrease is observed in the absorption capacity of the membranes for monovalent ions, i.e. at low concentrations of bivalent ions (similar to the ones found in seawater), the absorption capacity of monovalent ions decreases substantially.

Palabras clave: Salinity Gradient Energy (SGE), Reverse Electrodialysis (RED), Capacitive Reverse Electrodialysis (CRED), Renewable Energy, Membrane equilibria, Ion Exchange Membranes (IEM).

Content

List of figures

List of tables

Page.

List of symbols and abbreviations

Latin letters

Symbol	Term	Unit SI	Definition
A_Φ	Debye Huckel coefficient	-	Eq. (2.16)
A_m	Total membrane Area	m^2	Eq. (2.35)
$A_{T,m}$	Transversal membrane Area	m^2	Eq. (2.36)
b	width	m	Eq. (2.4)
C	Concentration	mol/m^3	Eq. (2.2)
	Capacitance	F	Chapter 3
D	Effective diffusion constant	m^2/s	Eq. (2.11)
D_i	Effective concentration average diffusion	m^2/s	Eq. (4.1)
E	Voltage	V	Eq. (2.34)
F	Volumetric flow	m^3/s	Eq. (2.2)
	Faraday constant	C/mol	Eq. (2.13)
G	Gibbs free energy	J/s	Eq. (2.1)
ΔG_{mix}	Gibbs free energy of mixing	J/s	Eq. (2.1)
I	Electrical Current	A	Eq. (2.34)
J	Volumetric or mol flux	$m^3/m^2 s$, $mol/m^2 s$	Eq. (2.6)
	migration current	A	Eq. (2.13)
K	Equilibrium constant	-	Eq. (4.9)
K_i	Partition coefficient	-	Eq. (4.1)
L	Length of the compartment	m	Fig. (2.2)
M	Molar mass	Kg/mol	Eq. (2.11)
N	Number of cells	-	Eq. (2.22)
P	Pressure	Pa	Chapter 1
	Steady state permeability coefficient	-	Eq. (4.1)
P_d	Power density	W/m^2	Eq. (2.22)
$P_{d\text{-}total}$	Total power density	W/m^2	Eq. (2.23)
$P_{d\text{-}net}$	Net power density	W/m^2	Eq. (2.24)
$P_{d\text{-}hydr}$	hydraulic losses	W/m^2	Eq. (2.25)
ΔP	Pressure drop	Pa	Eq. (2.27)
Q	Charge	C	Chapter 1
R	Universal gas constant	$J/mol\,K$	Eq. (2.2)

Symbol	Term	Unit SI	Definition
T	Absolute temperature	K	Eq. (2.2)
t	time	s	Eq. (2.4)
t_{res}	residence time	s	Eq. (2.29)
V	Volume	m^3	Chapter 1
v	linear velocity	m/s	Eq. (2.26)
vis	viscosity	$Pa\ s$	Eq. (2.26)
X	Exergy flow	J/s	Eq. (2.34)
x	axial flow direction	-	Chapter 2

Greek letters

Symbol	Term	Unit SI	Definition
α	selectivity	-	Eq. (2.14)
$\Delta\Phi$	Potential difference	V	Eq. (2.13)
γ	Activity Coefficient	-	Eq. (2.14)
μ	Ionic strength	-	Eq. (2.15)
η_T	Thermodynamic efficiency	-	Eq. (2.30)
δ	Thickness	m	Eq. (2.4)
ρ	Density	Kg/m^3	Eq. (2.11)
Λ	Molar Conductivity	$S/m^2 mol$	Eq. (2.20)
$\Delta\Phi_D$	Donnan Potential Difference	V	Eq. (4.2)

Sub-indexes

Sub index	Term
AEM	Anion Exchange Membrane
c	Concentrated, consumed
Cell	cell
CEM	Cation Exchange Membrane
d	Diluted, density
di	diffusion
i	Ion, species
in	Inlet
int	Internal
M	Membrane
m	Membrane, mix
mi	migration
NaCl	Salt
out	Outlet
Tot	total
w	Water
∞	Bulk, solution

Abbreviations

Abbreviation	Term
AAS	Atomic Absorption Spectroscopy
AEM	Anionic Exchange Membrane
APE	Alkaline Polymer Electrolyte
CapMix	Capacitive Mixing
CEM	Cationic Exchange Membrane
CRED	Capacitive Reverse Electrodialysis
ED	Electrodialysis
EDL	Electric Double Layer
EDLC	Electric Double Layer Capacitor
IEM	Ion Exchange Membrane
IC	Ion Chromatography
MD	Membrane Distillation
OCV	Open Circuit Voltage
PRO	Pressure Retarded Osmosis
RED	Reverse Electrodialysis
SGE	Salinity Gradient Energy
SGP	Salinity Gradient Power

1. Introduction

The humankind has always required enormous amounts of energy for its progress, in 2013 the energy consumption per capita was 3.1 KWh, and this number has been on the rise for the last 30 years [1]. Furthermore, these energy requirements have been principally supplied by fossil fuels, in 2013 81.2% of total energy consumption came from fossil fuels [1], in addition in 2015, 3000 million people in the poorest countries still used pollutant fuels like kerosene, wood, carbon and manure for basic necessities like cooking [2].

Since 1992 the United Nations has accepted that: “human activities have been substantially increasing the atmospheric concentrations of greenhouse gases, that these increases enhance the natural greenhouse effect, and that this will result on average in an additional warming of the Earth's surface and atmosphere and may adversely affect natural ecosystems and humankind”. The united nations have set the goal to stabilize greenhouse gases concentrations in the atmosphere at a level that can prevent dangerous anthropogenic interference with the climate system [3], [4].

In the light of these statements, one of the most effective ways to reduce CO_2 emissions, favoring at the same time economic growth is to develop revolutionary production, distribution, storing and energy conversion technologies. It is necessary to boost new energy generation systems that are in harmony with natural earth cycles.

The main classes of renewable energies are: Solar energy, wind energy, hydroelectric energy, biofuels, geothermic and marine energy [5]. The newest of marine energies is salinity gradient energy (SGE) that harness the natural water cycle to produce energy.

Energy generation through salinity gradients converts into electrical energy, the free energy available in the mixing of two streams with different salt concentrations. It was first mentioned in 1954 by R. Pattle, who stated that: “When a volume V of pure solvent mixes irreversibly with a much larger volume of a solution the osmotic pressure of which is P, the free energy lost is equal to PV. The osmotic pressure of seawater is about 20 atm, so that

when a river mixes with the sea, free energy equal to that obtainable from a waterfall 680 ft. (200 m) high is lost. There thus exists an untapped source of power which has been unmentioned in the literature." [6].

The theoretical SGE potential at river mouths has been previously estimated between 1.4 and 2.6 TW, equivalent to 74% of the worldwide electricity consumption [7] [8]. However, considering site suitability and environmental constrains from river mouths worldwide, global SGE potential was recently estimated to be 65 GW, which corresponds to 625 TWh/year of renewable energy, contributing to 3.5% of global energy consumption [9], [10].

SGE has a large potential in Colombia due to the great abundance of river and seawater in the country. Table 1-1 shows mean annual discharge of the six rivers accounting for the 99% of the fresh water discharged into the Colombian Caribbean basin [11], [12]. Recent studies show that in Colombia a potential of 15.6 GW could be achieved from salinity gradients with a capacity factor of 84% [10], [12].

Table 1-1. Mean annual discharge of the six rivers accounting for the 99% of the fresh water discharged into the Colombian Caribbean basin. Taken from [12].

River	Mean water discharge (Km^3/year)
Magdalena	228.1
Atrato	81.08
Sinú	11.76
Canal del dique	9.43
León	2.47
Don Diego	1.14
Total Colombian discharge to the Caribbean sea	337.68

Among the advantages of salinity gradient energy have been the continuous supply of "fuel" if river and sea water are used, the absence of atmospheric pollutants that intensify climate change, no thermal contamination, radioactive waste or sudden changes in energy production. Actually salinity gradient power has one of the highest capacity factor among the renewable energy technologies like wind, solar, tidal and wave energies [13].

Notwithstanding the previous advantages, one disadvantage of the technology is that energy density is relatively poor compared to traditional energy generation systems. Another careful matter is that the use of this energy may generate changes in the salinity structure of the rivers if water extraction of the river surpasses 20% of the mean discharge,

affecting directly very important ecosystems like mangrove forests and estuaries [10], [13]. Thus a specific site potential analysis should be assessed before the construction of any SGE plant.

1.1 Current technologies

From the moment the idea of generating energy through salinity gradients was conceived 60 years ago until now, many technologies have arisen and major improvements have been developed for harnessing this type of energy. The four most outstanding technologies are described in this section.

1.1.1 Reverse Electrodialysis (RED)

In Reverse Electrodialysis (RED) the free mixing energy between to water streams with different salt concentration is converted into electrical energy by doing a less thermodynamically irreversible process.

In order to do this, two water streams with different salt concentration enter the stack and distribute in different compartments. Using anionic and cationic selective membranes (AEM and CEM) the movement of anions or cations from the concentrated to the diluted compartments is allowed. The ion selective membranes as well as the concentrated and diluted compartments are intercalated between them. The salinity gradient generated with the intercalation constitutes an electrochemical potential difference across each membrane, approximately 80 mV between river and sea water [14]. The total potential difference generated in a stack is calculated as the sum of each of the membrane potentials.

Electric field through the stack is generated because the electrochemical potential difference between compartments causes an ionic current of positive ions in one direction, and negative ions in the opposite direction. The ionic current and the voltage are converted into electrical energy through the use of a couple of electrodes at the stack ends, in contact with an electrolyte solution that generate oxidation and reduction reactions.

As a result of electrode reactions, an electron current is produced from the anode to the cathode through an external circuit, providing electrical work to the surroundings. Figure 1.1 shows a simple scheme of a Reverse Electrodialysis (RED) cell.

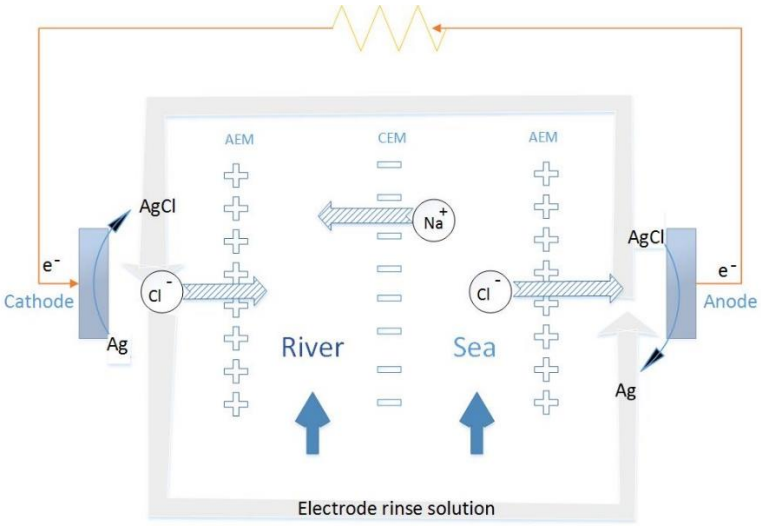

Figure 1.1. Scheme of a RED cell

1.1.2 Pressure Retarded Osmosis (PRO)

In this system, two water streams with different salt concentration are separated by a water semipermeable membrane. Driven by the chemical potential difference, water passes from the diluted to the concentrated stream. If the concentrated stream is pressurized before entering PRO system, the water transport inside the PRO stack will increase the flow and the pressure of this concentrated stream. The intensified flow of the pressurized stream passes through a hydroelectric turbine, which delivers electrical power [15]. Figure 1.2 explains the operation of a PRO system.

PRO and RED technologies are the most widely studied and developed Salinity Gradient Energy (SGE) systems. Different researches have been developed in order to understand which of them is the most efficient and has more energy density. In some studies it has been found that RED is more suitable for systems where concentrations of the water streams are the ones found in river and sea water [14], [16].

On the other hand a more recent study stated that membranes for PRO have had significant progress in the past few years, and that power density achievable could be up to 4.5 W/m^2 [17]–[19]. In contrast, the highest reported power density for RED is 2.2 W/m^2 [20], and the near future projections are 2.7 W/m^2 [21], which are less than half of energy obtainable with the best PRO membrane. Nonetheless the study for PRO does not take into account losses in the system associated with pressurizing the system and turbine efficiency.

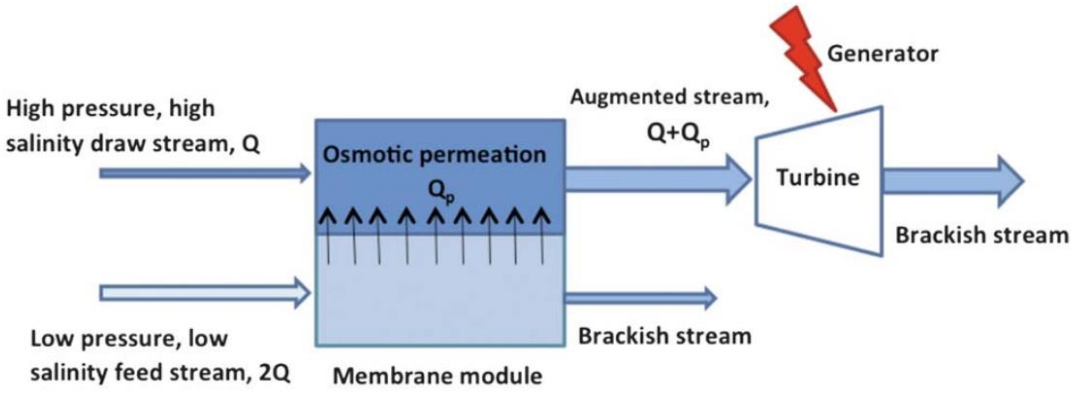

Figure 1.2. Scheme of a PRO energy generation system. Taken from [17].

1.1.3 Capacitive mixing

Capacitive mixing (CapMix) principle was first described by Brogioli in 2009. It consists in extracting energy from the expansion and contraction effect of the electrical double layer (EDL) when the concentration of the solution is changed at constant stored charge [22]. When a capacitor is charged in the presence of a solution with concentration C, it will store a certain amount of charge Q, if the external circuit is disconnected, and concentration of the solution is decreased, diffusion will cause an ion movement from the capacitor surface to the bulk solution, which is actually against electrostatic forces. This new equilibrium distribution of the Electric Double Layer (EDL) causes a net gain in the electrostatic energy of the system which can be used for energy generation [22], [23].

A CapMix cell is shown in Figure 1.3 composed by two activated carbon supercapacitors that are put in contact with a concentrated solution of NaCl. For extracting energy it is necessary to do a four step cycle [23]–[26]:

- Exchange the concentrated solution for a diluted solution at open circuit configuration.
- Discharge the capacitors through an external load.
- Change again the electrolyte solution for one with higher salt content at open circuit configuration.
- Charge the capacitors with an external resistance until cell voltage is equal to external voltage in order to restart the cycle.

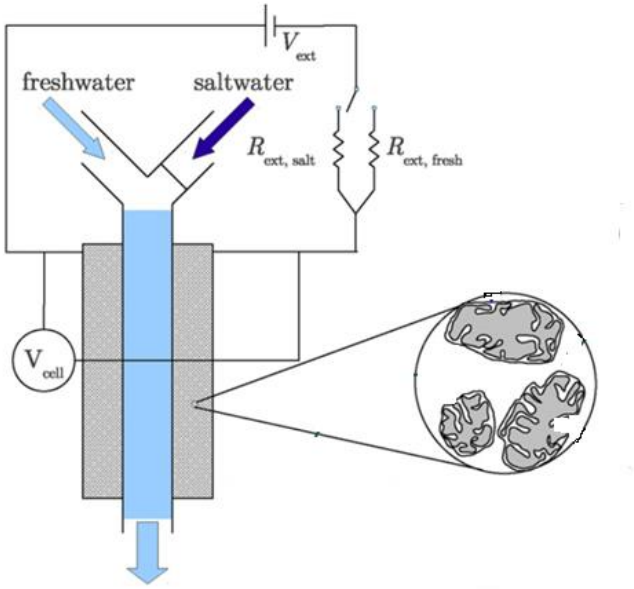

Figure 1.3. Scheme of a CapMix Cell. Taken and modified from [23]

1.1.4 Capacitive Reverse Electrodialysis (CRED)

Capacitive Reverse electrodialysis is a recently developed energy generation system that combines RED and Capacitive mixing (CapMix) principles [27], [28]. CRED technology has a membrane pile core identical to RED, but instead of electrodes, at both ends of the stack, two supercapacitors are put in contact with a NaCl solution.

Electroneutrality principle causes that while ions accumulate on the solution side of the capacitors, electronic configuration of the activated carbon reorganizes to complement the charge excess in the capacitors surface, which causes an electron movement through an external circuit. When the capacitors are saturated and energy is extracted, an interchange

of the feed waters must be done in order to reverse the ionic flux, and thus to reinitiate the process in the opposite direction. The scheme of a CRED cell is shown in Figure 1.4. The concept will be extended in chapter 3.

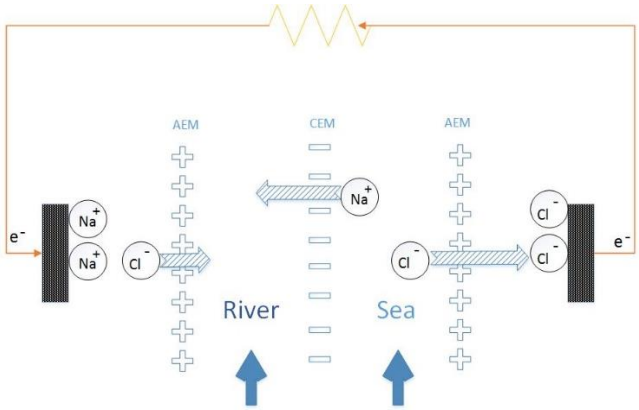

Figure 1.4. Scheme of a CRED cell

1.2 RED Applications

RED has been a widely studied technology in the recent years, and apart from energy extraction at river mouths, other sources of salinity gradient have been identified. For example, the replacement of river water for non-reused municipal waste water effluents as diluted water stream has been proposed [17]. Moreover, the use of saline natural sources like hypersaline lakes and salt domes as concentrated affluent, mixed with seawater as diluted stream has also been proposed [16].

Recently the first RED pilot plant for power production using brine as concentrated water stream and sea water as diluted water stream was constructed in Trapani, Italy. The RED pilot plant obtained the brine from a salt work that produces sea-salt by evaporating water from seawater [29], [30]. Other studies have been performed using the effluents of desalinization process as concentrated stream and seawater as diluted stream in order to recover some of the energy spent in the process and at the same time to mitigate the adverse impacts of desalination plants [31]. Finally, hybrid systems consisting in membrane distillation modules (MD) coupled with reverse electrodialysis have been investigated to harvest low temperature thermal energy [31], [32].

In addition, a number of new applications have been recently investigated like Hydrogen production coupling RED with alkaline polymer electrolyte (APE) in a water electrolysis cell [33] and microbial reverse electrodialysis for treatment of wastewater contaminated with Chromium ions [34]. On top of that, new waste heat conversion systems using ammonium bicarbonate concentrated and diluted solutions for generating the salinity gradient in RED stacks in thermal driven electrochemical generators [35] have been experimentally validated. Finally a new energy storage system has been proposed using the chemical potential of the solutions by combining RED with ED in salinity gradient flow batteries, [36].

1.3 RED Challenges

Although new applications have been found for RED, the technology still faces major challenges to be commercially viable for its application at river mouths. The first one is power density, which has been limited by the internal resistance of the stack, especially the river water compartment and the membrane resistance [17], [37]. In order to reduce the thickness of the river water compartment, improvements in the stack design like reducing thickness of the diluted compartment [20], [38], using new stack geometries and even microfluidic devices have been proposed [39], [40]. Another way is to change nonconductive spacers for profiled membranes [21], [41]–[43], conductive spacers [44], or resin beads [45], [46]. Specially the decreasing of cell length and using profiled membranes have been the most studied and have had better results as strategies for enhancing net power density. Another not too mentioned in literature alternative, is to reduce membrane thickness in order to reduce overall resistivity of the membrane, in case membrane resistance cannot be further improved.

Another important problem is fouling under natural conditions. It can be caused by biological agents, chemical agents (e.g. presence of multivalent ions, clay) or particles that may clog the system [47]. Biological agents have been treated using air sparging inside the stack and periodical water switching with good results [48]. The last strategy is based in the fact organisms that live in river water cannot live in salinity conditions of sea water and vice versa. Other anti-fouling strategy is to do membrane surface modifications [49]. There have been efforts to reduce the adverse effects in power density in the presence of multivalent ions using monovalent membranes, however currently available monovalent selective membranes were not found to be very effective to address the problem [50]. Lastly, system clogging has been a great concern for RED applied in river and sea water because it is

necessary to use 20μm filters in order to avoid blocking of the RED stack thin compartments. This kind of pretreatment can have economical and energetic costs that could be in the same order of energy production using river and seawater [51].

1.4 Aims

1.4.1 General Aim

To propose and validate a model from the construction and operationalization of a RED and CRED energy generator

1.4.2 Specific Aims

- To propose a model that describes energy generation for RED and CRED
- To design and to construct an energy generation system for RED and CRED.
- To validate the theoretical model proposed with experimental results of the operationalization of the energy generation system and with literature data.

2. Reverse Electrodialysis

2.1 Introduction

Salinity gradients are found in nature when rivers meet the sea. Artificially, they are found in desalination plants which have concentrated salt brines effluents that are usually discharged directly to the sea, and bring adverse impacts on vulnerable ecosystems like mangrove forests, salt marshes, coral reefs, or generally, low energy intertidal areas [52]–[54].

Estimations of practical global energy potential for salinity gradients between river and sea water, suggests that 3% of the world energy demand could be satisfied [10]. Only for Magdalena river in Colombia, taking into account its environmental constrains, a technical potential for an installed capacity greater than 15 GW has been calculated [13], which makes it the sixth river with more extractable energy in the world [10].

Colombia is rich in both, river and sea water, and its oceanographic and climate conditions favor the harnessing of Salinity Gradient Power (SGP) more than other types of marine energy [55]. This power could be a clean source of energy for Colombia, replacing coal plants, small diesel generators from rural and off grid areas, and even used for cogeneration systems, mitigating environmental impacts in desalination plants [29], [56].

Electrical power cannot be extracted under spontaneous mixing conditions, because the process is thermodynamically irreversible [6]. The technologies for extracting SGP allow to transform the diminution of Gibbs free energy available when mixing two solutions with different salt content, in electrical energy, performing the mixing under controlled conditions

Several technologies are being developed for harnessing artificial or natural SGP [14], [27], [57], [58]: Pressure Retarded Osmosis (PRO) uses the Osmotic pressure difference with membranes selective for water [59], [60], Capacitive Mixing uses the expansion and contraction effect of the electrical double layers using activated carbon capacitors [58], and

Reverse Electrodialysis (RED) uses the electrochemical potential difference with ion selective membranes (IEM) [61].

RED is one of the most extensively studied technology in the recent years, it has been demonstrated that it can be suitable for different applications like waste heat recovery using ammonium bicarbonate solutions [35], wastewater treatment when coupled with biological processes [34], water electrolysis for hydrogen production [33] and energy extraction with redox or capacitive electrodes [27]. Due to its possibilities and advantages, RED is the focus of this chapter.

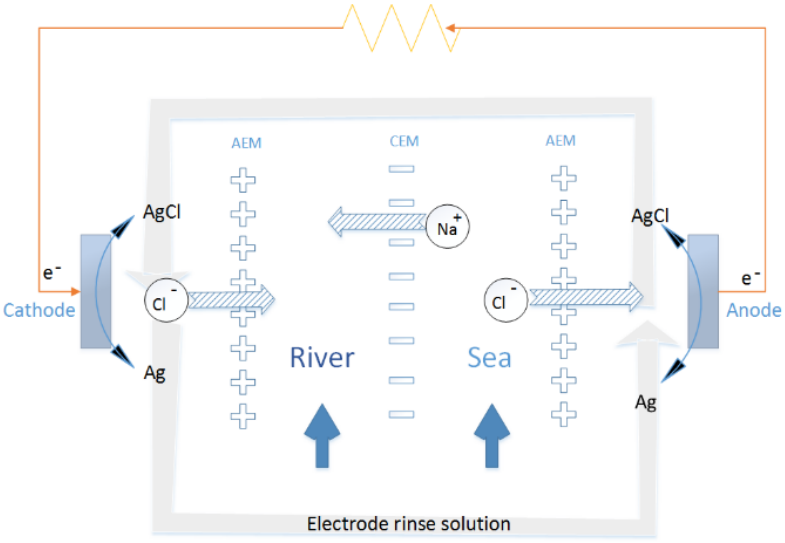

Figure 2.1. Schematic view of a RED cell.

Figure 2.1 shows the scheme of the RED cell used in this work. It consists in a set of ion exchange membranes, alternating cation (CEM), and anion exchange membranes (AEM), which are charged negatively and positively respectively. Using this membrane arrangement, river and sea water flow intercalating between membranes, and in this way compartments are formed. Due to the difference in salt concentration between the waters, there is an electrochemical potential difference, which is the motive force for ions to flow through the membranes from the sea water compartments, to the river water compartments. This part of the system is the ionic circuit, it performs the mixing process in a thermodynamically reversible way, making possible the generation of electrical power.

Using this membrane circuit allows cations to move in one direction and anions to move in the opposite direction. As a result of the controlled ion movement, an electrical potential difference arises in the membranes. The total voltage obtained from the stack, is the sum of electrochemical potential of each of the membranes.

In order to convert the ionic flux in the membrane circuit into electrical current, the generated voltage is used to perform reversible reduction/oxidation reactions in the electrodes that allow to transport electrons through an external circuit, and thus power is produced.

2.2 Theoretical model

The model formulation is based in the model presented by Veerman [38] using the methodology proposed by Alvarez et al [62]. It is given in SI units.

2.2.1 Maximum obtainable energy

The theoretical available energy in mixing (mix) a concentrated (c) and a diluted (d) solution, corresponds to the Gibbs free energy of mixing ΔG_m [63].

$$\Delta G_{mix} = \sum_i G_{i,m} - (G_{i,c} + G_{i,d}) \tag{2.1}$$

$$\Delta G_{mix} = 2RT \left[F_c C_c \ln \frac{C_c}{C_m} + F_d C_d \ln \frac{C_d}{C_m} \right] \tag{2.2}$$

With

$$C_{mix} = \frac{F_c C_c + F_d C_d}{F_c + F_d} \tag{2.3}$$

Where R is the universal gas constant (8.314 J/mol K), T is absolute temperature (K), F is volumetric flow (m^3/s) and C_c and C_d are salt concentration of concentrated and diluted solutions respectively. Factor 2 corresponds to dissociation of NaCl.

2.2.2 Mass balance

Mass balances for NaCl in both compartments have been developed. Figure 2.2 shows a scheme that explains salt and water transport through the compartments with length L, width b, and thickness δ.

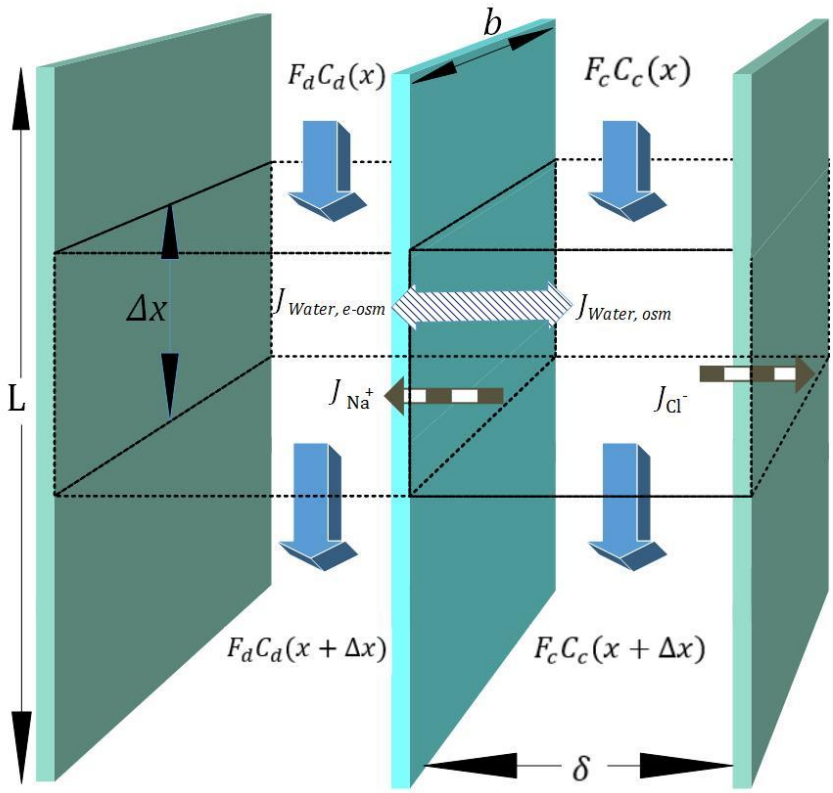

Figure 2.2. Mass balance for concentrated and diluted compartments. Source: The authors

Convective flow is defined in the *x* direction. In the length differentials, transport of ions occurs from the concentrated to the diluted compartments through the membranes due to a salt concentration gradient. Water passes in the same direction as salt due to electro osmotic drag. In the opposite direction an osmotic effect is presented and the non-ideal behavior of membranes causes water transport in the opposite direction as well.

A mole balance within the length differential, in concentrated and diluted compartments leads to Eq. (2.4) and Eq. (2.5) respectively

$$\frac{(b\ \delta\ \Delta x)\ dC_c(x)}{dt} = F_c C_c(x) - (\ F_c + b\ \Delta x\ J_w) C_c(x+\Delta x) - b\ \Delta x\ J_{NaCl}(x) \qquad (2.4)$$

$$\frac{(b\ \delta\ \Delta x)\ dC_d(x)}{dt} = F_d C_d(x) - (\ F_d - b\ \Delta x\ J_w) C_d(x + \Delta x) + b\ \Delta x\ J_{NaCl}(x) \quad (2.5)$$

Where C_c and C_d represent NaCl concentration in the concentration and diluted compartment respectively (mol/m^3). F_c And F_d are volumetric flows in the concentrated and diluted comparments (m^3/s). J_w Is volumetric water flux (m^3/m^{2}s) driven by osmosis. J_{NaCl} is salt flux through the membranes (mol/m^{2}s) induced by migration and diffusion [8, 22].

$$J_{NaCl} = J_{mi} + J_{di} \quad (2.6)$$

Dividing Eq. (2.4) by F_c and Eq. (2.5) by F_d and applying limits when Δx tends to cero, allows to obtain partial differential equations that describe the change of concentration in time and space. The development of the partial differential equations is explained in Appendix 1.

$$\frac{dC_c(x)}{dt} = \frac{F_c}{b\ \delta}\frac{\partial C_c(x)}{\partial x} - \frac{1}{\delta}\ J_w C_c(x) - \frac{1}{\delta}\ J_{NaCl}(x) \quad (2.7)$$

$$\frac{dC_d(x)}{dt} = \frac{F_d}{b\ \delta}\frac{\partial C_d(x)}{\partial x} + \frac{1}{\delta} J_w C_d(x) + \frac{1}{\delta} J_{NaCl}(x) \quad (2.8)$$

In stationary state, the concentration differential in time is cero, and the mole balance leads to Eq. (2.9) and Eq. (2.10)

$$\frac{dC_c}{dx} = -\frac{b}{F_c} T_{NaCl}(x) - \frac{b}{F_c} C_c(x) T_w(x) \quad (2.9)$$

$$\frac{dC_d}{dx} = \frac{b}{F_d} T_{NaCl}(x) + \frac{b}{F_d} C_d(x) T_w(x) \quad (2.10)$$

2.2.3 Transport equations

To solve mole balance equations, requires defining transport models for salt and water through membranes.

- **Water transport**

Water transport is given by Fick's diffusion model

$$J_w = \frac{2D_w}{\delta_m}(C_c - C_d)\frac{M_w}{\rho_w} \tag{2.11}$$

Where D_w is effective water difussion constant (m^2/s), δ_m is membrane thickness (m), M_w is molar mass (Kg/mol) and ρ_w (Kg/m^3) is density of water. The factor M_w/ρ_w is added to convert mole flux into volumetric flux [38], [56].

- **Salt transport**

Transport of NaCl through the membranes is considered to be driven by two major effects: Migration of counter-ions due to potential difference, and diffusion of co-ions due to non-idealities in membrane selectivity. Diffusion transport is described by Fick's model.

$$J_{di} = \frac{2D_{NaCl}}{\delta_m}(C_c(x) - C_d(x)) \tag{2.12}$$

Where D_{NaCl} is the diffusion constant of salt through membranes (m^2/s), and δ_m is the thickness of the membranes (m). The factor 2 accounts for the presence of 2 membranes in a cell. Diffusion transport is unwanted because only migration contributes to electrical current and its effect is analogous to self-discharge of batteries [64].

For describing migration, Ohm's principle is used.

$$J_{mi} = \frac{1}{F}\frac{N\Delta\varphi}{R_{cell}} \tag{2.13}$$

Where $\Delta\varphi$ is the potential (V), N is the number of cells, R_{cell} is the cell resistance (Ω m^2) and F is the Faraday constant (96485 C/mol), which is needed to convert coulombic flux into mol flux. $\Delta\varphi$ Can be calculated with Nernst equation, depending on the ion concentration in each side of the membrane.

$$\Delta\varphi = \alpha_{CEM}\frac{RT}{F}\ln\left(\frac{\gamma_c^{Na^+}(x)C_c^{Na^+}(x)}{\gamma_d^{Na^+}(x)C_d^{Na^+}(x)}\right) + \alpha_{AEM}\frac{RT}{F}\ln\left(\frac{\gamma_c^{Cl^-}(x)C_c^{Cl^-}(x)}{\gamma_d^{Cl^-}(x)C_d^{Cl^-}(x)}\right) \quad (2.14)$$

Where α is the permselectivity of the membrane and γ are activity coefficients of the ions in the solutions. For diluted and concentrated solutions, activity coefficients may be estimated from the Pitzer model [65], which can be simplified for symmetric electrolytes to Eq. (2.15) - (2.18).

$$\ln\gamma = |z_M z_X| f^\gamma + mB_{MX}^\gamma + m^2 C_{MX}^\gamma \quad (2.15)$$

$$f^\gamma = -A_\phi\left[\frac{\mu^{1/2}}{1+b\mu^{1/2}} + \frac{2}{b}\ln(1+b\mu^{\frac{1}{2}})\right] \quad (2.16)$$

$$B_{MX}^\gamma = 2\beta_{MX}^{(0)} + \frac{2\beta_{MX}^{(1)}}{\alpha^2\mu}\left[1 - e^{-\alpha\,\mu^{\frac{1}{2}}}\left(1+\alpha\,\mu^{\frac{1}{2}} - \frac{1}{2}\alpha^2\mu\right)\right] \quad (2.17)$$

$$C_{MX}^\gamma = \frac{3}{2}C_{MX}^\phi \quad (2.18)$$

Where μ is the ionic strength of the solution, A_ϕ is the Debye Huckel coefficient for osmotic function (0.392 for water at 25 °C), values of α and *b* are 2 y 1.2 respectively and values of $\beta_{MX}^{(0)}$ $\beta_{MX}^{(1)}$ y C_{MX}^ϕ vary depending on the electrolyte used (0.0765, 0.2664, 0.00127 respectively for NaCl) [65].

On the other hand, the resistance of the cell R_{cell} is the sum of resistances of anion and cation exchange membranes, the river water compartment and the sea water compartment.

$$R_{cell} = R_{CEM} + R_{AEM} + R_c + R_d \quad (2.19)$$

R_{CEM} And R_{AEM} are membrane resistances, which is a property given by the membrane manufacturer ($\Omega\,m^2$). The resistance of the compartments can be calculated with Eq. (2.20)-(2.21).

$$R_d = \frac{\delta_d}{\Lambda_m * C_d} \quad (2.20)$$

$$R_c = \frac{\delta_c}{\Lambda_m * C_c} \quad (2.21)$$

Where δ_c and δ_d are the thickness of the compartments (m), Λ_m is the molar conductivity of the solution (S m^2/mol) and C the solution concentration (mol/m^3). Λ_m Is dependent on concentration, but if a suitable value is used for low concentration compartment, calculated resistance of the river compartment is reliable [38]. As the sea water compartment resistance is much lower, its value has low influence on the total stack resistance.

Other models have a correction factor in the calculation of compartments resistance that accounts for the volume occupied by the spacer material f_v, wich is a measure of the increase in electrical resistance due to negative effect of nonconductive spacers, such as tortuosity in the ion flux trajectory and decrease in available volume for solution to flow [38], [56]. In this research f_v was not used because stack was designed in two configurations: without spacers and with conductive spacers. It has been proven that stacks without spacers present half the electrical resistance of stacks with spacers [8]. For calculating stack resistance with conductive spacers, the resistivity of such spacers was taken into account.

2.2.4 Response parameters

- **Power density**

Once the system of equations is solved through the flow trajectory x, local power density P_d (W/m^2) delivered to an external circuit can be found. In the particular case of maximum power, external resistance R_u should be equal to the internal resistance R_i.

$$P_d(x) = \frac{1}{2N} J^2(x) R_u \tag{2.22}$$

The factor ½ is due to the fact that area is duplicated, because of the use of two membranes (CEM y AEM) per cell. Total power density produced is obtained with the integration of P_d over the length of the compartment *L* in the *x* direction, divided by the total membrane area.

$$P_{d-total} = \frac{2Nb \int_0^L P_d(x)\, dx}{2NLb} \tag{2.23}$$

Net power density produced can be calculated as the difference between total power produced and hydrodynamic losses of the stack corrected for total membrane area.

$$P_{d-net} = P_{d,total} - P_{d,hydr} \tag{2.24}$$

Where hydrodynamic losses P_{d_hydr} are calculated as the pressure drop over the stack, times the volumetric flow of each stream, divided by total membrane area.

$$P_{d\_hidr} = \frac{\Delta P_c \, F_c + \Delta P_d \, F_d}{2Lb} \tag{2.25}$$

For calculating the pressure drop over the stack, Reynolds number is used to know flow regime of streams inside the compartments

$$Re = \frac{vD\rho}{visc} \tag{2.26}$$

In this case v respresents mean velocity, D is the hydraulic diameter, ρ is liquid density and $visc$ is the dynamic viscosity (0.9 x 10^{-3} Pa s for water). For the flow between to plane parallel plates, hydraulic diameter is equal to 2 times the distance between them. Applying this equation to small cells (0.1 m x 0.1 m and a thickness compartment of 200 μm), for low residence times, a Reynolds number of the order of 0.01 is obtained, which can be interpreted as laminar flow over the compartments [38]. For laminar flow, pressure drop over the compartments is defined as:

$$\Delta P_c = \frac{2viscLF_c}{b \, {\delta_c}^3} \tag{2.27}$$

$$\Delta P_d = \frac{2viscLF_d}{b \, {\delta_d}^3} \tag{2.28}$$

Eq. 2.24 is used for calculating total residence time

$$t_{res} = \frac{Lb\delta N_c}{F_{tot}} \tag{2.29}$$

Where L is the length, b is the width and δ is the thickness of the compartment, N_c is the number of cells and F_{tot} is the total water flow measured at the outlet of the compartment.

- **Thermodynamic efficiency**

The thermodynamic efficiency of the process is a crucial parameter to quantify the behavior of the stack [64]

$$\eta_T = \frac{P_u}{X_{cons}} \tag{2.30}$$

Where P_u is the actual power obtained from the RED stack (W) and X_{cons} is the exergy decrease in the feed waters (W). Exergy decrease may be calculated from

$$X_{cons} = X_{in} - X_{out} \tag{2.31}$$

Where X_{in} is the exergy flow ingoing to the stack and X_{out} is the outlet exergy flow. They

$$X_{in} = 2RT\left[F_c C_c Ln\left(\frac{C_{C,in}}{C_{m,\,in}}\right) + F_d C_d Ln\left(\frac{C_{d,in}}{C_{m,in}}\right)\right] \tag{2.32}$$

$$X_{out} = 2RT\left[F_c C_c Ln\left(\frac{C_{C,out}}{C_{m,\,out}}\right) + F_d C_d Ln\left(\frac{C_{d,out}}{C_{m,out}}\right)\right] \tag{2.33}$$

Where R is the universal gas constant, T is temperature (K), F_c and F_d are the flow rates of concentrated and diluted streams respectively. C_c And C_d are the inlet concentration of the concentrated and diluted streams, while $C_{c,\,out}$ and $C_{d,\,out}$ are the outlet concentration of the concentrated and diluted streams. $C_{m,\,in}$ And $C_{m,\,out}$ can be calculated with Eq. (2.3).

2.3 Experimental methodology

2.3.1 Reverse Electrodialysis stack

The stack used for the experiments was designed and built in Colombia, based on previous works in literature [66]. The dimensions of the cell were 5 cm x 10 cm, but the shape of the gaskets was designed in order to prevent leakages, which caused the real active membrane area to be 17.02 cm^2 (Figure 2.3). Stack was equipped with 300 μm silicon gaskets and Fujifilm ion exchange membranes AEM and CEM Type 1 (Fujifilm Manufacturing Europe BV, The Netherlands), membrane properties given by the membrane manufacturer are presented in Table 2-1.

Electrode system chosen for this research was made of Ag/AgCl electrodes in contact with NaCl solution 0.5 M. This redox couple was initially proposed by Audinos [67], it is highly reversible, cost effective and it can be easily fabricated. Furthermore, the rinse electrolyte solution is nontoxic, it does not causes membrane poisoning and the electrode rinse solution could be readily replaced by seawater, making it scalable without major trouble.

Electrodes fabrication was done using two plates of silver cut in a circular shape. Silver chloride was formed in one plate by applying a constant potential of -0,1 V vs Ag/AgCl in a NaCl solution 3 M during 30 minutes; the other one was left as raw silver.

Table 2-1. Membrane properties given by the manufacturer

Membrane	AEM Type I	CEM Type I
Resistance ($\Omega.cm^2$)[1]	1.3	2.7
Perm selectivity	0.92	0.92
Thickness (μm)	125	135
Water permeation (ml/bar.m^2.h)	6	10

[1]Measured in 0.5 M NaCl

NaCl concentrated solution was 0.5 M, which is the typical seawater concentration. Diluted NaCl solution was 0.01 M. Although typical NaCl concentration in river water can be lower than the value chosen, 0.01 M was the value used in previous works [38].

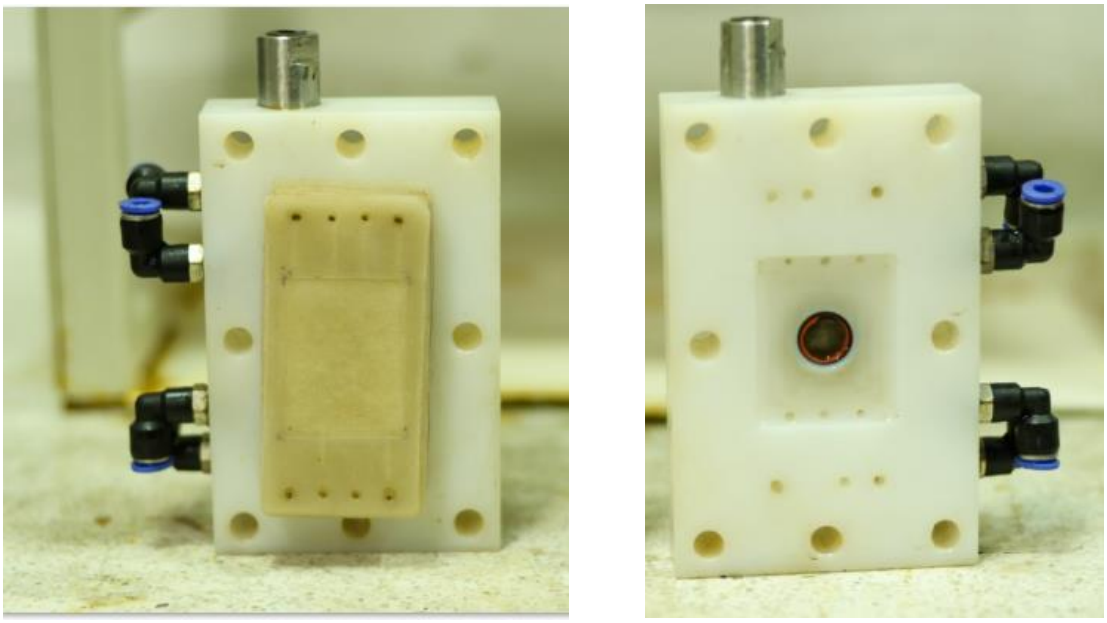

Figure 2.3. Picture of the RED stack used in the experiments.

2.3.2 Electrochemical measurements

The experimental set up is shown in Figure 2.4. The experiments did not count with flow control, no pumps were used in the experiments, and water flowed by gravity with a 30 cm height difference between water containers and stack. Electrode rinse solution was not recirculated. Salt solutions were made using reagent grade NaCl (Merck) and tap water.

Inside the stack, water flow was from the bottom to the top of the RED stack, this was done to improve water distribution inside the compartments. Water flow was measured gauging a 25 mL volumetric balloon in the stack outlet.

Experiments were carried out using 3 multimeters UNI-T (UT71D) for recording data in time, in combination with a manually variable resistance. Stack voltage was measured in Ag/AgCl reference electrodes and in the electrodes terminals. The first method allows to leave losses associated with electrode reactions out of consideration, and to read real membrane circuit voltage changes with resistance. This can be done because the electrode losses are dominant in a stack with few cells, but in practice, these losses can be neglected due to the great amount of cell pairs needed for pilot or commercial scale [64], [68].

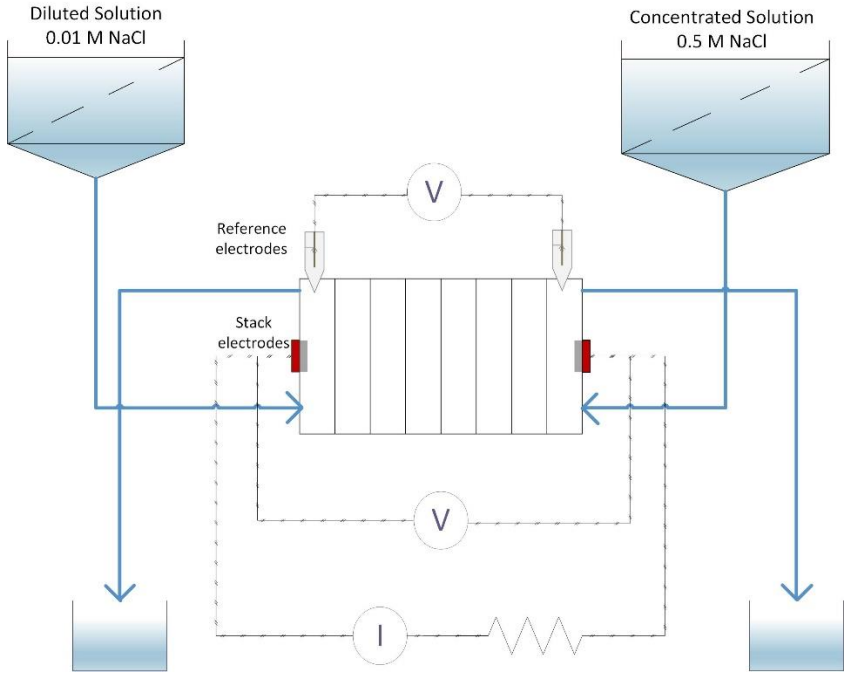

Figure 2.4. Experimental set up for RED experiments.

2.3.3 Experimental conditions

Initially, the effect of the number of cell pairs N was investigated for stacks without spacers, however it has been reported that spacerless stacks present higher non-ohmic resistances associated with smooth hydrodynamic conditions and concentration polarization effects in the diffusion boundary layer (DBL) [8].

In order to decrease the non ohmic resistance of the stack, conductive spacers were tested. Ion conductive spacers have been proven to enhance power generation in RED and to decrease the internal resistance of the stack related to spacer shadow effect in the presence of nonconductive spacers [44]. Conductive spacers were made of Fujifilm anion and cation exchange membranes. The arrangement of the spacers inside the channels consisted in an AEM membrane, AEM spacer, CEM spacer and CEM membrane, this is called a normal configuration [44].

Spacers were cut manually and they were designed inspired in chevron geometry (Figure 2.5). Chevron geometry has been found to be the most promising geometry for corrugated membranes: it enhances mass transfer, it reduces channel dead flow zones and it does not drastically increase the pressure drop of the stack [41]

A B

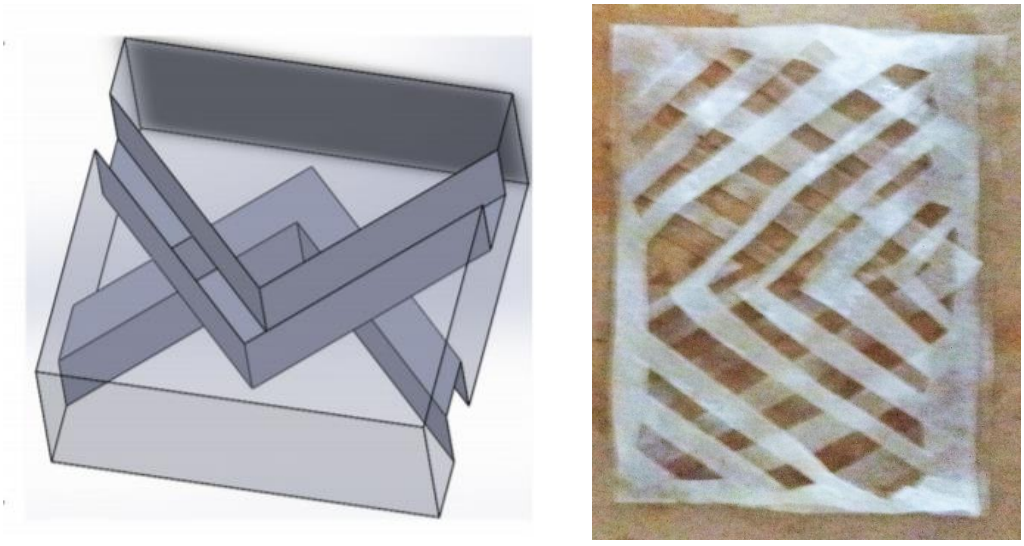

Figure 2.5. A) Chevron Geometry recommended for RED [41]. B) Spacers cut by hand used in the stacks.

Experiments were performed in parallel current configuration. Additional experiments were operated in counter current mode. Ultimately one test was performed using real Caribbean Sea water and Magdalena river water. Table 2-2 summarizes the effects investigated in the experiments.

Table 2-2. Experiments carried out in the research

Number of cells	**1**	**3**	**5**	**10**
Without spacers and parallel	X	X	X	X
With spacers and parallel current		X	X	
With spacer and counter current		X		
With spacers, parallel current and real river and sea water		X		

2.3.4 Calculation of experimental values

Power obtained from the stack experimentally was calculated with Eq. 2.34

$$P_u = E * I \tag{2.34}$$

Where E is the voltage measured at the electrodes (V) and I is the current that passed through the ammeter (A). Power Density obtained was calculated with Eq. (2.35)

$$P_d = \frac{P_u}{A_m} \tag{2.35}$$

Where A_m is the total membrane area (AEM and CEM) that contribute to voltage build up [38] [20].

Current density was calculated as the current measured with the ammeter divided by the transversal membrane area (AEM and CEM) available for ion exchange.

$$I_d = \frac{I}{A_{T,m}} \tag{2.36}$$

Internal resistance of the stack was calculated experimentally in the condition of maximum power with Ohm's law

$$R_{int} = \frac{E}{I} \tag{2.37}$$

Where E is the voltage in the electrodes and I is the current passing through an external circuit.

2.4 Results and discussion

Electrochemical characterization measurements were made to determine stack performance.

2.4.1 Dynamic model results

Dynamic model was solved using Matlab ® with parameters presented in literature [38], [61]. Results are presented in Figure 2.6 for co current and counter current operation for RED. Concentration profiles in stationary state are properly predicted with this model. Each line represents changes of salt concentration with time through the compartment, arrows show the direction of time in the profiles obtained.

The last time lines in Figure 2.6 show the developed concentration profiles in stationary state for diluted and concentrated solutions, which are in agreement with models developed for stationary state [61]. This validates that the model is able to represent dynamic behavior of concentration profiles inside the compartments.

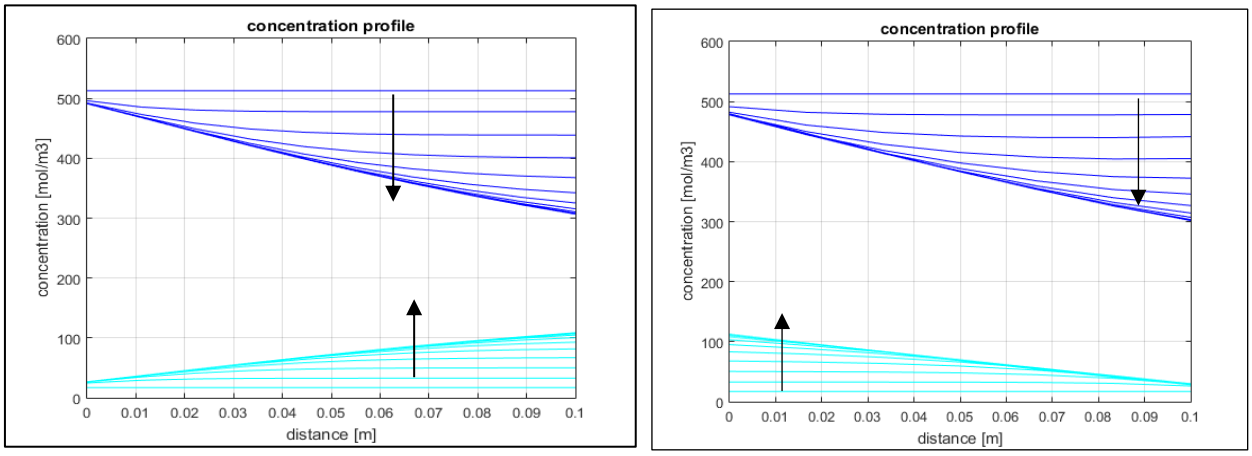

Figure 2.6 Results of the dynamic model for concentration profiles. A) in co current mode. B) in counter current mode. Arrows show the direction of time

Figure 2.7 shows the concentration changes in the compartment with time, each line represents one of the volume differentials used for solving the model. In Figure 2.7 the model predicts that the time required for reaching stationary state is equal to the residence time, which proves the capacity of the model to represent dynamic behavior. It can be seen that when 50 seconds have passed there are not any more changes in concentration.

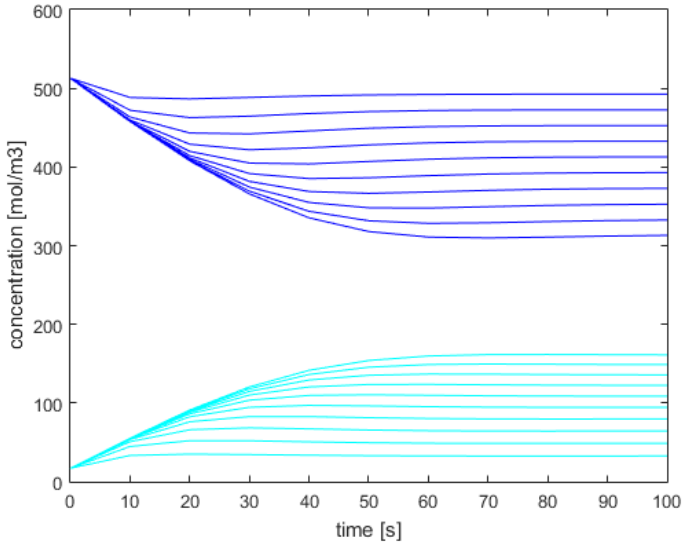

Figure 2.7. Concentration of salt water (blue) and fresh water (cyan) in time.

2.4.2 Results for 1 cell

Figure 2.8 presents the results obtained in stack electrodes for 1 cell. Figure 2.8 A shows experimental results (circles) compared with expected theoretical polarization curve (line). It is possible to notice that the values of OCV at cero current are very similar. Unfortunately with the development of the polarization curve, voltage drops drastically until half of the value expected in theory. This effect may be ascribed to the electrode losses, which are dominant in a stacks with few cells [68].

Due to the great difference between stack electrodes resistance and expected theoretical resistance, the actual resistance measured in the electrodes was an input in model to calculate power density. Figure 2.8 B presents the power vs current curve for the stack. It is possible to notice that experimental and theoretical are very similar when internal resistance obtained experimentally is used for the calculation.

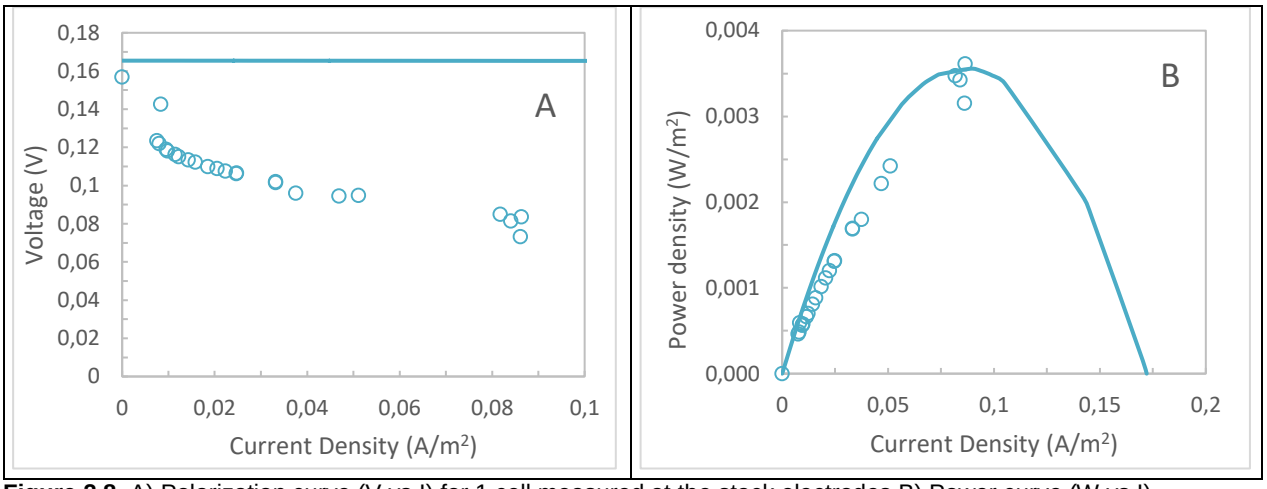

Figure 2.8. A) Polarization curve (V vs I) for 1 cell measured at the stack electrodes B) Power curve (W vs I) for 1 cell measured at the stack electrodes. ○ Experimental, -- Theoretical.

2.4.3 Results for 3 cells

Results in Figure 2.9 show, A polarization curves and B power density curves for the stack measured at the terminals of the electrodes (circles) and at the reference electrodes (triangles).

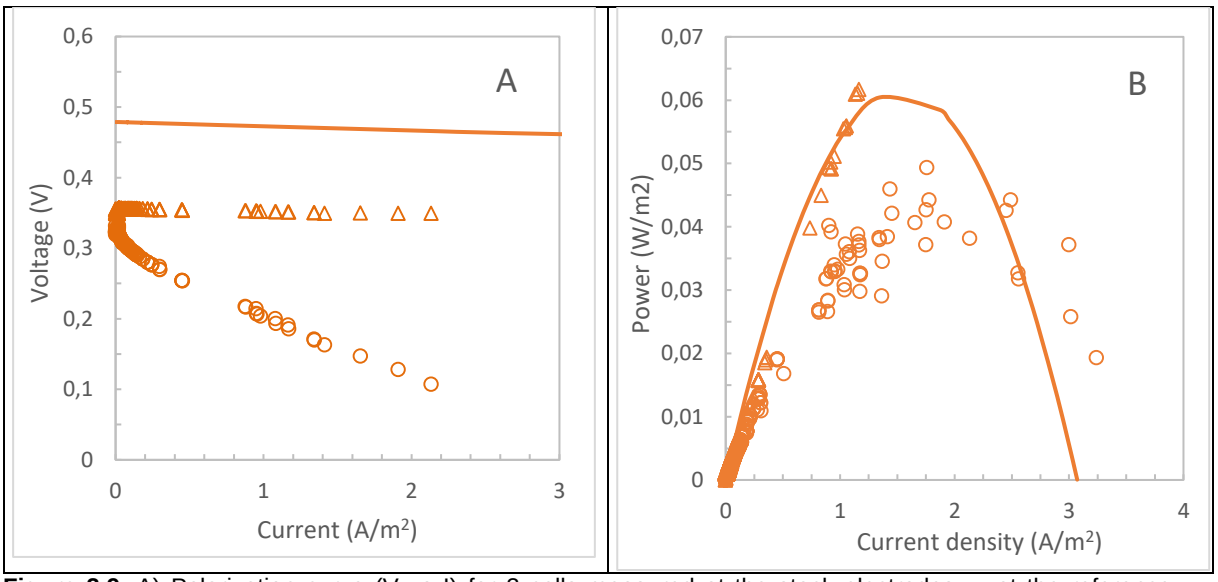

Figure 2.9. A) Polarization curve (V vs I) for 3 cells measured at the stack electrodes ○, at the reference electrodes Δ, and theoretically calculated -- B) Power curve (W vs I) for 3 cells measured at the stack electrodes ○, at the reference electrodes Δ, and theoretically calculated --

In Figure 2.9A, it is worth noting that voltage measured with reference electrodes (triangles), as well as Power density calculated (Figure 2.9B), is much higher than the results obtained for the stack electrodes (circles). Stack electrodes presented a very high resistance, this was a common problem in all the experiments. It was caused because there was a leakage

problem in the stack terminals. The junction between Ag electrodes and copper terminals produced a galvanic couple when water slightly leaked into the external circuit compartment. Thus, oxidation occurred, causing bad contacts between metals. The final result was a drastic increase in the internal resistance of the stacks. Unfortunately, because of this problem it was not possible to achieve higher current densities, and experiments were performed in only a small range of current densities.

Measurements in the reference electrodes on the other hand, exhibited a very small slope in the polarization curve, consistent with theory (Figure 2.9A). This confirms that the high internal resistance measured experimentally had its origin in the stack electrodes. Figure 2.9B shows the power curve. Theoretical calculations for Figure 2.9B were made using internal resistance measured in the stack electrodes.

Although stack electrodes do not achieve high power densities, when power is calculated using the value of internal resistance measured with reference electrodes, expected power density is much higher than actual obtained power (Figure 2.10).

In Figure 2.10, a zoom is shown for the initial part of the power curve. It is possible to notice that experimental data was only obtained for a small part of the power curve, nevertheless, results of the model are able to predict in this initial ranges the behavior of the stack.

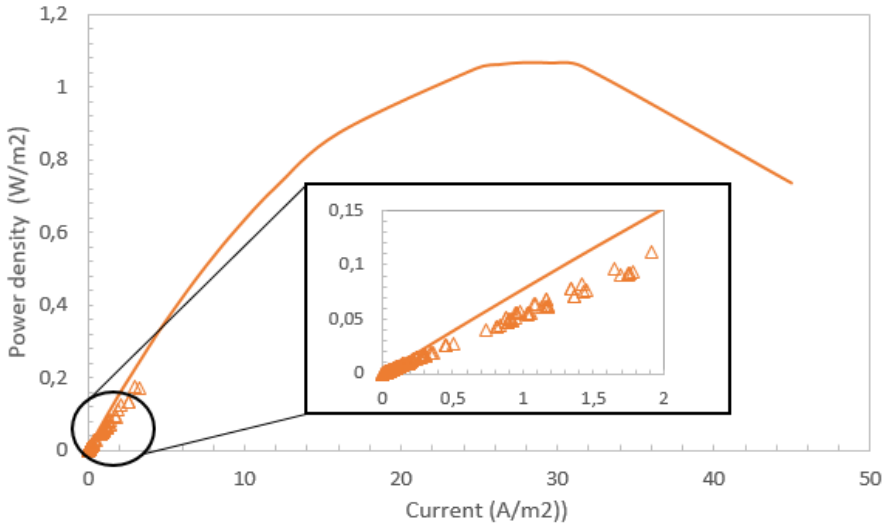

Figure 2.10. Expected Power density from the stack. Reference electrodes Δ, and theoretically calculated —.

- **Effect of ion conductive spacers**

Figure 2.11 present polarization curves for A stack electrodes and B reference electrodes. The same problem mentioned in previous sections was observed for conductive spacers. In fact, when voltage is measured with stack electrodes, stacks with spacers appear to have a negative effect in the behavior of the stack. This unwanted effect is because oxidation of the electrodes caused very high variability in the voltage measurements in the electrodes.

On the contrary Figure 2.11A shows polarization curves measured with reference electrodes. It is clearly seen that the use of conductive spacers in parallel current operation (blue) cause an increase in OCV. Furthermore, the operation of the stack in counter current configuration with spacers (green) presents the best results, compared to parallel current operation. This effect may be ascribed to the fact that in counter current operation the salinity gradient is preserved during the flow path, keeping constant the motive force that causes ion flux. In parallel current operation, the salinity gradient decreases with length, causing some areas to have less potential difference than others, and the overall effect is a decrease in voltage. Another thing to notice is that in the 3 cases investigated in Figure 2.11B, the slope is similar to the theoretical predicted slope during operation range investigated.

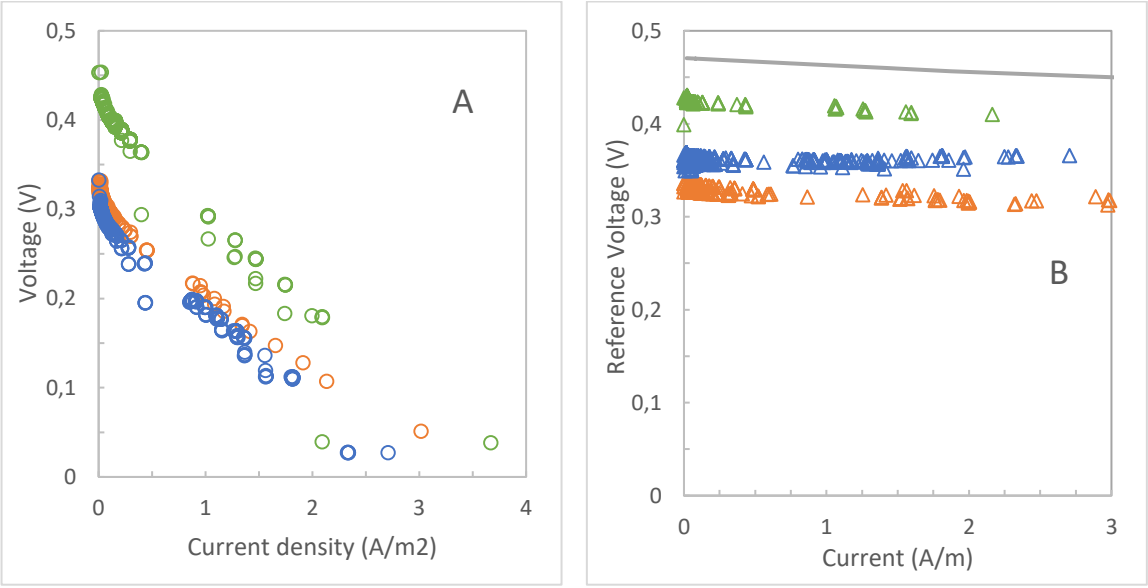

Figure 2.11. Polarization curves for A) stack electrodes (circles), B) reference electrodes (triangles). For stacks with 3 cells without spacers (orange) with conductive spacers in parallel current (blue), and conductive spacers in counter current operation (green)

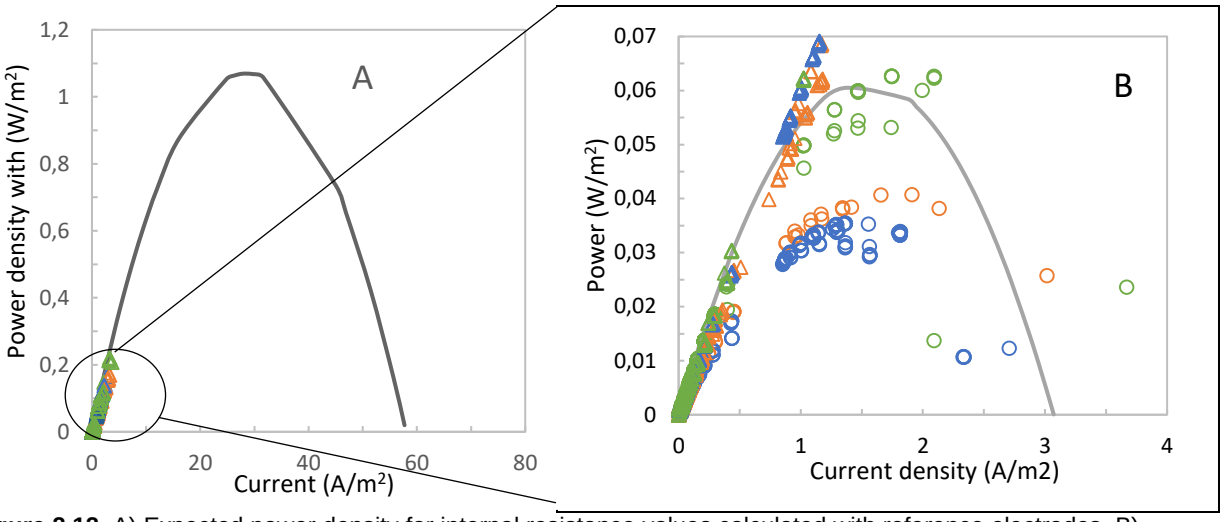

Figure 2.12. A) Expected power density for internal resistance values calculated with reference electrodes. B) Real obtained power density for stack electrodes and reference electrodes for stacks without spacers, with spacers in parallel current and spacers in counter current.

Figure 2.12 are Power density vs Current density curves. Figure 2.12A shows the expected behavior of the cell in the absence of problems related to leakages in the external circuit compartments. The circle in the initial part of the curve indicates the real experimental values obtained in the reference electrodes. Figure 2.12B is the zoom of Figure 2.12A, but theoretical power is calculated using real internal resistance of the stack. Figure 2.12B also contains experimental power density obtained in stack electrodes (circles).

- **Use of real river and sea water**

In order to assess the potential of salinity gradient energy in Colombia, water from the Caribbean Sea and from the Magdalena River was collected in the Bocas de Ceniza River mouth, in Barranquilla, Colombia, by researchers of Universidad del Norte. The water was kept in a refrigerator for 6 months until it was used in these experiments. Table 2-3 shows the concentration of different ions in the waters used for the experiments

Table 2-3. Ion composition of real seawater used in the experiments

Ion composition (mg/L)	**Na^+**	**Mg^{++}**	**Ca^{++}**	**Cl^-**	**SO_4^{--}**
Magdalena River	6.6	3.3	15.8	5	12.9
Caribbean Sea	11494.5	1312.8	485.7	24700	2640

Results in Figure 2.13 show a comparison of results obtained with artificial waters prepared in the laboratory (blue) and results obtained with real sea water (purple). From Figure 2.13A it is possible to notice that OCV is higher in tests with real water than with artificial water. Additionally, even for the small current range studied, it is possible to notice a slightly

steeper slope for real waters. This behavior may be attributed to the presence of Mg^{++}, Ca^{++} and SO_4^{--} ions, which have been proven to increase electrical resistance of the membranes [69]–[71].

In Figure 2.13B no relevant information can be drawn. The reason is that results obtained account only for the initial part of the power density curve and real operation conditions of the cell should be in a much higher current density range of operation (20 – 40 A/m^2) according to the theoretical model and literature in the subject [64] .

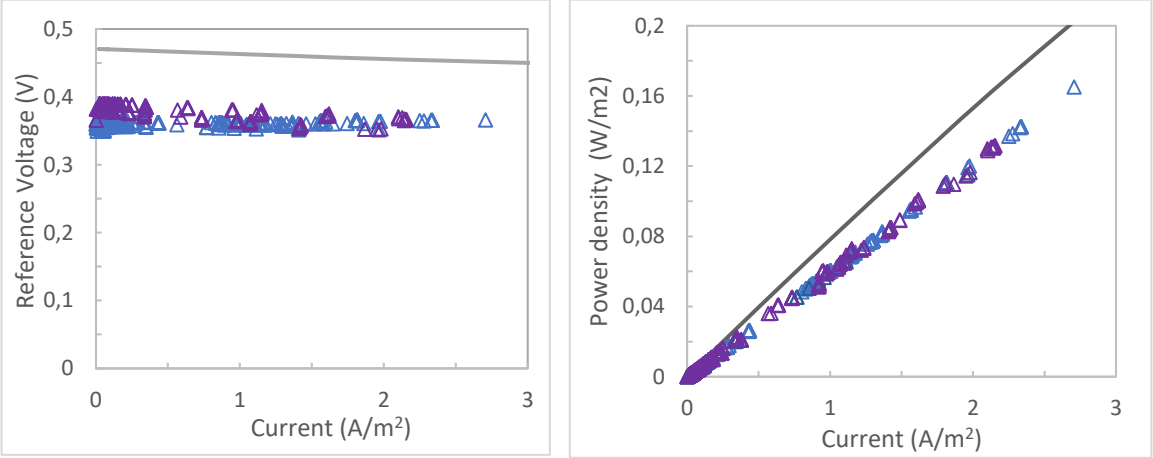

Figure 2.13. A) Polarization curves found for reference electrodes B) Power density curves found for reference electrodes. Δ Tests with water from Magdalena River and Caribbean Sea in stacks with spacers, Δ Tests with artificial sea water in stacks with spacers.

2.4.4 Results for 5 cells

Effect of spacers was also investigated for 5 cells. Figure 2.14 is a comparison of polarization curves for a stack with 5 cells with (dark blue) and without (gray) spacers. Results in Figure 2.14A confirm the great variability that resistance measured in stack electrodes can have. Even for the same conditions and stack configuration, different slopes of the polarization curves may be obtained.

Figure 2.14B also shows variability in the results probably associated to the absence of flow control, and to the non-uniform flow distribution. However, the slopes, and thus the resistances found, are consistent with theoretical model and are repeatable through the experiments.

Apart from the preceding, Figure 2.14B presents a difference of 0.1 V between theoretical calculation and the best experimental results. Some authors have described these differences using perm selectivity parameter. In this case, as the model calculation is done with the reported properties of the membrane manufacturer, the difference between theoretical calculation and experimental results could be due to a lower membrane perm selectivity value than the reported by the manufacturers.

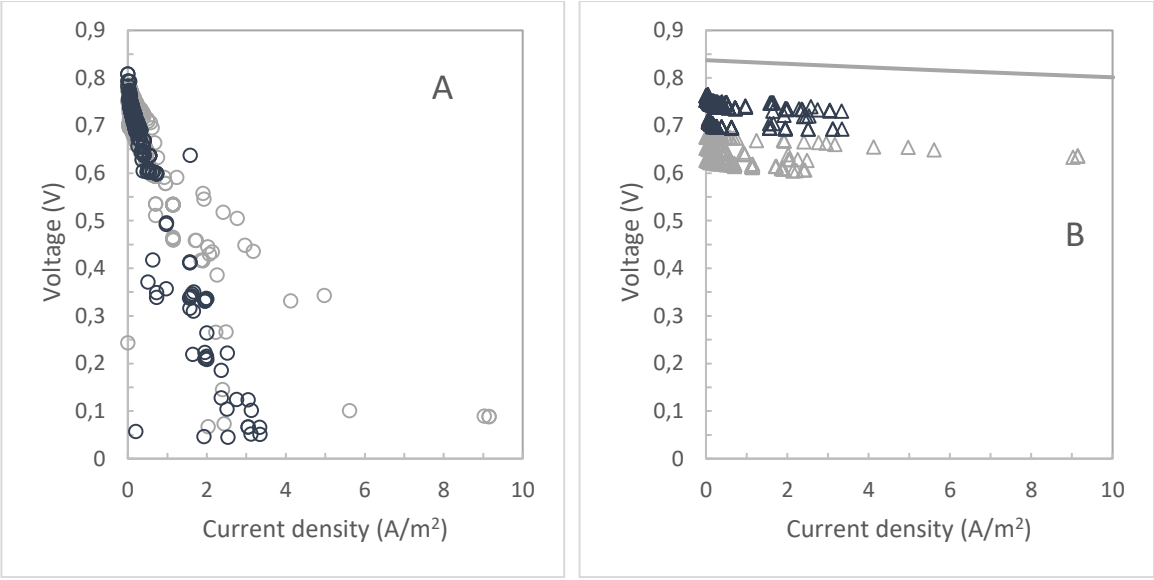

Figure 2.14. Polarization curves with 5 cells stack. A) Measured with stack electrodes in stacks without spacers ○ and with spacers ● B) Measured with Reference electrodes in stacks without spacers △ and with spacers ▲

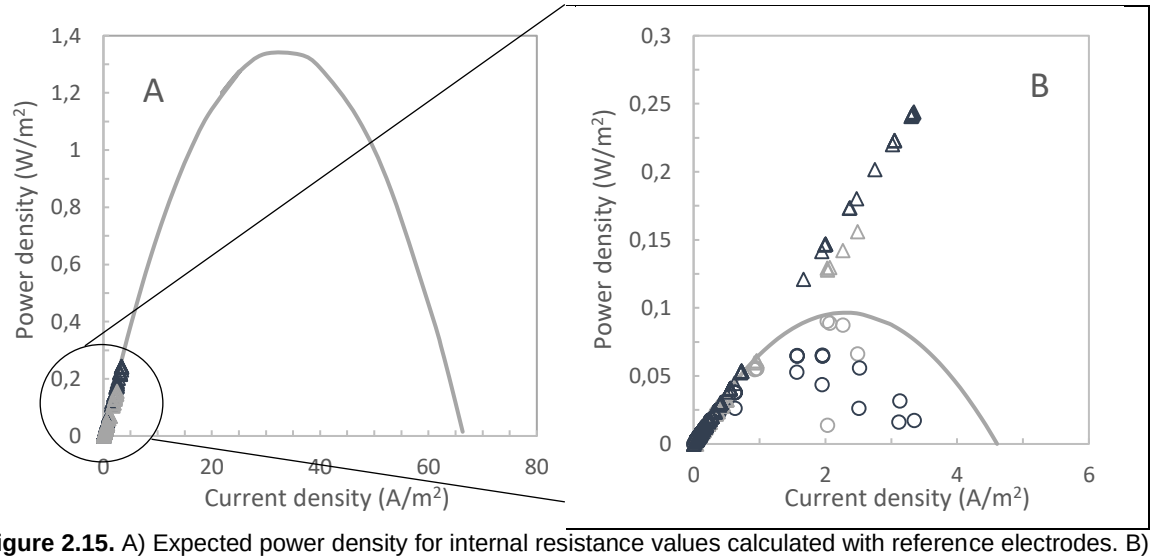

Figure 2.15. A) Expected power density for internal resistance values calculated with reference electrodes. B) Real obtained power density. Theoretically calculated --. Experimentally obtained in stack electrodes with ● and without ○ spacers. Experimentally obtained in reference electrodes for stacks with ▲ and without △ spacers.

Figure 2.15 are Power density curves. Figure 2.15A shows the expected behavior of the cell in the absence of problems related to leakages in the external circuit compartments and the circle in the initial part of the curve indicates the real experimental values obtained. Figure 2.15B is the real behavior of the cell measured in the stack electrodes (circles) and in the reference electrodes (triangles) for stacks with spacers (dark blue) and without spacers (gray). In Figure 2.15B, the calculated theoretical power is also shown. The calculation was performed, substituting the theoretical value of internal resistance, with the real internal resistance values measured with stack electrodes.

2.4.5 Results for 10 cells

Figure 2.17 shows results obtained for 10 cells. Figure 2.17A is the polarization curve measured in stack electrodes (circles) and in reference electrodes (triangles). It is clearly visible that OCV measured at the stack electrodes is much higher than OCV measured at the reference electrodes. Nevertheless the slope of the polarization curves is much steeper in stack electrodes than in reference electrodes. When working electrodes would acquire a different potential difference than the reference electrodes, evidence for the occurrence of reactions would appear in the copper terminal of the stack (Figure 2.16).

Figure 2.16. Oxidation reactions in copper stack terminals.

According to results obtained in this and in previous research [63], [64], it could be said that the difference in OCV between reference and working electrodes, could be a way to recognize the occurrence of unwanted irreversible reactions in the electrode system.

Figure 2.17B is the power density curve obtained for 10 cells. Theoretical calculations were obtained substituting the theoretical calculated resistance, with real resistance values obtained from the working electrodes of the stack. Experimental results obtained from the reference electrodes (triangles) and from the working electrodes (circles) are shown. The theoretical power curve can partially predict experimental results and differences between theory and experiments may be ascribed to an increase in ohmic resistance with time and the generation of oxidation reaction at the stack terminals.

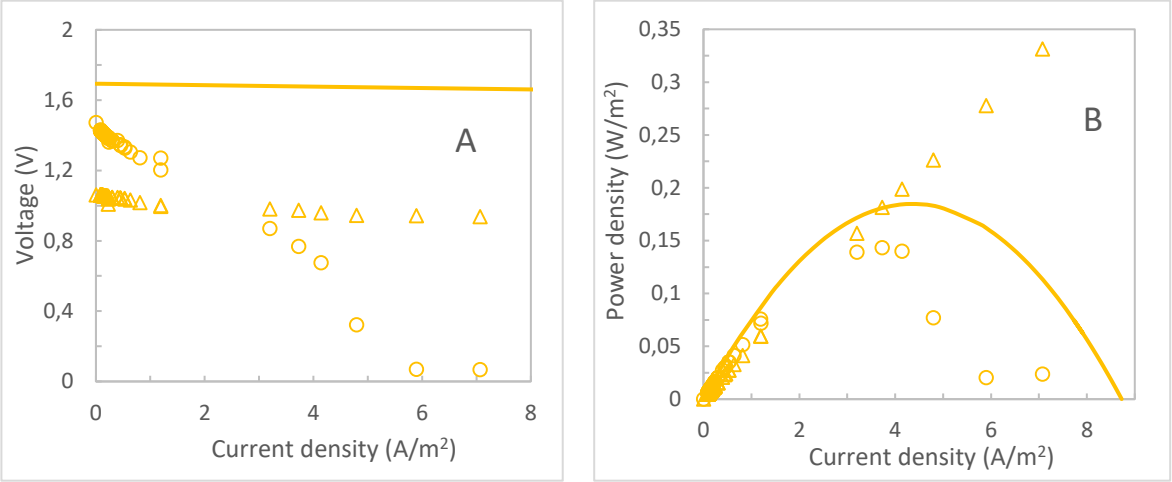

Figure 2.17. A) Polarization curve (V vs I) for 10 cells measured at the stack electrodes ○, at the reference electrodes △, and theoretically calculated — B) Power curve (W vs I) for 3 cells measured at the stack electrodes ○, at the reference electrodes △, and theoretically calculated —.

2.4.6 General Analysis and discussion

Figure 2.18 summarizes results obtained for working electrodes in all the stacks tested without spacers. Polarization curves in Figure 2.18A reveal that OCV increases with the number of cell pairs. On the other hand, slope of the polarization curves does not change with a defined trend and it can have a great variability, which was a problem exhibited during the experimental section.

Figure 2.18B are power density curves obtained in the working electrodes for stacks without spacers. In spite of the great variability in the results with the stack electrodes, maximum power achieved for 10 cells was 0.14 W/m^2, which is consistent with other experimental results presented in literature [63].

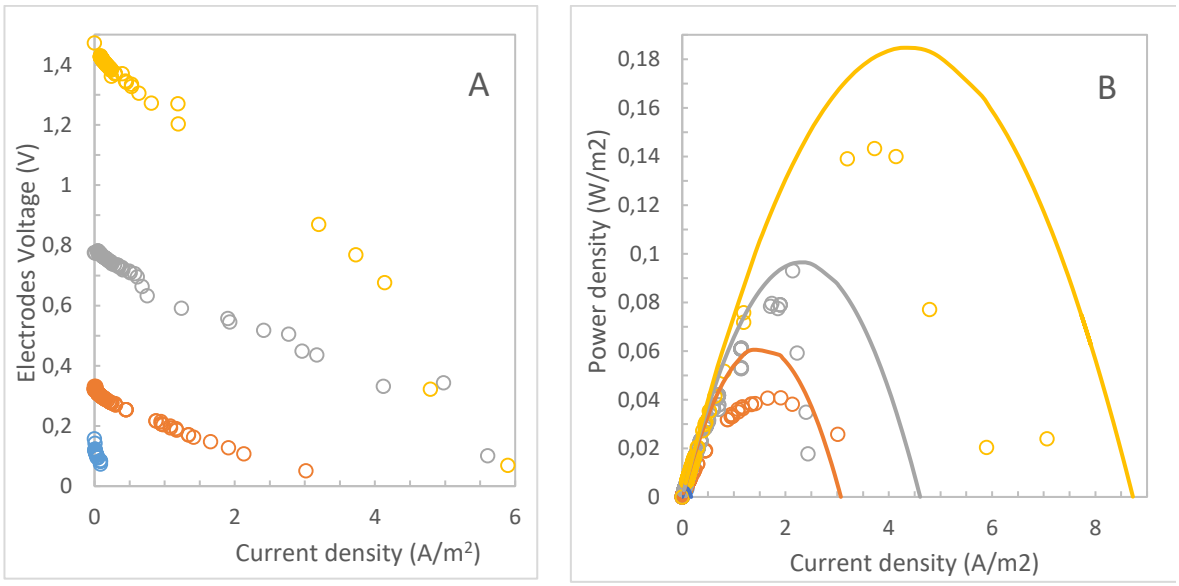

Figure 2.18. A) Polarization curves obtained with working electrodes for stacks with 1 ○, 3 ○, 5 ○ and 10 ○ cells. B) Power curves obtained with working electrodes for stacks with 1 ○, 3 ○, 5 ○ and 10 ○ cells.

Figure 2.19 summarizes polarization curves obtained for all the stacks tested with reference electrodes. It is possible to notice that the use of conductive spacers increased the voltage compared to stacks without spacers. The number of cell pairs, also has a positive effect on stack voltage, and in this case the slope of the polarization curves is less variable and more consistent with theory than the one presented in Figure 2.18A.

In general Power density curves obtained in this research for reference electrodes do not exhibit important information. The reason is that data obtained during the experiments accounts only for the initial part of the total power density curve. The typical power curve should exhibit a maximum value, and it is expected to reach current density values of more than 30 A/m^2. Although the information shown in Figures 2.8, 2.10 and 2.13 shows that results obtained for reference electrodes fit the initial part of the power curve described by the model, the experimental results cannot be extrapolated, and thus, the summary of power density results measured in reference electrodes are not shown in this section.

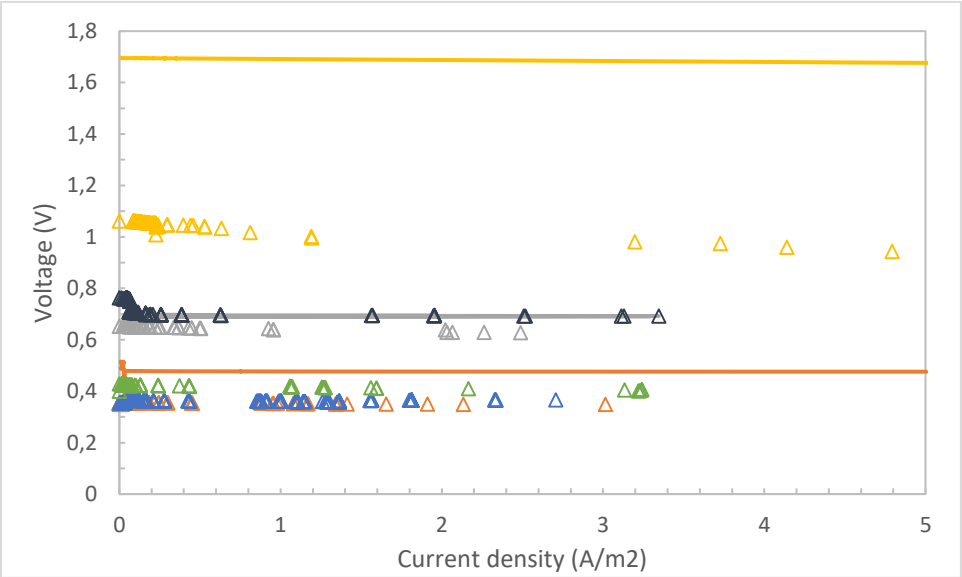

Figure 2.19. Polarization curves obtained theoretically and experimentally with reference electrodes for 3 cells without spacers Δ, 3 cells with spacers Δ, 3 cells with spacers in counter current mode Δ, 5 cells without spacers Δ, 5 cells with spacers Δ and 10 cells Δ.

Experimental resistance of the cells are illustrated in Figure 2.20. Results in gray represent real stack resistance measured in the working electrodes, light green describes cell resistance measured with reference electrodes, while solid dark green line represents the theoretically calculated values.

In previous sections, the unexpected response of the stack was explained with the high resistance of the stacks. In Figure 2.20 it is possible to notice that internal resistance measured with working electrodes can be from 10 to 70 times higher than the experimentally obtained results with reference electrodes or the calculated values with theory. This difference can be ascribed to the occurrence of irreversible oxidation reactions in the stack terminals due to water leakage into the external circuit. This reactions would cause a low conductance oxidation layer that would restrict electrons flow through the external circuit, causing some times behaviors of polarizable electrodes.

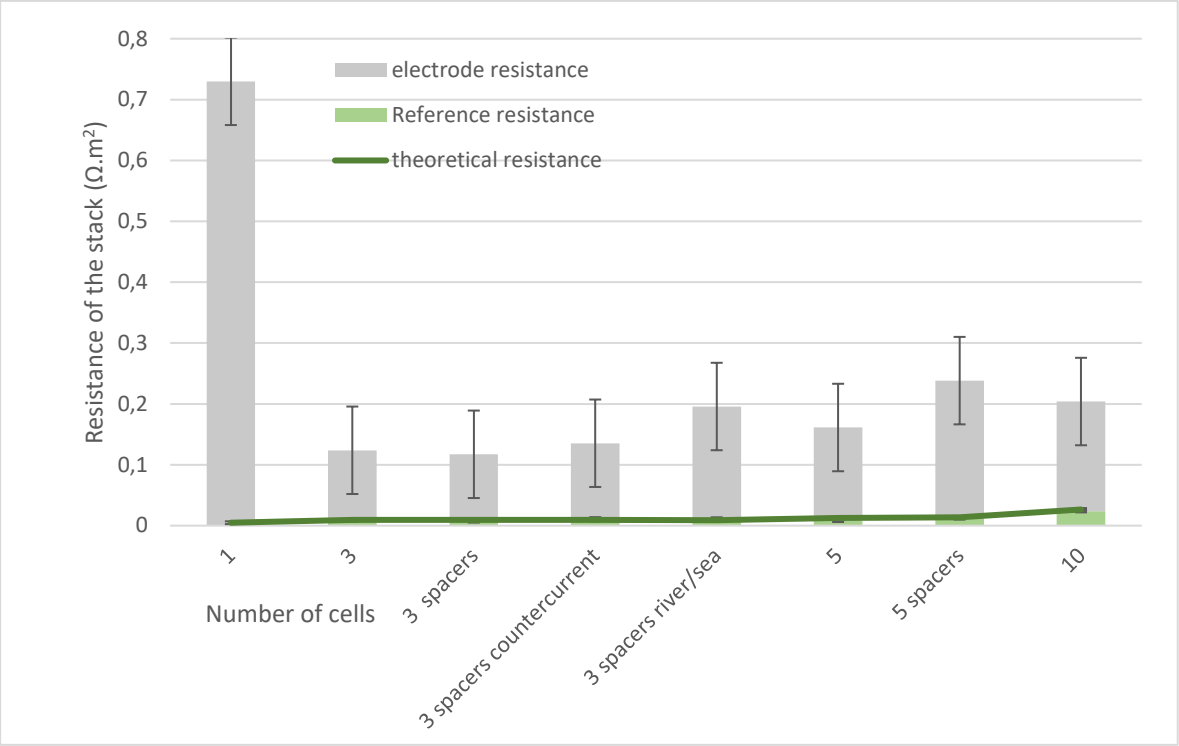

Figure 2.20. Internal resistance of the stacks calculated theoretically and obtained experimentally

Despite the large electrical resistance presented in the stack electrodes, experimental results obtained with reference electrodes are in good agreement with theoretical calculations. Figure 2.21 shows the expected theoretical internal resistance (dark Green) compared to the internal resistance measured with reference electrodes (light green) for each of the stacks. In some cases experimental values are higher than theoretical values and in some others they are lower.

This small differences encountered might be associated with the use of average flow to calculate internal electrical resistance. Even though water flow was measured at the stack outlet, it was not a controlled variable, and each test had different flows for concentrated and diluted solutions, thus theoretical calculations were performed with average flows. Another source of error is that membrane resistance is measured by the manufacturer in 0.5 M NaCl, while in RED, the membrane is exposed to a much lower ion concentration (0.01 M), which has been proven to cause an increase membrane resistance [72]. In this research resistance of the membranes was not measured experimentally and thus, theoretical calculations were performed with resistance values given by the manufacturers.

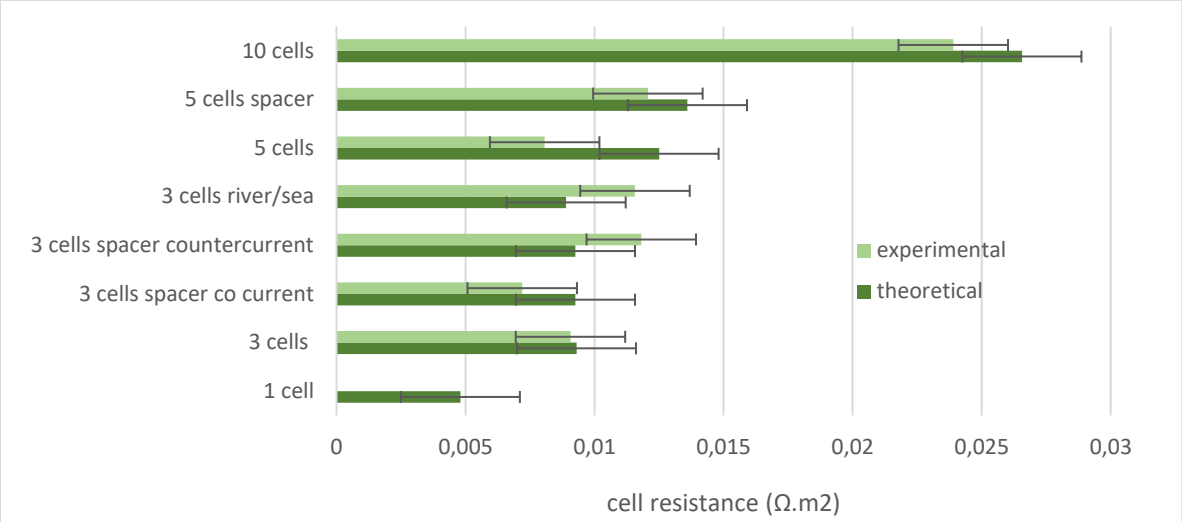

Figure 2.21. Comparison between theoretical results calculated with model and experimental results obtained with reference electrodes

Figure 2.22 shows results for OCV obtained in the reference electrodes (red), in the working electrodes (light red) and theoretically expected results (orange). In most cases OCV obtained with electrodes was higher than obtained in references. Theoretical results were always higher than experimental values. The reason for this is that theoretical calculation does not account for concentration polarization effects which are present in the case of low linear velocities, especially in the absence of spacers. Besides, perm selectivity values are not guaranteed by the membrane manufacturer.

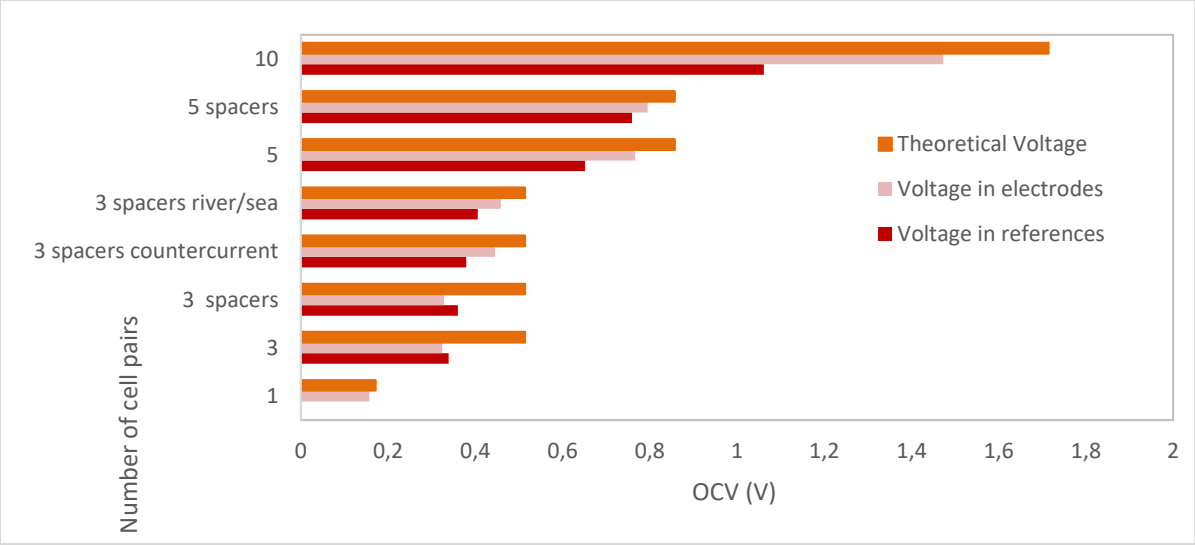

Figure 2.22. OCV measurements for electrodes, references and model

2.5 Conclusions

A stack has been designed and constructed in Colombia without the use of pumps as a first step to develop salinity gradient technology. A validated model has been tested successfully with the stack constructed.

The effect of conductive spacers with chevron geometry have proven to improve the behavior of the RED stacks. The stack presented the best results for counter current operation and thus it is recommended for generation of maximum power.

Water from the Caribbean Sea and from the Magdalena River was tested, and results obtained for power density were very similar to those for artificial NaCl solutions. This shows that it is theoretically possible to recover energy from the Bocas de Ceniza River Mouth in quantities similar to laboratory conditions. Results are a first step for the assessment of field implementation of a RED pilot plant in Colombia.

The Ag/AgCl electrodes are highly reversible and do not require pumping the rinse solution. In the experiments performed there was no evidence of side reactions in the electrode under the studied voltage ranges, and they were found to be mechanically stable after many cycles. On the other hand, although Ag^+ ions have low solubility in NaCl solutions, this ions could leak to the environment and cause a certain toxicity degree in the effluent waters. It is necessary to do further analysis regarding environmental and financial feasibility to determine the viability of Ag/AgCl redox couple.

A dynamical model has been proposed and solved for RED. This model gives insight of the transitory stages of RED, and it can be useful in the cases where this stages need to be studied, like feed water reversal for biofouling control. In larger time scales it can be helpful in the case where feed waters properties change with time and it can be used to model changes that might of occur in RED operation in time, like increasing internal resistance, for scheduling periodic cleaning treatments.

2.5.1 Recommendations

The leakage of electrolyte solution into the junction of an Ag/AgCl working electrode and a cooper terminal in the stack, resulted in bad operation of the equipment. In order to test the RED stack in conditions of stationary state, side reactions in the electrodes can be avoided improving the seal or using only one big silver block as working electrode and stack terminal. These alternatives are cost effective compared to other options suggested in literature.

RED operation involves a lot of variables. In order to validate the models and to calculate thermodynamic efficiency of the stack it is necessary to measure concentrations at stack outlet, to measure water flow at the stack inlet and outlet and to use peristaltic pumps to control water flow. It would also be interesting to use an electrical load that can be controlled computationally in order to control the load change in time, which has also different effects in the results. All of the data should be collected in an integrated unit that records in time each of the measured variables, otherwise it is a bigger effort to consolidate the results.

2.5.2 Outlook

From the theoretical point of view, it would be more accurate to include the dependence of the molar conductivity with concentration in the model. It would also be interesting to do CFD modelling with spacers designed for this research, and to include different configurations of the spacers designed in order to predict which would be the best one.

Experimentally it is necessary to study stability in big time scales of the stack in operation with river and sea water. The next step for assessment of a RED pilot plant implementation is to understand fouling effects that waters from the Caribbean Sea and the Magdalena River might produce.

3. Capacitive Reverse Electrodialysis

3.1 Introduction

3.1.1 Advantages of CRED compared to previous technologies

Capacitive Reverse electrodialysis is a recently developed energy generation system that combines RED and Capacitive mixing (CapMix) principles [27]. This process uses carbon based super capacitors instead of electrodes and electrochemical reactions. It has the advantage of not requiring redox reactions to convert salinity gradient energy into electrical energy.

Most papers published in the literature for studying RED technology use Ferro cyanide Redox couple ($[Fe(CN)_6]^{-4}$ / $[Fe(CN)_6]^{-3}$) [73][74][75]. Although this is a very reversible couple and thus it allows to study the properties and characteristics of the hydroelectric pile, it is not a feasible redox couple for commercial applications because there exists a big risk that some of the ions used for the redox reaction leak into the waters that enter the cell, and decompose in free cyanides in the presence of sunlight and oxygen [73]. This problem was addressed in the second chapter, using a highly reversible, nontoxic redox couple Ag/AgCl with a nontoxic electrolyte (NaCl 0.5 M).

On the other hand, the advantage of CRED with respect to CapMix is that the constant water flow through the ionic circuit generates a continuous ionic current towards the surface of the activated carbon, which allows to extend the charging and discharging processes of the capacitor [27].

Apart from that, it is important to go deeper into the study of CRED system in order to understand which is the maximum power obtainable and if it is possible to generate more power density with this system than with RED.

3.1.2 Electrical Double Layer Capacitors

In general, it has been found that Electrical Double Layer Capacitors (EDLC) are preferable than electrode reactions in any application in which high power density, fast response, rapid charging, and high cycle life are more important than energy density [76].

The current response transient for charging a supercapacitor interface under the influence of a step in potential is shown in Figure 3.1 Where an exponential decay of the current is expected. In the presence of a faradaic current, the total current will not tend to cero, but to the value of the faradaic current.

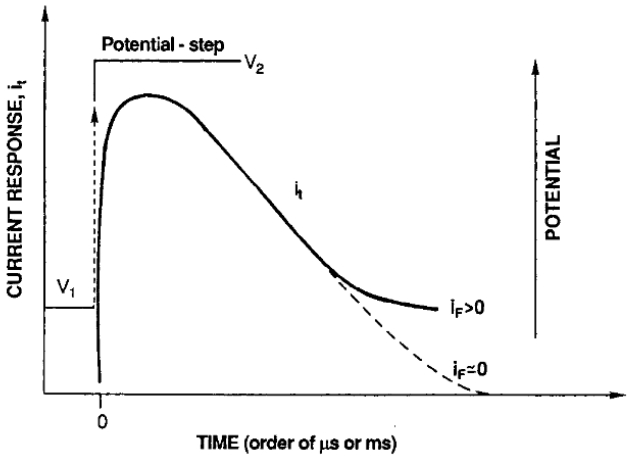

Figure 3.1. Current response transient for charging a supercapacitor interface under the influence of a step in voltage [77].

3.1.3 CRED Operation

CRED technology has a membrane pile core identical to RED, shown in Figure 3.2. The fundamental difference between the technologies is that CRED operates alternating feed waters in the compartments every certain time, while RED can be operated as a continuous process.

In CRED, the voltage produced in the membrane circuit is used to charge two supercapacitors located at both ends of the cell that are in contact with a saline solution. Because of electroneutrality principle, while ions accumulate on the solution side of the capacitors, electronic configuration of the activated carbon reorganizes to complement the

charge excess in the capacitors surface, which causes an electron movement through an external circuit.

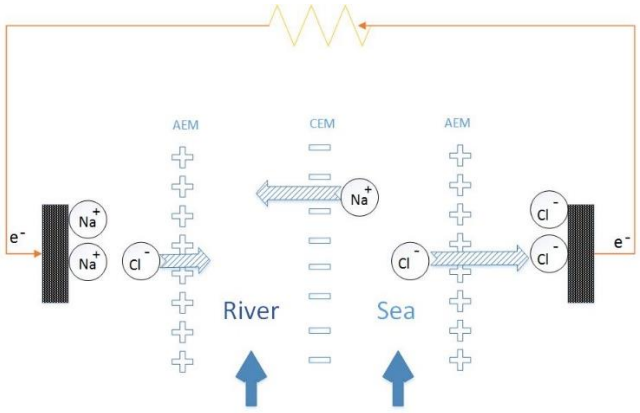

Figure 3.2. CRED Principle of operation

Once the capacitors are saturated with ions, it is necessary to invert the flow of the waters and to open the external electrical circuit. Where there used to pass river water, seawater starts to pass and vice versa.

The water interchange gives rise to a movement of ions in the opposite directions, which makes positive ions start to accumulate in the capacitor that was collecting negative ions before, and the carbon that was storing negative ions, starts accumulating positive ones instead.

The most interesting effect in CRED system is that voltage measured in the capacitors after the exchange reaches a higher value than the one obtained with regular RED or CapMix operation [27], [58].This effect is the sum of membranes voltage, as calculated in RED process, plus a contribution due to polarity change in the electrochemical compartments at constant charge, similar to CapMix effect. The difference in OCV voltage between RED and CRED has been attributed to the stored charge in the capacitors [27].

After system attains this stable voltage, the external circuit is again connected through an external resistance. In this way electronic configuration of the external circuit shifts again, and causes an electrical current to pass through a resistor. Thus the process changes repeatedly and power is generated. Figure 3.3 explains the operation of CRED cycles

3.2 Theoretical model

The full development of the model is presented in chapter 2. This section presents only the basic equations and the modifications of the RED model, as it is essentially the same. In this case, a stationary state solution is not included, because the behavior of CRED is intrinsically dynamic.

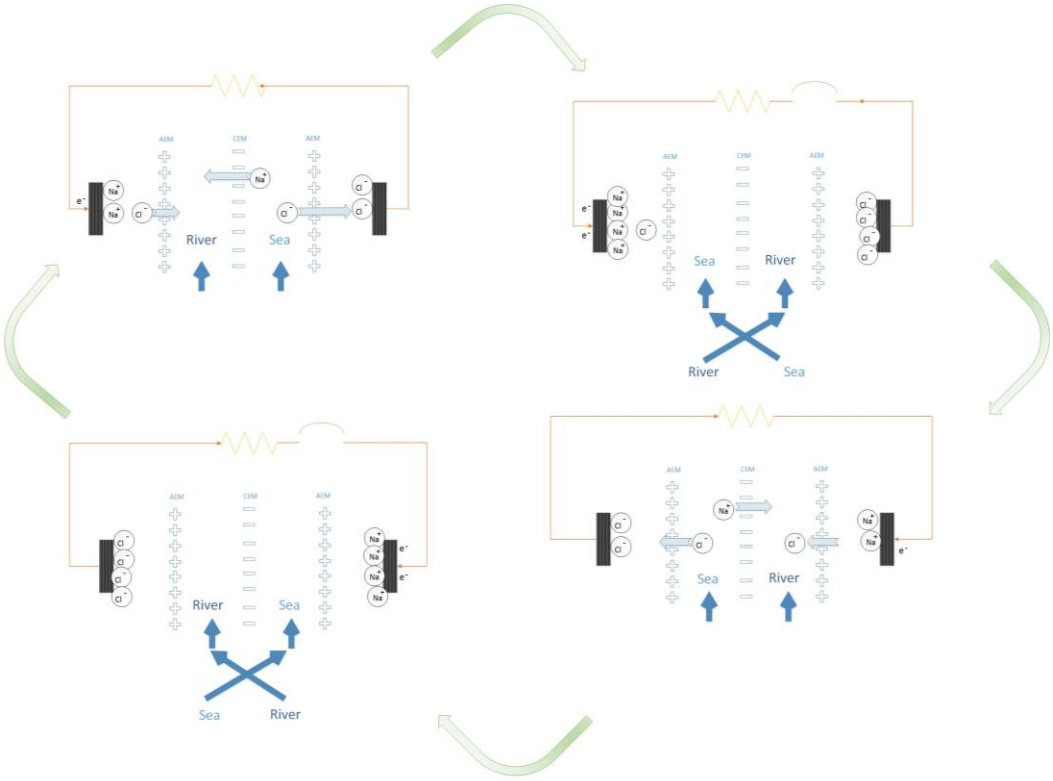

Figure 3.3. CRED cycle operation

The equations that simulate concentration change in time inside the compartments are

$$\frac{dC_c(x)}{dt} = \frac{F_c}{b\,\delta}\frac{\partial C_c(x)}{\partial x} - \frac{1}{\delta}J_w C_c(x) - \frac{1}{\delta}J_{NaCl}(x) \tag{3.1}$$

$$\frac{dC_d(x)}{dt} = \frac{F_d}{b\,\delta}\frac{\partial C_d(x)}{\partial x} + \frac{1}{\delta}J_w C_d(x) + \frac{1}{\delta}J_{NaCl}(x) \tag{3.2}$$

Except for J_{NaCl}, all the terms in Eq. 3.1 and Eq. 3.2 are calculated as explained in the previous chapter. The difference of the model is that NaCl transport by migration is now calculated as a transient process defined by the equation of current response in a capacitor

$$J_{mig} = \frac{E}{R_t}\exp^{-t/R_t C} \tag{3.3}$$

Where E is the voltage attained by the system (V), t is time in seconds, C is the capacitance (F), and R_t is the total resistance of the system, including internal and external resistance.

$$R_t = R_i + R_u \tag{3.4}$$

Finally Power density was calculated using Eq. (3.5) [27], [38]

$$P_d = \frac{1}{2N(t_2 - t_1)}\sum I^2 R\Delta t \tag{3.5}$$

The rest of the model has been explained in the previous chapter, and thus, it is not necessary to repeat equations for the calculations of power, power density or energy efficiency, between others.

3.3 Experimental conditions

3.3.1 Reverse Electrodialysis stack

The stack used for the experiments was the same as described in the previous chapter. The methodology for the construction of the capacitors was based in literature review [27], [78]. Activated carbon particles with a size of 38 µm or less were used. The activated carbon was dispersed in a solution of IPA-H_2O using ultrasound for 5 minutes. The mixture was dried during the night at 80ºC. After this procedure, the activated carbon was mixed with dispersed PTFE (85:15 ratio) and then the final mixture was put into an ultrasonic bath for 15 minutes. Subsequently the suspension was heated to 80ºC and it was vigorously agitated during 28 minutes until the mixture looked homogenous. The resulting paste was extended over an opaque Steel sheet, guaranteeing a 200 µm thickness of the film.

Electrochemical characterization of the supercapacitor was done using cyclic voltammetry and it was found to have a specific capacitance of 98.73 mF per cm^2 projected area. The geometrical area of the capacitors was 1.3 cm^2.

In order to be able to compare results obtained with previous literature, concentration values of the waters where 0.5 M NaCl for the concentrated solution, (typical seawater concentration) and 0.01 M NaCl for diluted solution [38].

3.3.2 Electrochemical measurements

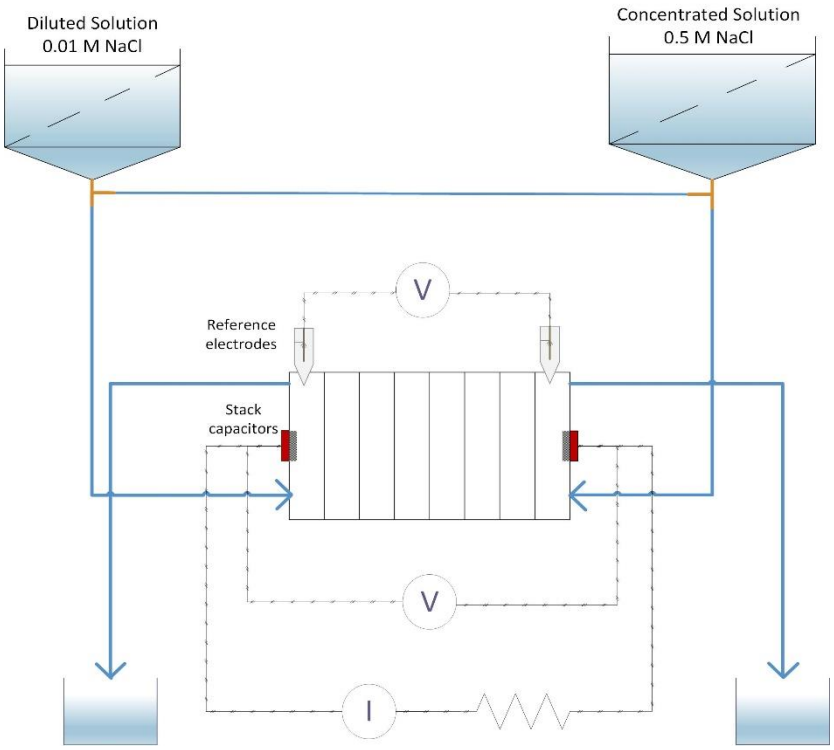

Figure 3.4. Experimental set up for CRED experiments.

The experimental set up is shown in Figure 3.4. The experiments did not count with flow control, no pumps were used in the experiments, and water flowed by gravity with a 30 cm water column. Three way valves where added to the experimental set up in order to easily exchange waters. Electrode rinse solution was not recirculated. Salt solutions were made using reagent grade NaCl (Merck) and tap water. Inside the stack, water flowed bottom up in order to improve water distribution inside the compartments. Water flow was measured gauging a 25 mL volumetric balloon in the stack outlet.

Experiments were carried out using 3 multimeters UNI-T (UT71D) for recording data in time, in combination with a manually variable resistance. Register of voltage and current was done every two seconds. Stack voltage was measured in Ag/AgCl reference electrodes and in the stack terminals.

3.3.3 Experimental conditions

Stacks with 1, 3, 5 and 10 cells were investigated with artificial solutions. The experiments consisted in measuring voltage response to the salinity gradient. Once the voltage reached a stable value, an external resistance was applied and current response to the perturbation was measured at the stack terminals, as shown in Figure 3.4. After current values were very small, the external resistance was disconnected and the waters were shifted. This process was done repeatedly for all the experiments.

Unfortunately results showed a lot of variability and low reliability. Thus, only for illustrating purpose, results for 3 cells are shown. Furthermore, in order to decrease the non ohmic resistance of the stack, conductive spacers were tested. Ion conductive spacers used in the experiments were described in the previous chapter. Finally, one test was performed using real Caribbean Sea water and Magdalena river water. All the experiments in this section were performed in parallel current configuration. Table 3-1 summarizes the effects investigated in the experiments.

Table 3-1. Experiments performed for CRED system

Number of cells	No spacers	spacers	
	Artificial solution	Artificial solution	Water from Magdalena river and Caribbean sea
3	x	x	x

3.3.4 Calculation of experimental values

Calculation of experimental values was explained in the previous chapter, and thus, it is not necessary to repeat equations for the calculations of power, power density and current density. It is important to clarify that for CRED, values of power were calculated point by point in time in order to obtain dynamical behavior of the system.

Due to the great variability of the results in the experiments, and taking into account that the system was tested only with a few values of external resistance, internal resistance of the stack was not calculated. Instead, a total resistance, including internal and external resistance was obtained by the least squares method.

3.4 . Results and discussion

3.4.1 Model results

Model predictions for CRED for 3 cells and 4 cycles, using the capacitance found experimentally with cyclic voltammetry and the geometrical area of the capacitors are shown in Figure 3.5 A. Figure 3.5 B is the enlargement of Figure 3.5 A, it describes CRED system when an external resistance is connected to close the circuit for only one cycle.

The capacitance used in the model corresponds to a small area (geometrical area of the capacitors), thus from Figure 3.5 it is possible to notice that response time of the capacitors is in the order of milliseconds. The capacitors fabricated for this research were mainly made of Vulcan ® Activated Carbon, which has 256 m^2/g area. Besides the supercapacitors constructed weighted 2 mg. Thus, a superficial area in the order of $5*10^{-1}$ m^2 was taken as initial guess for the model calibration. It was found that an area that would fit experimental results is in the order of 0.15 m^2.

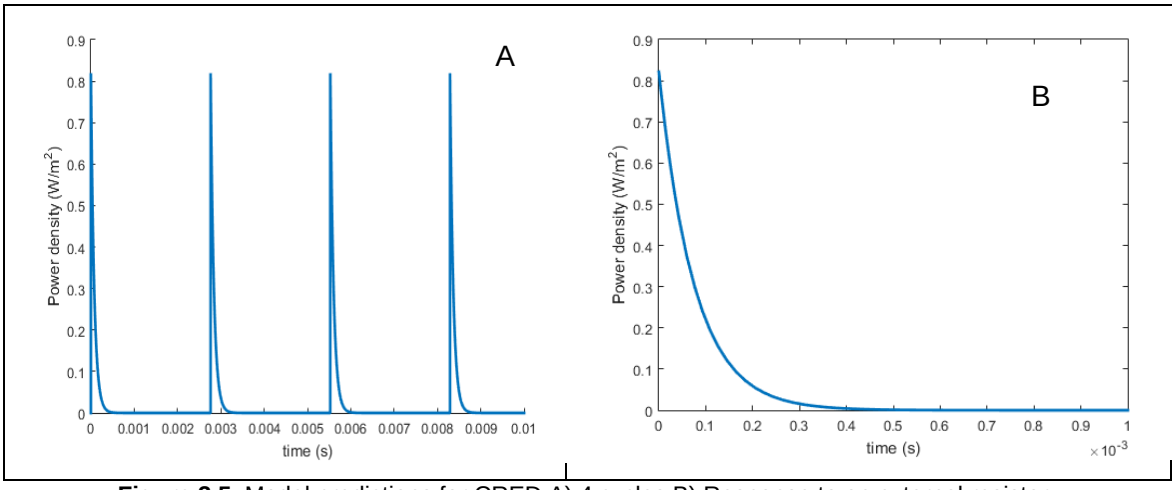

Figure 3.5. Model predictions for CRED A) 4 cycles B) Response to an external resistor.

3.4.2 . Experimental results

This section presents experimental results obtained for CRED experiments with a stack of 3 cells, and the calibrated model output.

- **Results for 3 cells without spacers**

Figure 3.6 shows the voltage vs time series obtained for a CRED stack with 3 cells without spacers measured at the reference electrodes and at the stack terminals. In general it is

possible to notice that the variability of the reference electrodes was smaller than the variability in the stack terminals.

The response of the voltage to the water exchange in the compartments was between 200 and 250 seconds. When the electrical resistance was connected, the voltage in the capacitors would drop sharply from one register to the next, while voltage at the reference electrodes remained constant.

This sudden abatement in capacitors voltage was accompanied of a peak current with an exponential decay, as shown in Figure 3.7. For reasons of clarity Figure 3.7 shows the behavior of current (values in the secondary axis) and voltage in the capacitors (orange circles), only for a couple of cycles. Although the voltage is expected to decrease rapidly from the beginning, it is also expected to increase when external circuit is disconnected. This behavior was observed in the experiments, especially in Figure 3.8 A.

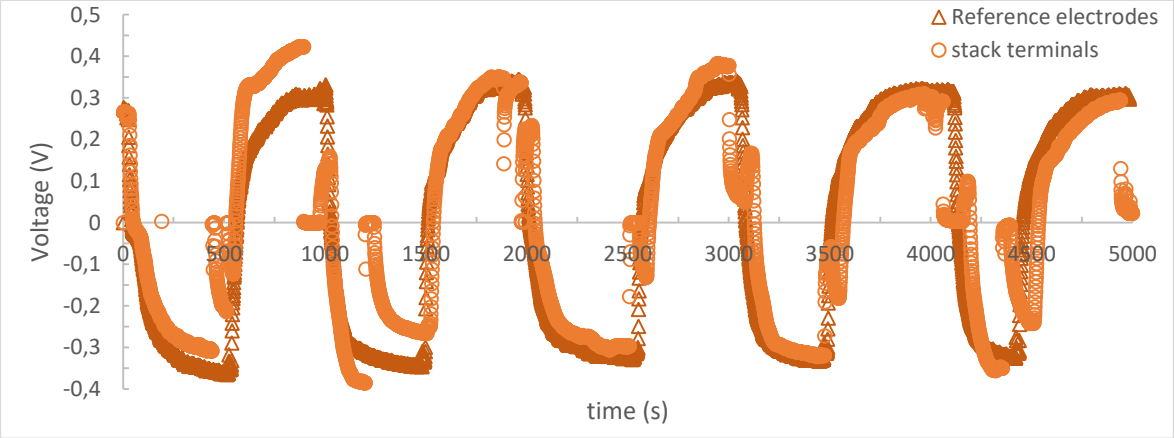

Figure 3.6. Obtained voltage from the stack in reference electrodes (Δ) and stack terminals (○) in CRED with 3 cells without spacers.

Figure 3.8 A shows only two cycles of the CRED experiments, for which external power was calculated. Figure 3.8 B is the characteristic power curve of the CRED cell, which was obtained by multiplying the electrode voltage times the current density results obtained in the same time interval.

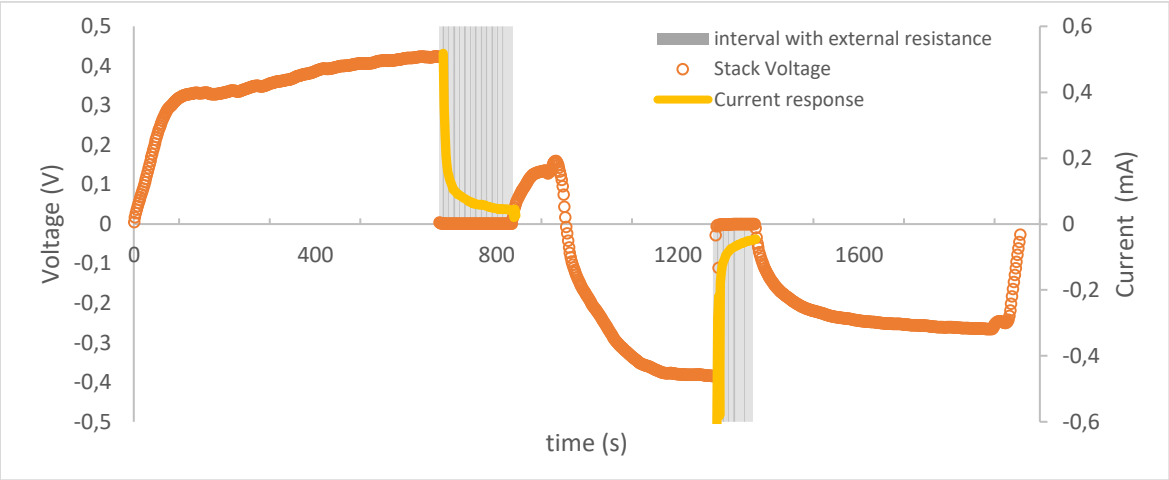

Figure 3.7. Current (--) and stack voltage (o) response to a perturbation in external resistance.

In order to validate the model, theoretical and experimental results were compared, and using minimum squared error it was possible to find total (internal plus external) resistance of the system. Although Figure 3.8 B shows good agreement between experimental and theoretical results, it is possible to notice that in the experiments the power does not drop down to cero, as the model predictions show. This phenomena appears to be a displacement of the potential that might be associated with internal leakages from the capacitors compartment to the external circuit, which caused electrochemical reaction to occur in the copper electrode terminals in contact with leaked NaCl solution.

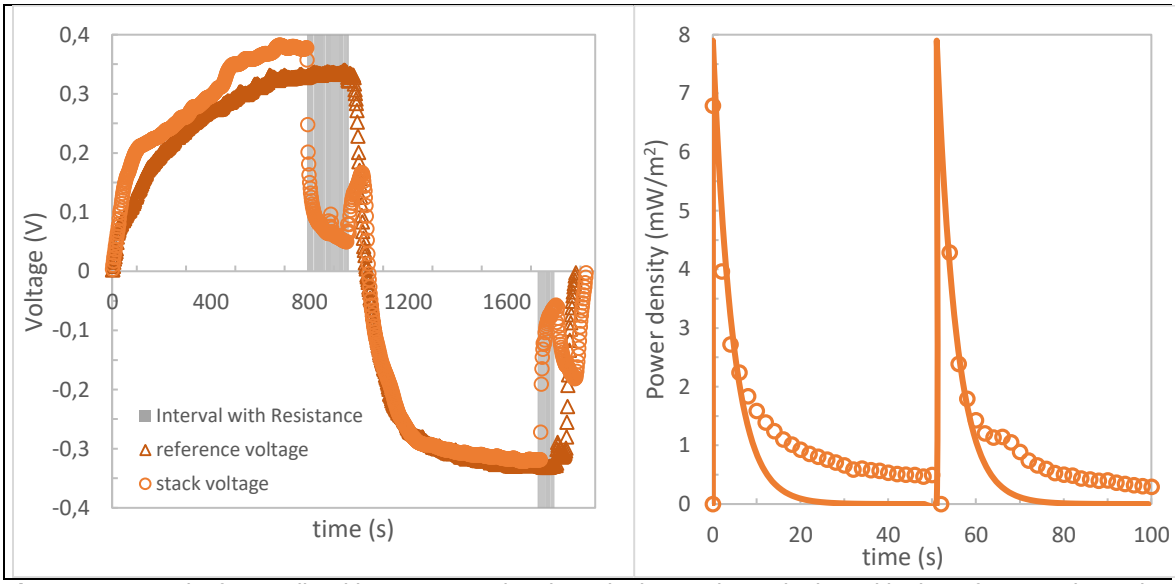

Figure 3.8. Results for 3 cells without spacer A) Voltage in the stack terminals and in the reference electrodes for the studied cycle. B) Power response of the stack after an external resistance perturbation for experimental (o) and model (--) results.

- **Results for 3 cells with spacers**

Figure 3.9 shows results for voltage at the capacitors and at the reference electrodes for the experiments performed with 3 cells and with spacers. After several cycles, voltage measured at the references remains unchanged, while for capacitors, voltage cycles did not stabilize. Looking at the negative part of the voltage, after each cycle the voltage reached by the stack terminals was smaller, while at the positive part, the stack voltage always achieved a stable value in the different cycles. It is believed that there was a leakage in one of the capacitors, which is the same problem mentioned along this research that has caused many inconvenient in the results.

On the other hand the expected results for stack with spacers was an increase in OCV and thus in power. For the voltage obtained in the capacitors and in the reference electrodes, an increase in OCV can be noticed, compared to the stack without spacers.

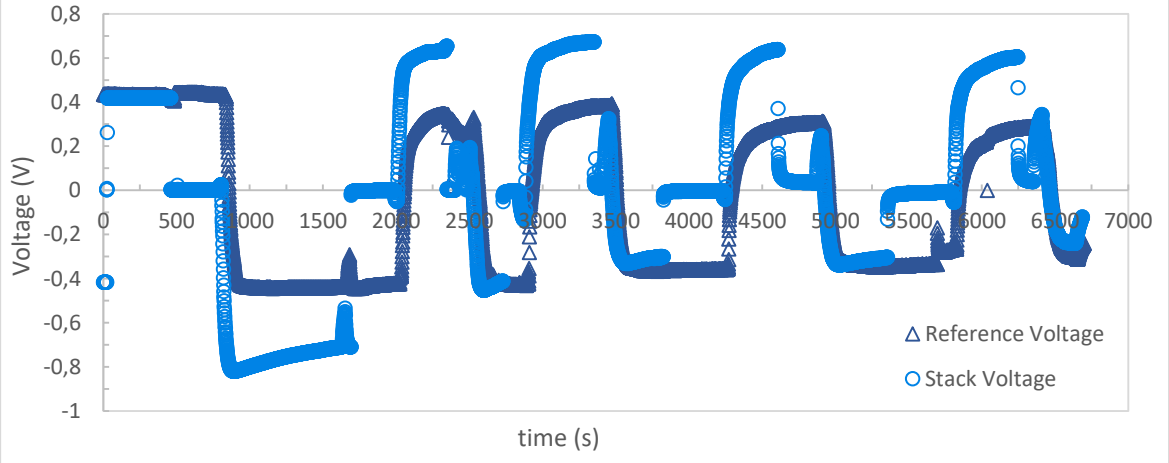

Figure 3.9. Obtained voltage from the stack in reference electrodes (Δ) and stack terminals (o) in CRED with 3 cells with spacers.

Figure 3.10 has the voltage and power response of the stack in the studied cycles. It is possible to notice a major difference between powers obtained from the 1st and 2nd cycle. The model was calibrated with the results obtained in the 2nd cycle, but applied to results in both studied cycles. It is possible to notice that for the first cycle, the model does not represent the results, probably because the internal resistance of the system was much higher.

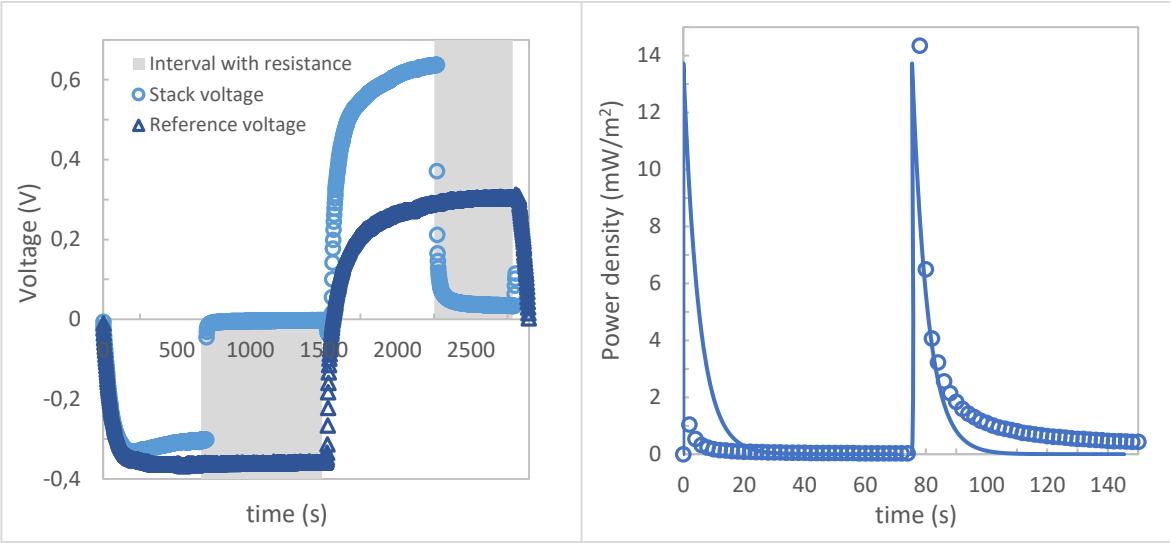

Figure 3.10. Results for 3 cells with spacer A) Voltage in the stack terminals and in the reference electrodes for the studied cycles. B) Power response of the stack after an external resistance perturbation for experimental (o) and model (—) results.

- **Results for stack with spacers and river and sea water.**

Figure 3.11 shows results for voltage in the stack terminals and in the reference electrodes. In these experiments voltage response was more stable. An improvement in voltage in the capacitors as well as in reference electrodes is noticed compared to the case without spacers.

An interesting thing should be noticed in this results, as well as in other results presented in literature [27]. Open circuit voltage in the capacitors is usually higher than voltage in the reference electrodes. The explanation for this open circuit voltage effect in the capacitors might be similar to CapMix effect, but it would be interesting to study deeper this phenomena.

From Figure 3.12 B it can be seen that in this case the peak power was almost double than the obtained in the previous case. However power declined drastically in less than 2 seconds.

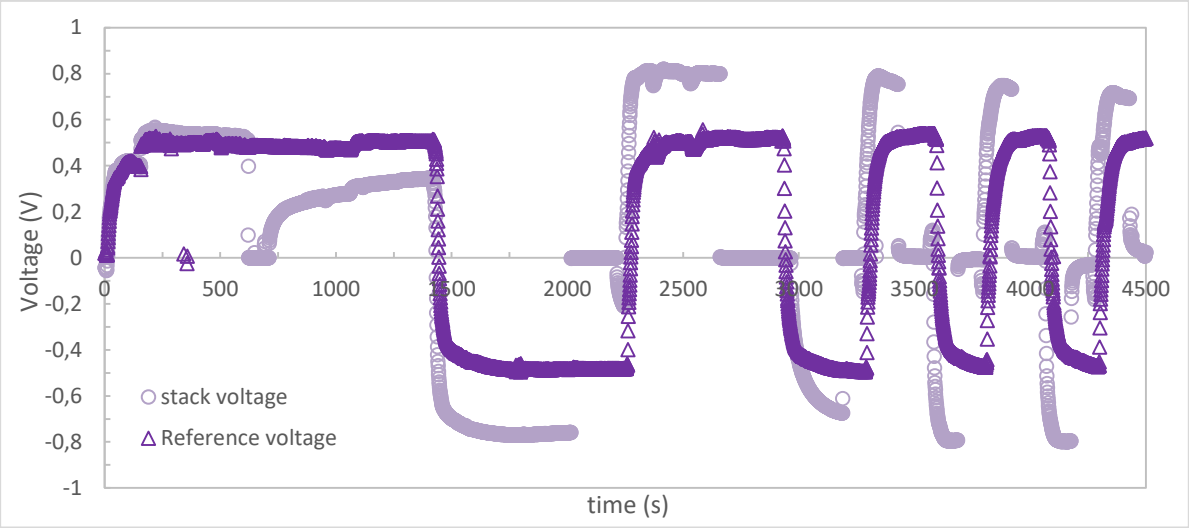

Figure 3.11. Obtained voltage from the stack in reference electrodes (▲) and stack terminals (○) in CRED with 3 cells with spacers with river and seawater.

From chapter two, it was found that power obtainable with river and sea water could be as good as using artificial NaCl solutions prepared in laboratory. In the previous chapter a proper current density sweep was not done with the equipment, and it was not possible to make a conclusion in the obtainable power density from river and sea water. In this chapter, due to the big variability of the results it is not possible to determine if peak power is a consequence of river and sea water, or if it was obtained because the stack had an overall better performance in this experiments than in the others.

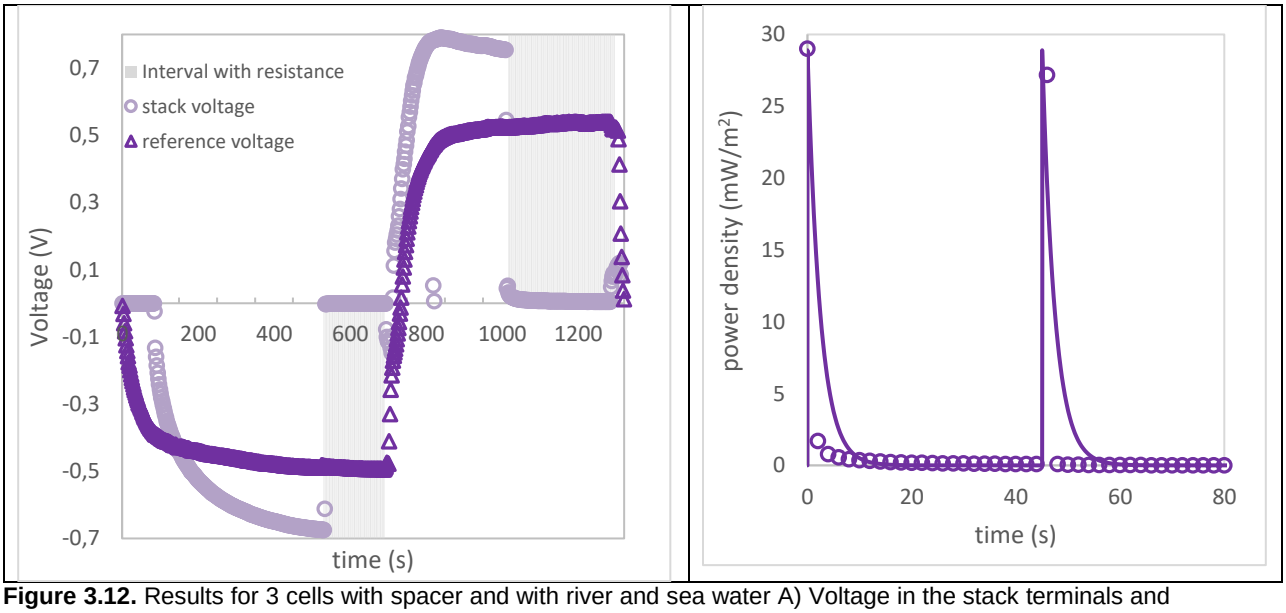

Figure 3.12. Results for 3 cells with spacer and with river and sea water A) Voltage in the stack terminals and in the reference electrodes for the studied cycles. B) Power response of the stack after an external resistance perturbation for experimental (○) and model (▬) results.

3.4.3 Optimization

With the aim to evaluate if it is possible to obtain more power density from a CRED system than a RED system, external resistance and capacitance were optimized for a period of 1200 seconds, where the last 200 seconds accounted for water interchange for CRED operation, and thus no power generation. The model was solved taking into account that voltage in the CRED system cannot exceed by more than 0.9 V the voltage obtained with the membranes in order to avoid reactions [27].

Maximum power is obtained when external resistance is equal to internal resistance, just as in RED process. It was found that in order to make CRED average power density marginally higher than RED (0.9580 W/m^2 for CRED 0.9518 W/m^2 for RED), it is necessary to have a capacitor with at least 55 F capacitance (Figure 3.13), which is easily achievable with current state of the art in capacitors fabrication [79]–[81]. Furthermore, the model revealed that a higher capacitance allows to decrease voltage drop in the capacitors in time, avoiding reactions in operation (Figure 3.14).

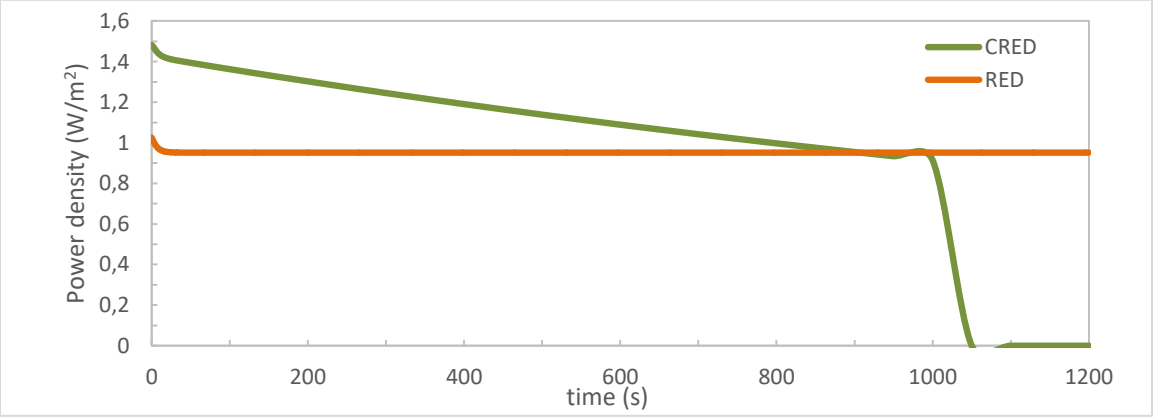

Figure 3.13. Results of optimization of CRED (green) and comparison with RED (orange) using the same parameters.

It is evident that higher capacitances will result in increased power generation. Optimization for CRED system was performed setting an upper limit of 200 F for the capacitance of the material. In this conditions a maximum average power of 1.153 W/m^2 can be generated with CRED, in contrast with 0.952 W/m^2 generated with RED in the same conditions, which is 21% more power density. Optimization of power density showed that in order to maximize power density with these parameters, switching interval should be every 1800 s (30 minutes) which is 11% of characteristic time constant of the system.

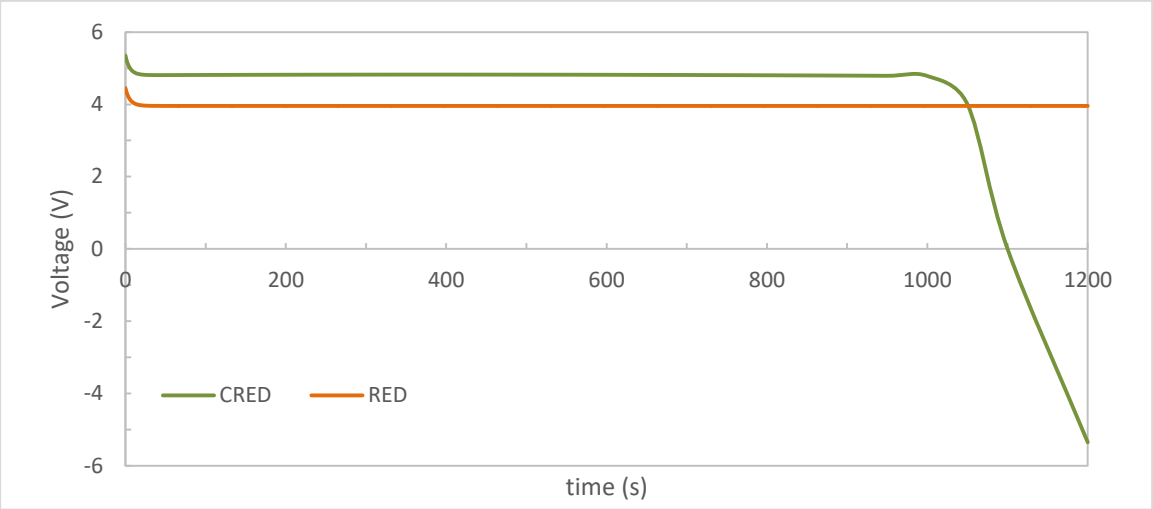

Figure 3.14. Voltage vs time curves for RED and CRED

Furthermore, 200 F is a very conservative value considering the latest studies, that have fabricated graphene based materials with capacitances up to 231 F/g and specific surface area of 3523 m^2/g [79]. With this values in improvement of 39% in power density is envisaged.

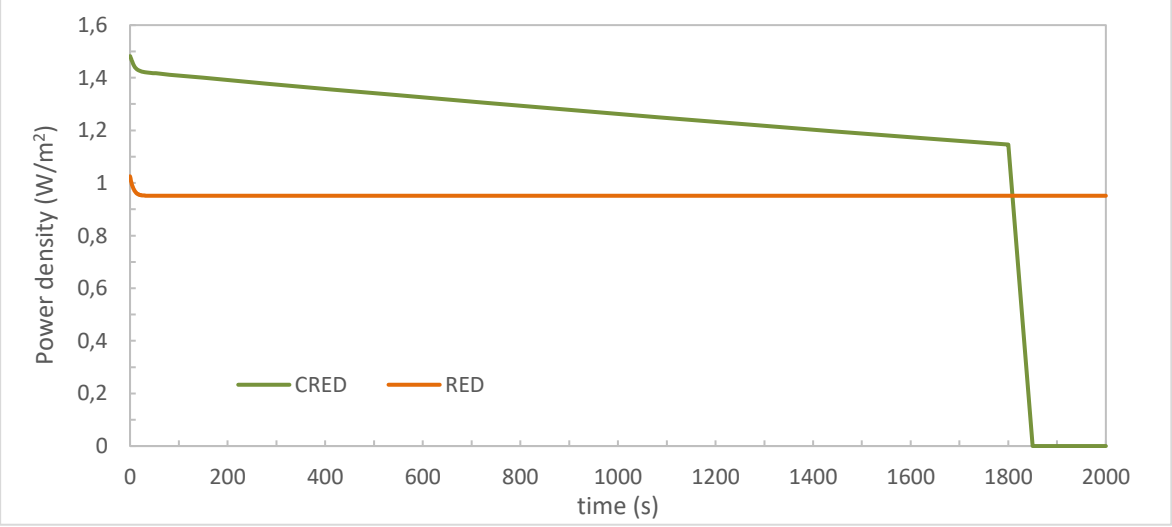

Figure 3.15. Results for CRED optimization and comparison with RED in the same conditions.

3.5 Conclusions

The experimental results show in general a greater internal resistance for CRED than for RED, attributed to the fact that the support of the capacitor did not have good mechanical stability. Thus it was not possible to make good contact between stack copper terminals and capacitors, because if a lot of pressure was done, the capacitors would break.

It was found good agreement between the model and experimental results, which confirms this model can be used to predict the behavior of CRED stacks. The dynamical model was used as a tool for optimizing CRED operation. It was found that it is possible to increase power density of CRED over RED up to 39% using the most advanced supercapacitors, and changing the feed waters at 11% of the characteristic time constant (RC) of the capacitor. Thus, the best RED systems that have shown a maximum power density of 2.7 W/m^2 could increase up to 3.7 W/m^2 the produced power density. This is a step forward towards the implementation of salinity gradient power in real field conditions.

3.5.1 Recommendations

For studying CRED it is necessary to register as continuously as possible the current and voltage responses to the external resistance, because due to its very fast dynamic behavior, a lot of information is probably lost during 2 seconds.

It is very important to find a different material for supporting the capacitors with good mechanical stability. For example, graphite has better mechanical stability and electrical conductivity than the material used for this research. It is possible to think in using a graphite terminal and to support the capacitor directly into this material in order to avoid bad contacts between capacitors and terminals.

Finally it is important to find better methodologies and materials (*e.g.* graphene) for the fabrication of the capacitor in order to increase the capacitance of the material. Another way to improve performance of CRED is to enlarge the area of the capacitor, which allows to extend the characteristic time for capacitor discharge.

It is important to refine the theoretical model and to take into account the time necessary to charge the capacitor again, after the water streams exchange.

3.5.2 Outlook

Although it was found that power generation could be greatly increased using supercapacitors, this number could be much higher if non aqueous electrolytes are used. The advantage of this kind of electrolytes is that they are stable in a wider voltage window, nonetheless they can be very toxic to the environment, and thus this alternative should be considered with great care. Moreover, It is possible to think in hybrid combinations of capacitors and electrodes in order to increase migration current, and possibly increasing overall power density obtainable with salinity gradient energy [59].

The dynamical model could be used as a tool for optimizing and for designing control of CRED systems. It is important to include mesoscale models in order to have a deeper understanding of the phenomena occurring in the supercapacitor, because until now the mesoscale models apply for CapMix, where the change in the thickness of the double layer is due to a decrease in ionic concentration in the solution, while in CRED, the phenomena is similar, but is definitely not the same, as there are no changes in the concentration of the solutions that are in contact with the capacitors.

4. Equilibrium in Ion Exchange Membranes

4.1 Introduction

One of the biggest challenges for the development of new membrane processes, is to work in real field conditions, where the water supplied contains multiple monovalent and bivalent ions. Actually, the presence of multivalent ions in feed waters for different electro-membrane processes (like ED, RED), has been a subject of study for several years [82].

In the context of energy generation through salinity gradients, it has been proven that in the presence of Mg^{2+}, there is both a decrease in power density for RED [32, 34, 42] as well as increase in membrane resistance [33, 34]. Deposition of solid salts in the membrane surface or membrane channels, also known as scaling, has been reported to occur in the presence of magnesium, calcium, barium, sulphate and bicarbonate ions for basic and neutral pH [43, 44]. Moreover, in the presence of multivalent ions an irreversible loss of the available energy is encountered due to decrease in open circuit voltage (compared to solutions containing only NaCl), and a transport of divalent ions against the concentration gradient is found, called uphill transport [34, 45].

Ion exchange equilibrium between a salt solution and an ion exchange membrane is reached whenever a membrane is placed in contact with an electrolyte solution, which likely contain counter-ions different from that in the membrane. In case of salt mixtures, all ions that are present in solution will be involved in the sorption equilibrium, according to their specific interaction with the membrane matrix. It has been reported that under equilibrium conditions (no electrical current), the affinity of divalent cations with CEMs is larger than for monovalent cations, due to higher electrostatic attraction of divalent ions with the fixed ion exchange sites in the membrane [86].

In general it is possible to asseverate that there exists a link between equilibrium parameters and transport processes. Specifically for ion exchange through membranes, it has been found that the equilibrium ratio between mobile ion concentration in a charged

membrane and its concentration in the adjoining electrolyte solution, also known as partition coefficient, strongly influences transport properties of membranes for applications like ED or RED. For instance, the steady state permeability coefficient is related to equilibrium sorption coefficient and the effective concentration averaged diffusion coefficient of solute in the polymer (Eq. 4.1) [87], [88].

$$P_i = K_i D_i \tag{4.1}$$

Where P_i is the steady-state permeability coefficient of solute *i* in the membrane, K_i is the equilibrium sorption or partition coefficient of solute *i* between external phase and membrane phase and D_i is the effective concentration averaged diffusion coefficient of solute in the polymer.

Thus, considering the foregoing, understanding experimentally and theoretically ion equilibrium in IEMs in the presence of multivalent ions, is crucial for a detailed description of the performance of any membrane process.

In the framework of theoretical advances, a number of modeling works have been focused on the description of ion equilibrium in IEMs [82], [87], [89], [90] . For instance, a common modeling approach is based on the definition of partition coefficients, in order to calculate concentration of ions in the membrane phase, where the ion partition coefficient is related to bulk concentration, to the concentration ratio of fixed charge groups in the membrane to bulk solution, as well as to the fixed charge sign and the valence [82].

Recently, Kamcev et al studied the equilibrium partitioning of ions and modeled ion sorption in the presence of NaCl, $MgCl_2$ and $CaCl_2$ using Donnan theory coupled with Manning's counter ion condensation theory to describe non ideal behavior of ions in the membranes [87]. According to Kamcev et al the assumption that activity coefficients inside the membrane are equal to those outside the membrane does not accurately describe real conditions inside the membrane, due to the fact that high fixed charge concentration density may result in non-ideal behavior of the ions. Thus he proposes a thermodynamic model where activity inside the membrane is calculated using Maning's counter ion condensation theory. He proves the model shows good agreement with experimental results with no adjustable parameters.

Another modeling approach has been proposed by Galama et al., who described the Donnan equilibrium by means of Boltzmann equation for NaCl solutions in the range of 0.01 – 3 M NaCl.

The aim of this work is to describe equilibrium in IEMs in the presence of multivalent ions by using the Boltzman equation, as previously demonstrated by Galama et al [89] for NaCl. Four different types of membranes have been tested with ion sorption experiments using different salt solutions, such as mixtures of NaCl with $MgCl_2$, $CaCl_2$ or Na_2SO_4 in different proportions maintaining total normality of the solution constant in 0.5 N. Mixture of more than two salts where also performed simulating the conditions of real sea water keeping constant the total normality of the solutions. Results show that higher counter ion concentration in solution leads to a major decrease in monovalent ion sorption inside the membrane.

4.2 Theoretical model

In ion exchange membranes (IEMs), counter ions have a higher concentration relative to the external solution outside the membrane, while the co-ion concentration is lower. Assuming electroneutrality is fulfilled inside the membrane, concentration of counter ions should be larger than X by the concentration of the co-ions, where X is the membrane charge density, defined as the number of fixed charges per unit aqueous volume phase [89]. Because of the ion transport through membranes, co-ion and counter ion concentration gradually change across the membrane thickness, and the concentration profiles for both counter ion and co ion can be obtained in line with the electroneutrality condition, as schematically depicted in Figure 4.1.

The Boltzmann relationship between ion concentrations in the membrane with external concentration is

$$c_{i,M} = c_{i,\infty} \exp(-z_i \, \Delta\varphi_D) \tag{4.2}$$

Where $c_{i,M}$ is the ion concentration inside the membrane (subscript M), $c_{i,\infty}$ represents ion concentration in the bulk solution (subscript ∞), z_i is the valence of the ion and $\Delta\varphi_D = \varphi^M - \varphi^\infty$ is the Donnan potential, defined as the difference between potential inside φ^M and outside φ^∞ the membrane.

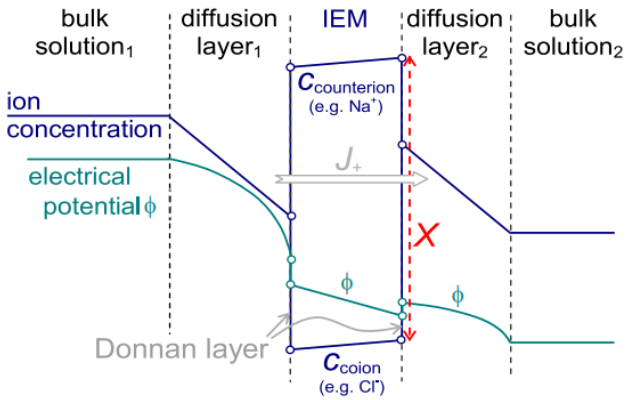

Figure 4.1. Schematic view of profiles of ion concentration and electrical potential in ion exchange membranes. The difference between counter ion and co-ion concentration is the membrane charge density X. Taken from [89]

The electroneutrality condition in the membrane is described by

$$X + c_{coion} = c_{counteion} \tag{4.3}$$

Where X is the membrane charge, c_{coion} is the concentration of coions in the membrane and $c_{counteion}$ is the concentration of counterions in the membrane.

From Eq.4.1 and Eq. 4.2, together with electroneutrality, Eq. 4.4 is obtained

$$X = v_{coion} c_{\infty} [\, \exp(-z_{counterion} f \Delta\varphi_D) - \exp(-z_{coion} f \Delta\varphi_D) \,] \tag{4.4}$$

Where v_{coion} is the number of dissociated co ions, z is the charge of the ion and f is the faraday constant.

For symmetrical electrolytes Eq. 4.4 may be reduced to

$$z_{coion} f \Delta\varphi_D = sinh^{-1}\left(\frac{X}{2C_{\infty}}\right) = \ln\left\{\frac{X}{2C_{\infty}} + \sqrt{\left(\frac{X}{2C_{\infty}}\right)^2 + 1}\right\} \tag{4.5}$$

Together with Eq. 4.1 and Eq. 4.2

$$c_{salt}{}^{M} = -\frac{X}{2} + \sqrt{\left(\frac{X}{2}\right)^2 + (c_{\infty})^2} \tag{4.6}$$

Where ${c_{salt}}^{M}$ is the free salt concentration in the membrane. As co ion concentration in the membrane is equal to ${c_{salt}}^{M}$, then the expression for salt concentration in the membrane is the same as the co-ion concentration in the membrane. Finally, applying electroneutrality principle we get an expression for the counter ion concentration in the membrane

$$c_{counterion} = \frac{X}{2} + \sqrt{\left(\frac{X}{2}\right)^2 + (c_\infty)^2} \tag{4.7}$$

Combining Eq. 4.5 and Eq. 4.6 we obtain

$$c_{counteion} + c_{co-ion} = \sqrt{X^2 + (2 * {c_\infty}^2)} \tag{4.8}$$

In the case of salt mixtures and nonsymmetrical electrolytes, Eq. 4.3 to Eq. 4.8 are no longer valid, thus it is necessary to reformulate the problem.

Let's consider an ion exchange membrane with fixed-charge groups $-R^z$. Initially the membrane has counter ions A^{z1}. After the membrane is put in contact with two different salts: salt 1 $A_{v1}^{z1}C_{v3}^{z3}$ and salt 2 $D_{v2}^{z2}C_{v3}^{z3}$. The ion exchange process can be described by the following formalism [91]

$$v_1 A^{z1}(M) + v_2 D^{z2}(\infty) \leftrightarrow v_2 D^{z2}(M) + v_1 A^{z1}(\infty)$$

Where M and ∞ refer to the membrane and the bulk solution phase, respectively, v is the number of dissociated ions, and z is the charge of the corresponding ion. The stoichiometric relation $v_1 z_1 = v_2 z_2$ must be satisfied. The thermodynamic equilibrium condition is represented by the mass action law [91], [92]

$$K_{12} = \frac{(c_1^\infty)^{v1}(c_2^M)^{v2}}{(c_1^M)^{v1}(c_2^\infty)^{v2}} \tag{4.9}$$

Where K_{12} is the ion exchange equilibrium constant, which can be expressed in terms of the ionic chemical partition coefficient as [14]

$$K_{12} = {K_{c,1}}^{-v_1} * {K_{c,2}}^{v_2} \tag{4.10}$$

Where $K_{c,i}$ is the ionic partition corfficient defined as $K_{c,i} = e^{-(\mu_i^{o,M} - \mu_i^{o,\infty})/RT}$ [14]. Likewise, similar expressions can be derived for K_{13} and K_{23}

$$K_{13} = \frac{(c_1^M)^{v_1}(c_3^M)^{v_3}}{(c_1^\infty)^{v_1}(c_3^\infty)^{v_3}} \tag{4.11}$$

$$K_{23} = \frac{(c_2^M)^{v_2}(c_3^M)^{v_3}}{(c_2^\infty)^{v_2}(c_3^\infty)^{v_3}} \tag{4.12}$$

Again K_{13} and K_{23} are ion exchange equilibrium constants for ions *i*=1, 2, and ions *i*=1, 3. Subscripts 2 and 3 in v correspond to the number of dissociated ions (ion I=1, 3) exchanged in the process. Combining equations 4.10 to 4.12 with electroneutrality condition for 2 counter ions and 1 co ion (Eq. 4.13).

$$X = c_1^M + c_2^M - c_3^M \tag{4.13}$$

We obtain expressions for concentrations of co ions and counter ions inside the membrane that depend on ion exchange equilibrium constants, concentrations in the external solution and stoichiometric coefficients.

$$X = \sqrt[v1]{\frac{K_{13}(c_1^\infty)^{v1}(c_3^\infty)^{v3}}{(c_3^M)^{v3}}} + \sqrt[v2]{\frac{K_{23}(c_2^\infty)^{v2}(c_3^\infty)^{v3}}{(c_3^M)^{v3}}} - c_3^M \tag{4.14}$$

$$X = \sqrt[v1]{\frac{(c_1^\infty)^{v1}(c_2^M)^{v2}}{K_{12}(c_2^\infty)^{v2}}} + c_2^M - \sqrt[v3]{\frac{K_{23}(c_2^\infty)^{v2}(c_3^\infty)^{v3}}{(c_2^M)^{v2}}} \tag{4.15}$$

$$X = c_1^M + \sqrt[v2]{\frac{K_{12}(c_1^M)^{v1}(c_2^\infty)^{v2}}{(c_1^\infty)^{v1}}} - \sqrt[v3]{\frac{K_{13}(c_1^\infty)^{v1}(c_3^\infty)^{v3}}{(c_1^M)^{v1}}} \tag{4.16}$$

This theory may be extended for more than 3 ions present in solution, defining one dissociation constant for each salt and solving the electroneutrality condition in the presence of more ions.

4.3 Experimental conditions

In the experiments, co-ion and counter ion concentrations in IEMs are measured as function of external salt concentration in a soak solution with external concentration C_∞. Two types of anion and cation exchange membranes were tested (AMX and CMX from Neosepta Tokuyama Soda Inc., Japan. And Fujifilms Manufacturing Europe BV, The Netherlands), and Table 1 shows the properties of the membranes used in the experiments. The

experimental procedure reported by Galama et al [89] has been adopted in this work, and it will be described in the following sections.

Table 4-1. Properties of Neosepta membranes provided by the manufacturer

	Neosepta		Fujifilms	
	CMX	AMX	CEM	AEM
Type	Strong Acid (Na Type)	Strong Base (Cl Type)	Homogeneous Type -1	Homogeneous Type -1
Electric Resistance (Ω cm²)	3	2.4	2.7	1.3
Thickness (mm)	0.17	0.15	0.13	0.14
pH range	0 – 10	0 – 8	4 - 12	2 - 10
Theoretical fixed charge concentration (M)[a]	5.7	4.8	3.5	3.8

[a]*Values taken from* [89], [93]

4.3.1 Pretreatment

Before cutting, membrane pieces of approximately 100 cm^2 are stored in 0.5 M NaCl solution for at least 48 hours to make sure Na^+ and Cl^- replace any other ions that may be present in the material as obtained from the manufacturer.

The membrane samples were afterwards washed and stored in deionized water for 2 days, replacing water twice per day in order to ensure equilibrium with the medium. Membranes were cut in pieces of approximately 18 cm^2. A scheme of the pretreatment procedure is shown in Figure 4.2

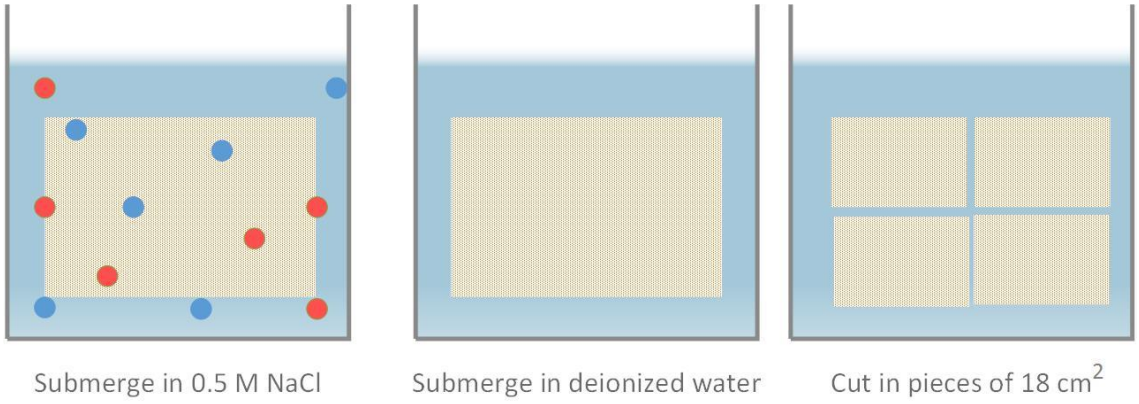

Figure 4.2. Pretreatment of membranes prior to cutting.

4.3.2 Soak

Membrane samples were equilibrated for at least 24 h in 200 mL of salt solutions with a salt concentration C_∞ in the range of 0.01 – 0.5 M, according to the salt solutions used during specific tests. During this period, the beaker was sealed with Para film to prevent water evaporation and contamination.

In order to understand equilibrium sorption, mixtures of salts listed in Table 4-2. **Experimental conditions for salts mixtures.** with total concentration of 0.5 N have been tested with each membrane. Solutions where designed in such a way as to gradually decrease NaCl concentration from solution 1 (which contains only NaCl 0.5 M), to the last solution, that does not contain NaCl at all.

Table 4-2. Experimental conditions for salts mixtures.

Salt Mixture	**NaCl - $MgCl_2$**			**NaCl - $CaCl_2$**			**NaCl - Na_2SO_4**		
	NaCl (M)	$MgCl_2$ (M)	$\frac{MgCl2}{NaCl}$	NaCl (M)	$CaCl_2$ (M)	$\frac{CaCl2}{NaCl}$	NaCl (M)	Na_2SO_4 (M)	$\frac{Na_2SO_4}{NaCl}$
Solution 1	0.5		0	0.5		0	0.5		0
Solution 2	0,438	0,031	0,071	0,469	0,0155	0,033	0,467	0,0165	0,035
Solution 3	0,385	0,057	0,149	0,479	0,0105	0,022	0,439	0,0305	0,069
Solution 4	0,250	0,125	0,500	0,35	0,075	0,214	0,25	0,125	0,500
Solution 5	0,150	0,175	1,167	0,25	0,125	0,500	0,15	0,175	1,167
Solution 6	0,050	0,225	4,500	0,15	0,175	1,167	0,05	0,225	4,500
Solution 7		0.250	∞	0,05	0,225	4,500		0,25	∞
Solution 8					0.25	∞			

All solutions were prepared with a total concentration of 500 mN.

Finally, in order to understand the membrane behavior under real conditions, 3 mixtures of artificial seawater were tested. Artificial seawater recipe was chosen taking into account the typical ion compositions of real seawater, considering only ions with concentration higher than 1 mg / L. Three different recipes were taken into account, mimicking ion composition of real seawater in different geographical areas: Wadden Sea, Mediterranean Sea and Caribbean Sea. Table 4-3 shows composition of artificial seawater used in the experiments.

Table 4-3. Ion composition artificial seawater.

Artificial sea water Mixture NaCl - $MgCl_2$ - Na_2SO_4 -$CaCl_2$	**Concentration (M)**				**Total Conc (M)**
	NaCl	**$MgCl_2$**	**Na_2SO_4**	**$CaCl_2$**	
Wadden	0.374	0.031	0.017	0.016	0.437
Mediterranean	0,303	0,058	0,031	0,011	0.676
Caribbean	0,313	0,054	0,028	0,012	0.407

All solutions were prepared with a total concentration of 500 mN.

4.3.3 Exchange

In order to quantify counter-ion concentration, membrane samples were transferred from the soak solution to a beaker containing $MgSO_4$ exchange solution (for all the tests performed with NaCl, $CaCl_2$) or K_2CO_3 (for tests with $MgCl_2$, Na_2SO_4), ensuring that the "exchange" solution did not contain the ions present in the membrane. Before membranes were placed in exchange solution, the membrane sample was rapidly rinsed (for only 2 seconds) in a beaker with 200 mL deionized water, allowing salt solution present on the external surface of the membrane to be washed off. This procedure is done because external salt does not account as membrane adsorption.

After placing the membrane sample into the exchange solution (200 mL, 50 mM $MgSO_4$, or 50 mM K_2CO_3, according to the test performed), the beaker was again sealed and stored for at least 24 h to reach equilibrium. Afterwards, samples were taken from the exchange solution and ion concentration was measured. Figure 4.3 depicts the procedure followed in the experiments.

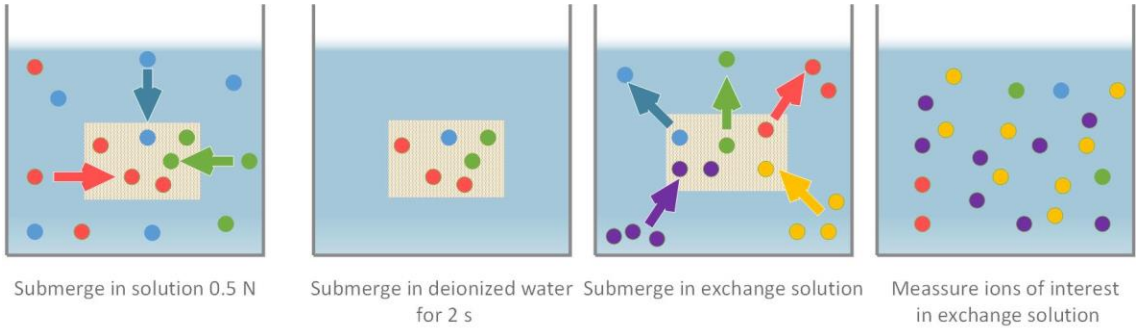

Figure 4.3. Schematic view of experimental procedure to determine membrane ion concentration.

4.3.4 Measurements

For all the investigated cations (Na^+, Mg^{++} and Ca^{++}), ion composition was measured through atomic absorption spectroscopy (AAS) with an AA300 Perkin Elmer. For Cl^- , the measuring technique used was potentiometric, using an Orion Dual Star thermoscientific potentiometer with Ion Selective Electrode (ISE) for Cl^- Methron. Finally, sulphate content was measured by turbidimetry with a Perkin Elmer UV-VIS lambda 45.

Membrane concentrations were calculated as the number of ions per litter water phase inside the membrane. In order to calculate this parameter membranes were soaked in a 0.5 M solution of NaCl for 24 hours, and wet membrane weight was measured right after taking the membranes out of the solution and removing excess water with filter paper. Afterwards membranes were dried in an oven for 24 hours at 105 ºC, after which they were put in an exciscator for 1 hour and weighted again. Volume water phase inside the membrane was calculated as the difference between membranes wet weight and dry weitght.

4.4 Results and discussion

This section shows the experimental results found during ion sorption tests on 4 different membranes: CMX, AMX (from Neosepta Tokuyama Soda Inc., Japan), CEM and AEM (from Fujifilms Manufacturing Europe BV, The Netherlands). Initially experiments were carried out using only NaCl. Subsequently, experiments with mixtures of two salts (NaCl - $MgCl_2$, NaCl - $CaCl_2$ and NaCl - Na_2SO_4) were performed. Finally, mixtures of 5 ions mimicking real seawater from 3 different geographical areas were investigated.

4.4.1 Ion sorption with Sodium Chloride

In this section, results of ion sorption tests for NaCl are presented. Experiments with Sodium chloride were performed in order to ensure the results by Galama et al [89] could be replicated using Absorption Spectroscopy as measuring technique.

Figure 4.4. **Concentration of co ions and counter ions in: CMX (a), AMX (b), Fuji CEM (c), Fuji AEM (d) as function of NaCl concentration in external solution. ◊ represents Cl and ○ is Na.**Shows concentration of co-ions and counter-ions inside CMX, AMX, Fuji CEM and Fuji AEM membranes as function of external NaCl concentration. Parameters for the theoretical calculation where fixed charged concentration and volume of aqueous solution in the membrane as 0.09 mL [89].

Small differences in the results, may be related to small differences in the size of the membrane pieces, due to the fact that membranes were cut by hand. Moreover, from Figure 4.4a it can be noticed that the technique used for measuring Cl^- ions (potentiometric with ISE) presents more variability than the analysis method for Na^+ (AAS).

From figures 4.4a and 4.4b it is also possible to see that the membrane charge of CMX and AMX membranes experimentally obtained (X=5.5 M for CMX and X=4.7 M for AMX) is slightly lower than the theoretical value given in table 1, which was the one assumed for the model calculations. This is not surprising, as membrane features may change from one membrane to another. Notwithstanding the differences previously mentioned, results were comparable with those obtained by Galama et al [89] and AAS was taken as a valid technique to continue the investigation.

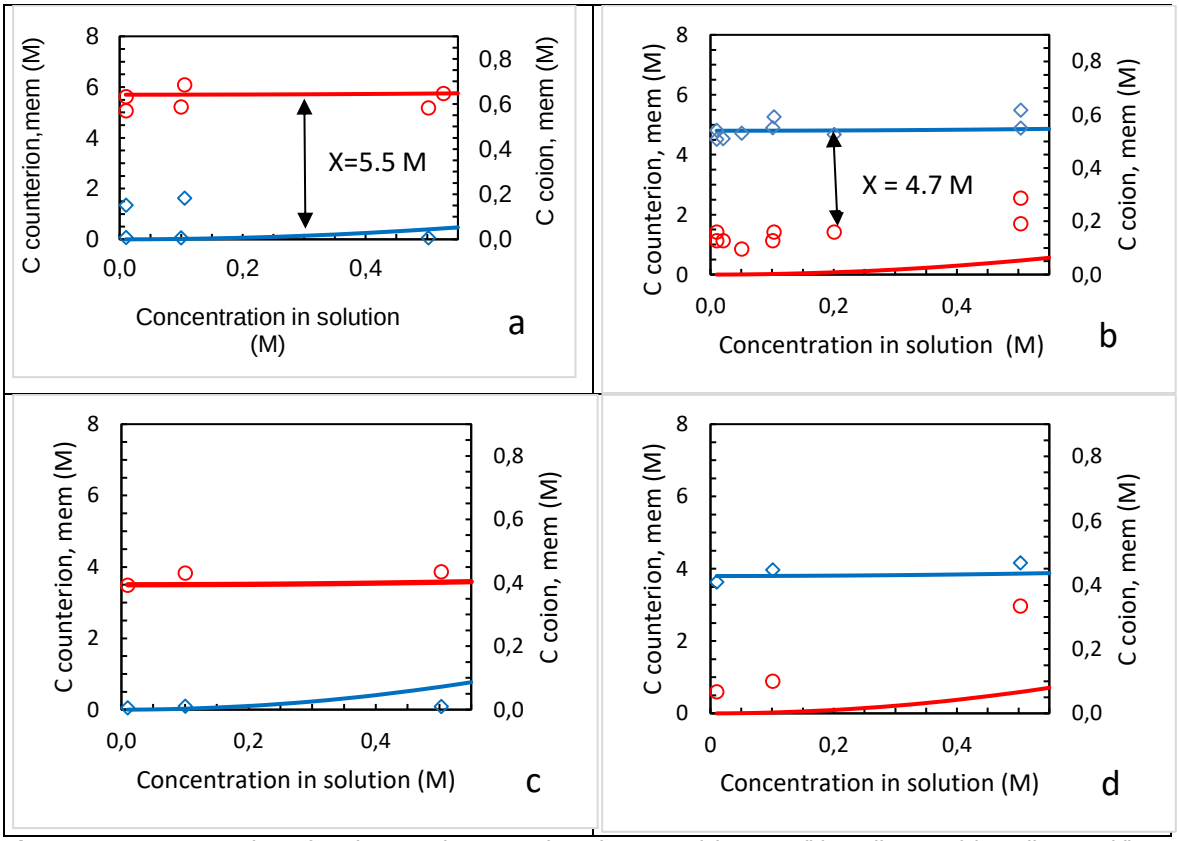

Figure 4.4. Concentration of co ions and counter ions in: CMX (a), AMX (b), Fuji CEM (c), Fuji AEM (d) as function of NaCl concentration in external solution. ◊ represents Cl and ○ is Na.

Following the procedure by Galama et al [89], a correction of the results was made, bearing in mind that water uptake in the membrane may change, depending on the external solution ion concentration. Figure 4.5. **Concentration of co ions and counter ions in: a) CMX, b),**

AMX, c) Fuji CEM, d) Fuji AEM as function of NaCl concentration in external solution and corrected for water content in the membrane. ◊ represents Cl and ○ is Na. Is the correction of Figure 4.4. **Concentration of co ions and counter ions in: CMX (a), AMX (b), Fuji CEM (c), Fuji AEM (d) as function of NaCl concentration in external solution. ◊ represents Cl and ○ is Na.**Taking into account the aforementioned.

According to Figure 4.5. **Concentration of co ions and counter ions in: a) CMX, b), AMX, c) Fuji CEM, d) Fuji AEM as function of NaCl concentration in external solution and corrected for water content in the membrane. ◊ represents Cl and ○ is Na.**water uptake dependence on external concentration does not seem to improve the experimental results, on the contrary experiments draw further away from theoretical calculations.

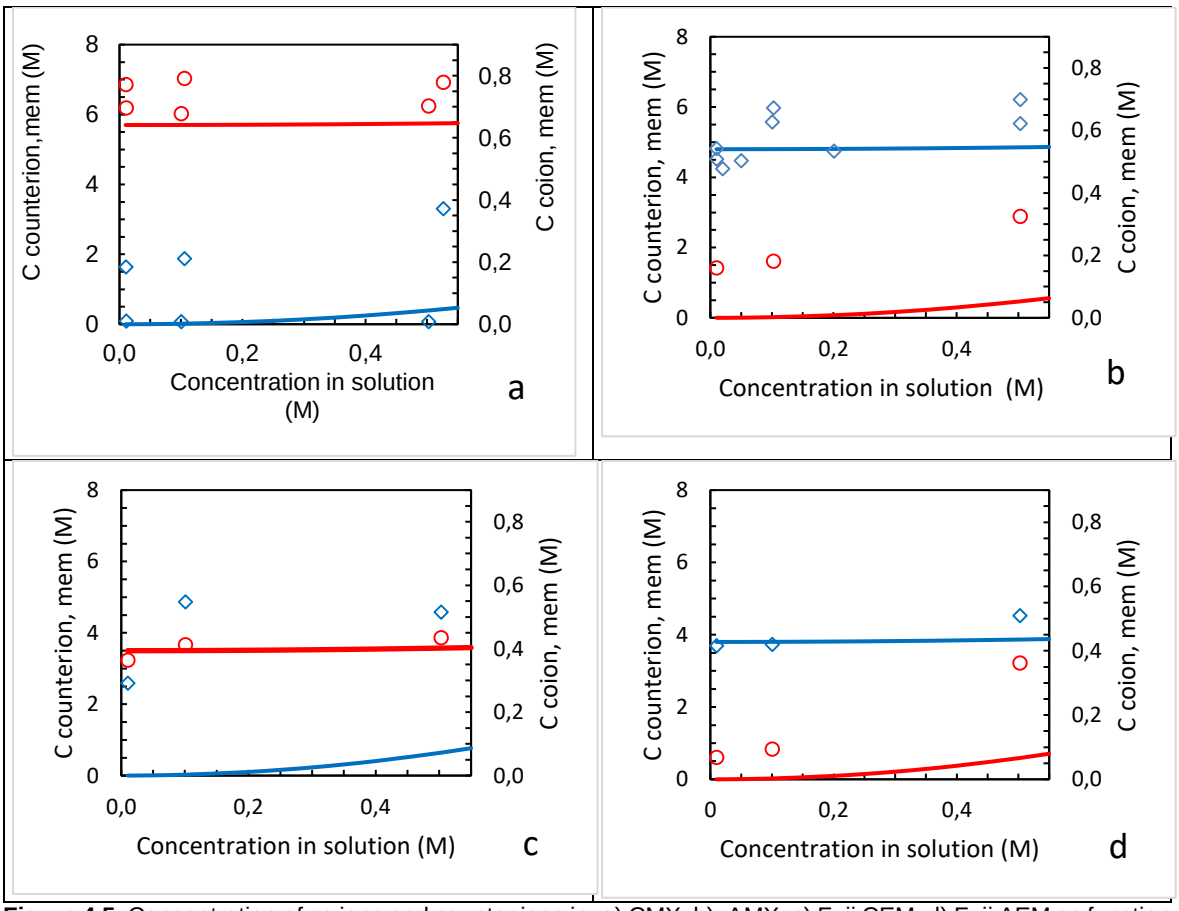

Figure 4.5. Concentration of co ions and counter ions in: a) CMX, b), AMX, c) Fuji CEM, d) Fuji AEM as function of NaCl concentration in external solution and corrected for water content in the membrane. ◊ represents Cl and ○ is Na.

4.4.2 Effect of Sulphate ions

In order to investigate the effect of sulphate ions, ion sorption tests on CMX, AMX, Fujifilm CEM and AEM, were carried out using mixtures of NaCl and Na_2SO_4. Figure 4.6 to Figure 4.9 summarize the results obtained for each of the membranes.

Figure 4.6. **Ion concentration (M) in AMX membrane as function of external ion concentration (M) for NaCl and Na_2SO_4. a) Concentration of Co ions and counter ions, b) Concentration of co ions in membrane as function of external concentration, c) concentration of Counter ion Cl^- in membrane as function of external solution, d) concentration of bivalent counter ion SO_4^{-2} in membrane as function of external concentration.**Shows results for AMX membranes with mixture of NaCl and Na_2SO_4. Subfigure 4.6a compresses the results of ions concentration inside the membrane for AMX membrane. Subfigure 4.6b presents results for the coion (Na^+), subfigure 4.6c shows the findings obtained for counter ion Cl^-, and finally subfigure 4.6d displays results for the second counter ion, SO_4^2. Darker colors represent solution 2 and lighter colors represent solution 3.

From figures 4.6 to 4.10 it is possible to notice that in most cases unrealistic values were obtained for SO_4^{2-} composition by turbidimetry. Many repetitions of the tests were done, in order to find a consistent result, however in each replication of the measurement, a different outcome would appear. For this reason, Ion Chromatography (IC) measurements will be performed at Wetsus to investigate the sulphate content.

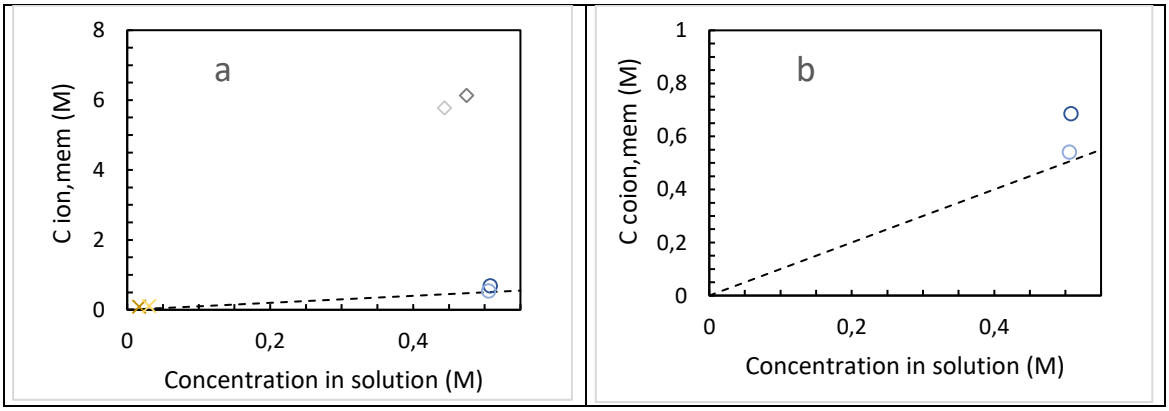

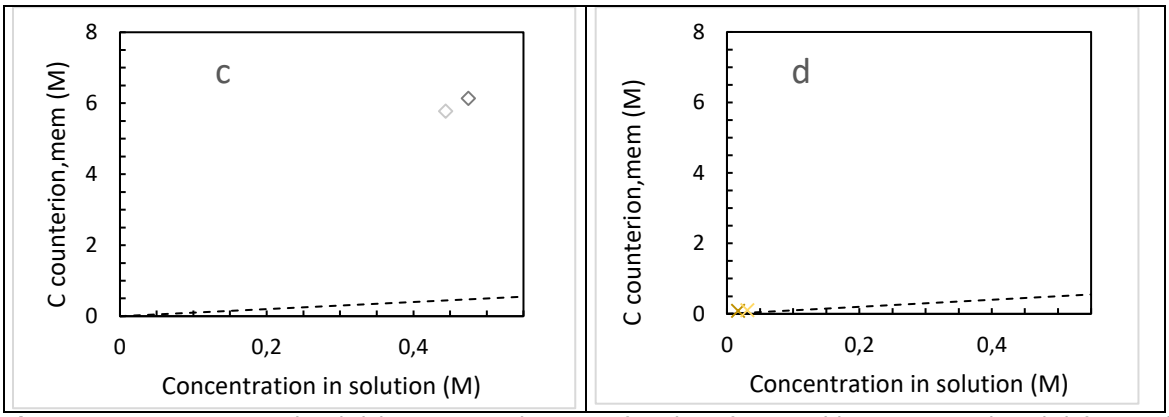

Figure 4.6. Ion concentration (M) in AMX membrane as function of external ion concentration (M) for NaCl and Na_2SO_4. a) Concentration of Co ions and counter ions, b) Concentration of co ions in membrane as function of external concentration, c) concentration of Counter ion Cl^- in membrane as function of external solution, d) concentration of bivalent counter ion SO_4^{-2} in membrane as function of external concentration.

Figure 4.7 shows results for Fujifilm AEM with mixture of NaCl and Na_2SO_4. For AMX as well as for Fuji AEM membranes, results for SO_4 seem to be extremely different from the foreseeable values. Due to the fact that $SO4^{-2}$ is a counter ion in AEMs, the experimental results for ion concentration inside the membrane of this counter ion are expected to be at least higher than the coion concentration inside the membrane.

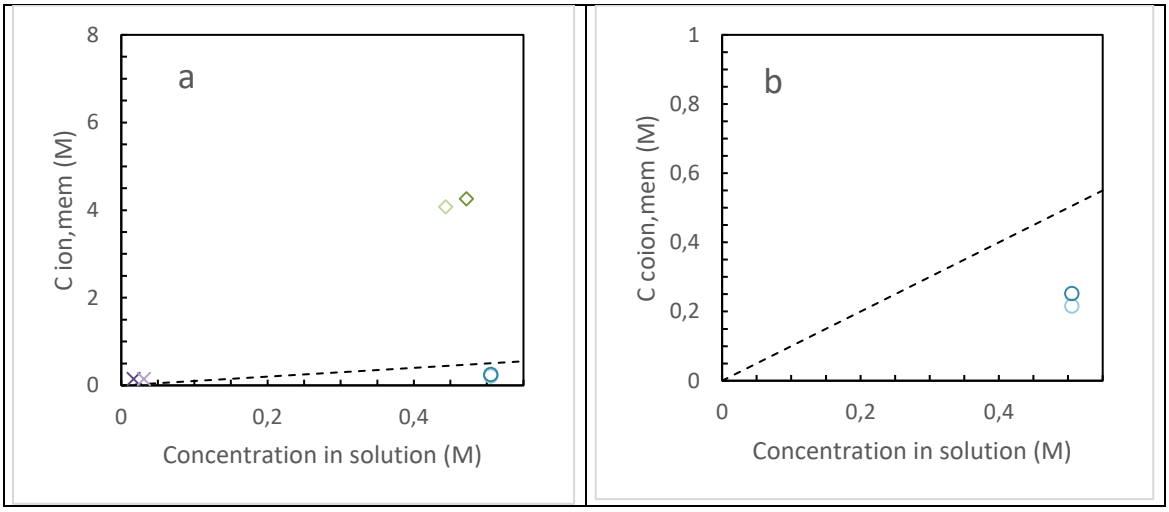

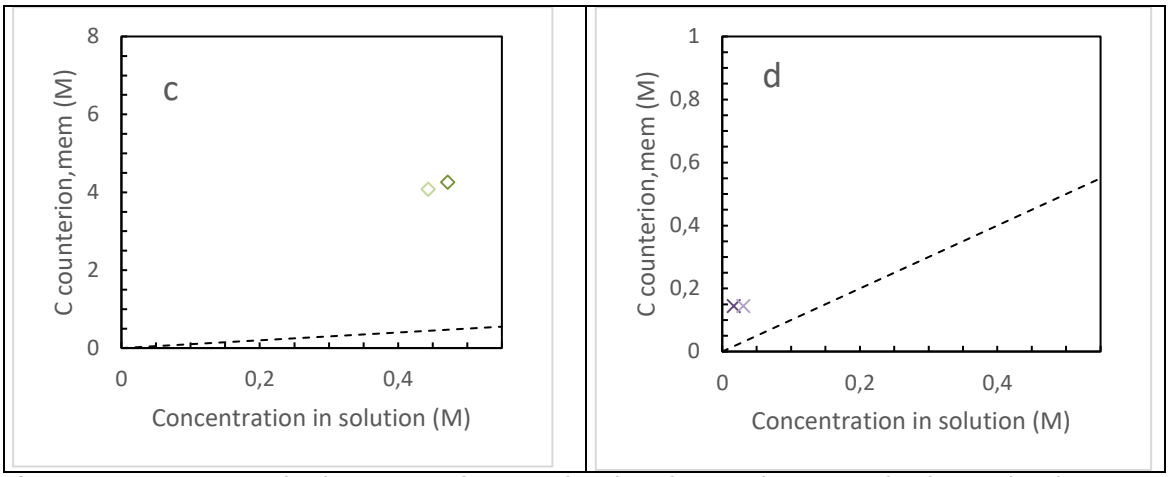

Figure 4.7. Ion concentration in AEM membrane as function of external concentration for NaCl and Na_2SO_4. .. a) Concentration of Co ions and counter ions, b) Concentration of co ion Na^+ in membrane as function of external concentration, c) concentration of Counter ion Cl in membrane as function of external solution, d) concentration of bivalent counter ion SO_4^{-2} in membrane as function of external concentration.

Figure 4.8 shows results for CMX membranes with mixture of NaCl and Na_2SO_4

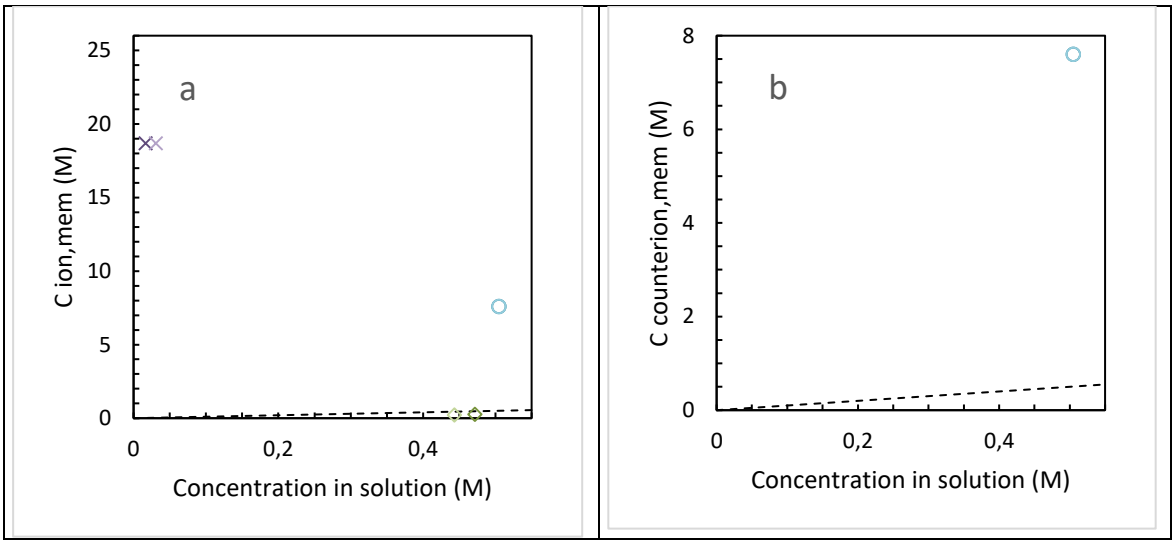

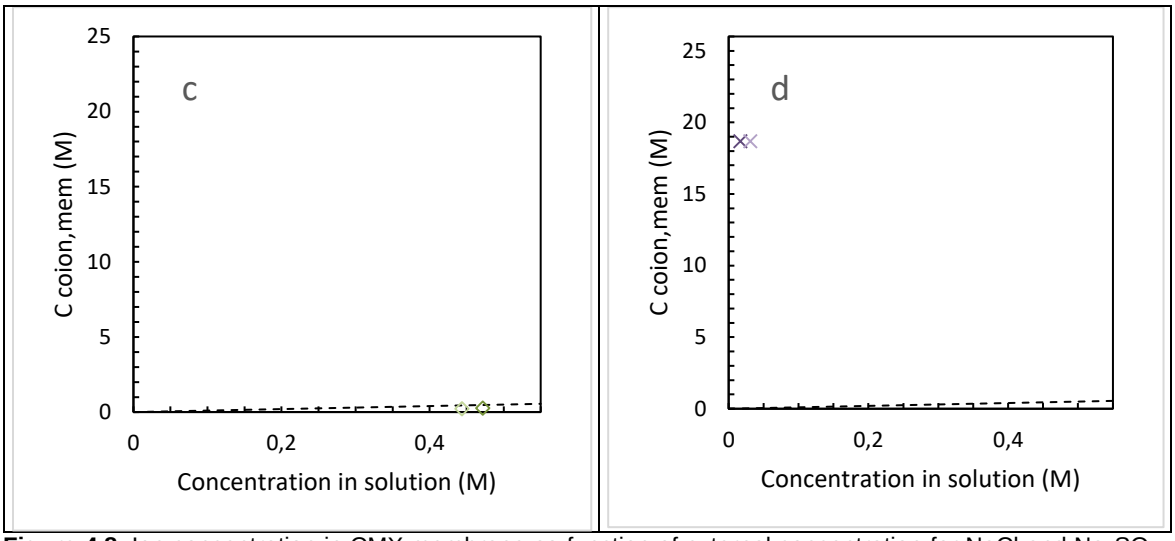

Figure 4.8. Ion concentration in CMX membrane as function of external concentration for NaCl and Na_2SO_4... a) Concentration of Co ions and counter ions, b) Concentration of counter ions in membrane as function of external concentration, c) concentration of co ion Cl^- in membrane as function of external solution, d) concentration of bivalent co ion SO_4^{-2} in membrane as function of external concentration.

Figure 4.9 shows results for CEM membranes with mixtures of NaCl and Na_2SO_4.

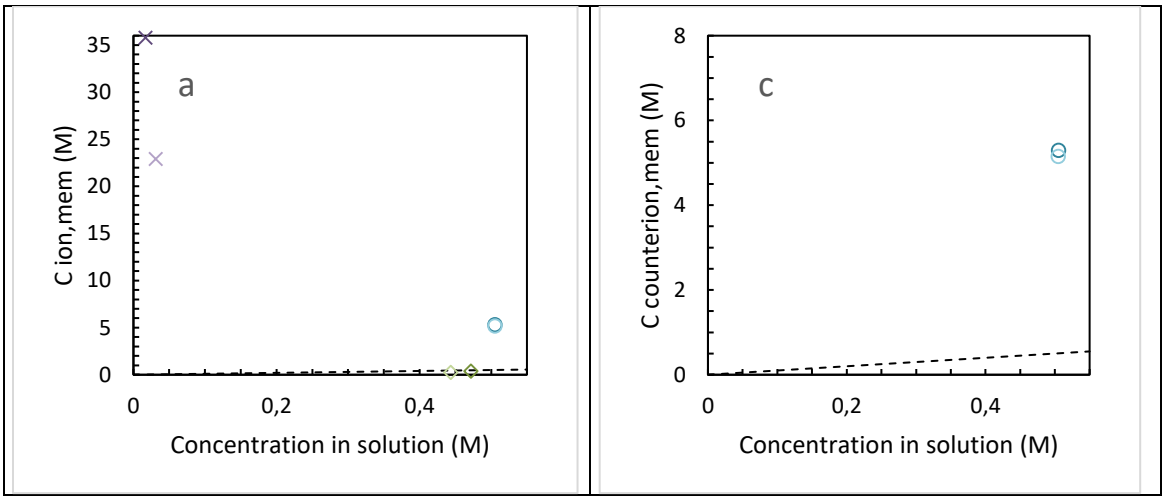

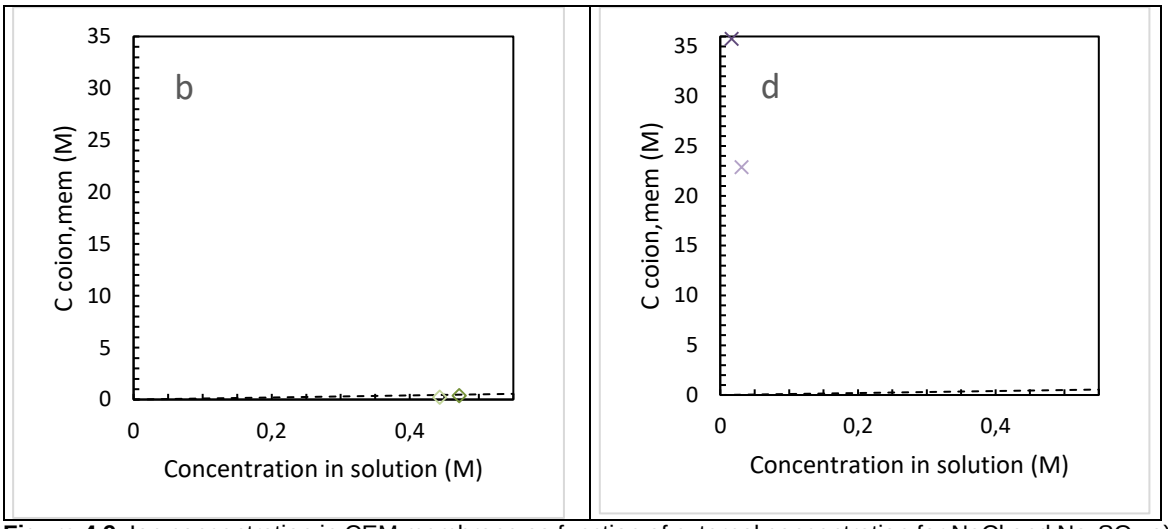

Figure 4.9. Ion concentration in CEM membrane as function of external concentration for NaCl and Na_2SO_4. a) Concentration of Co ions and counter ions, b) Concentration of counter ion Na^+ in membrane as function of external concentration, c) concentration of Co ion Cl^- in membrane as function of external solution, d) concentration of bivalent co ion SO_4^{-2} in membrane as function of external concentration.

In the case of CMX and Fuji CEM, even larger unrealistic values are obtained. SO_4^{-2} are co ions for cation exchange membranes and their ion concentration inside the membrane is expected to be negligible compared to counter ion sorption. Nonetheless results display that sulphate concentration inside the membranes is four times higher than the concentration of any counter ion.

Thus, taking into account all results obtained for sulphate ions, the only relevant conclusion that can be derived is that turbidimetry technique is not suitable for performing this kind of experiments.

4.4.3 Effect of Magnesium ions

The effect of Mg^{+2} ions has been investigated by performing tests with NaCl and $MgCl_2$ with 4 different membranes. Figures 4.10 to 4.13 review the effect observed on ions sorption, in the presence of Mg^{+2} ions in the external bulk solution. In this section, blue circles (○) represent Na^+ ions, gray rhombs (◊) symbolize Cl^- ions and orange squares (□) denote Mg^{+2} ions.

Solutions with the highest NaCl concentration (e.g. Solution 1 with only 0.5 M NaCl) are depicted in stronger colors, and in order to distinguish the mixtures investigated, the transparence of the color increases along the reduction of NaCl concentration from solution

1 to 7. Table 4-4. **Correspondence of symbols in the figures with the solutions given in Table 4.2** Helps to interpret the figures presented in this section

Table 4-4. Correspondence of symbols in the figures with the solutions given in Table 4.2

Solution	1	2	3	4	5	6	7
Na^+	○	○	○	○	○	○	
Mg^{+2}		□	□	□	□	□	□
Cl^-	◊	◊	◊	◊	◊	◊	◊

Figure 4.10 shows results for CMX membranes with mixture of NaCl and $MgCl_2$.

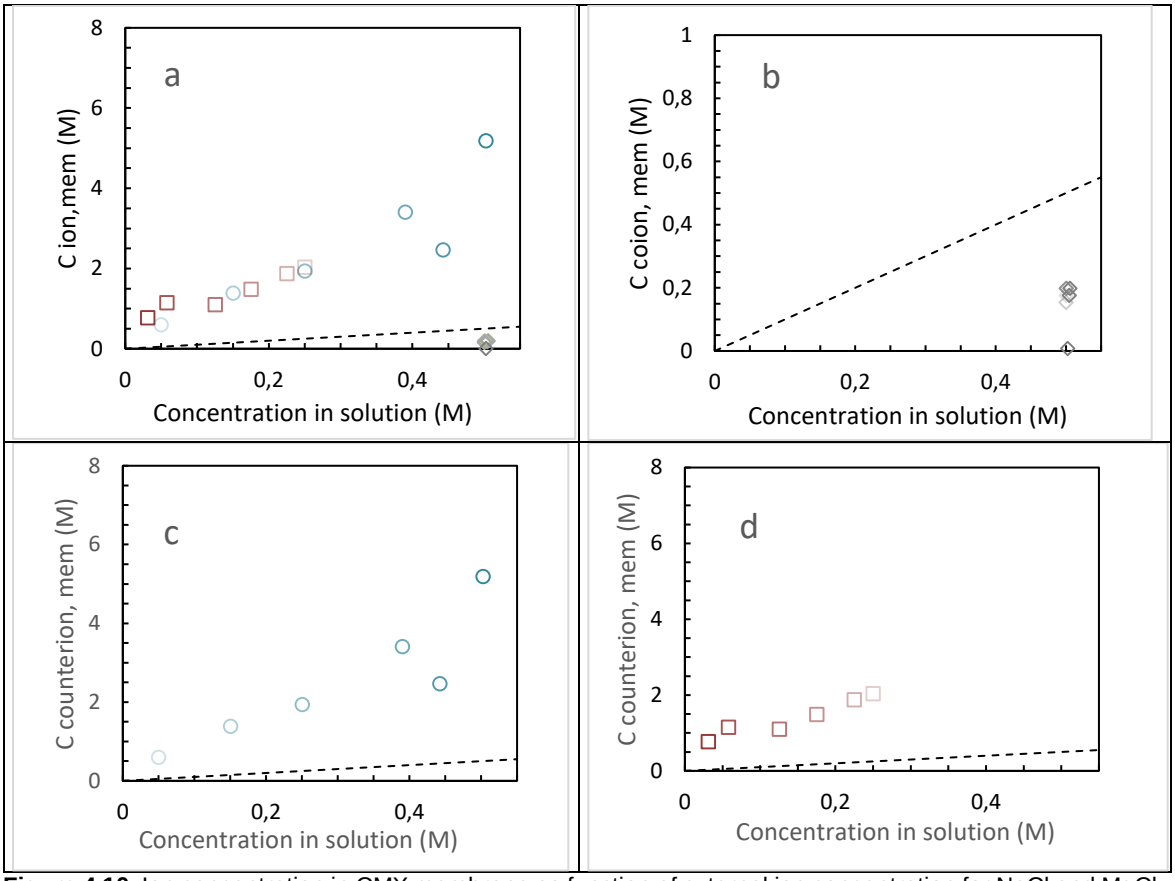

Figure 4.10. Ion concentration in CMX membrane as function of external ion concentration for NaCl and $MgCl_2$. a) Concentration of Co ions and counter ions, b) Concentration of co ions in membrane as function of external concentration., c) concentration of Na^+ in membrane as function of external solution, d) concentration of bivalent counter ion (Mg^{+2}) in membrane as function of external concentration

Figure 4.11 shows results for Fujifilm CEM membranes with mixture of NaCl and $MgCl_2$. From figures 4.10 and 4.11 it can be noticed that the presence of Mg^{+2} ions even in very small concentrations can reduce almost by half the capacity of the membranes to sorb Na^+ ions in cation exchange membranes. Furthermore, as the presence of Mg^{+2} increases linearly

in solution, the decrease in Na^+ concentration inside the membrane follows an exponential trend.

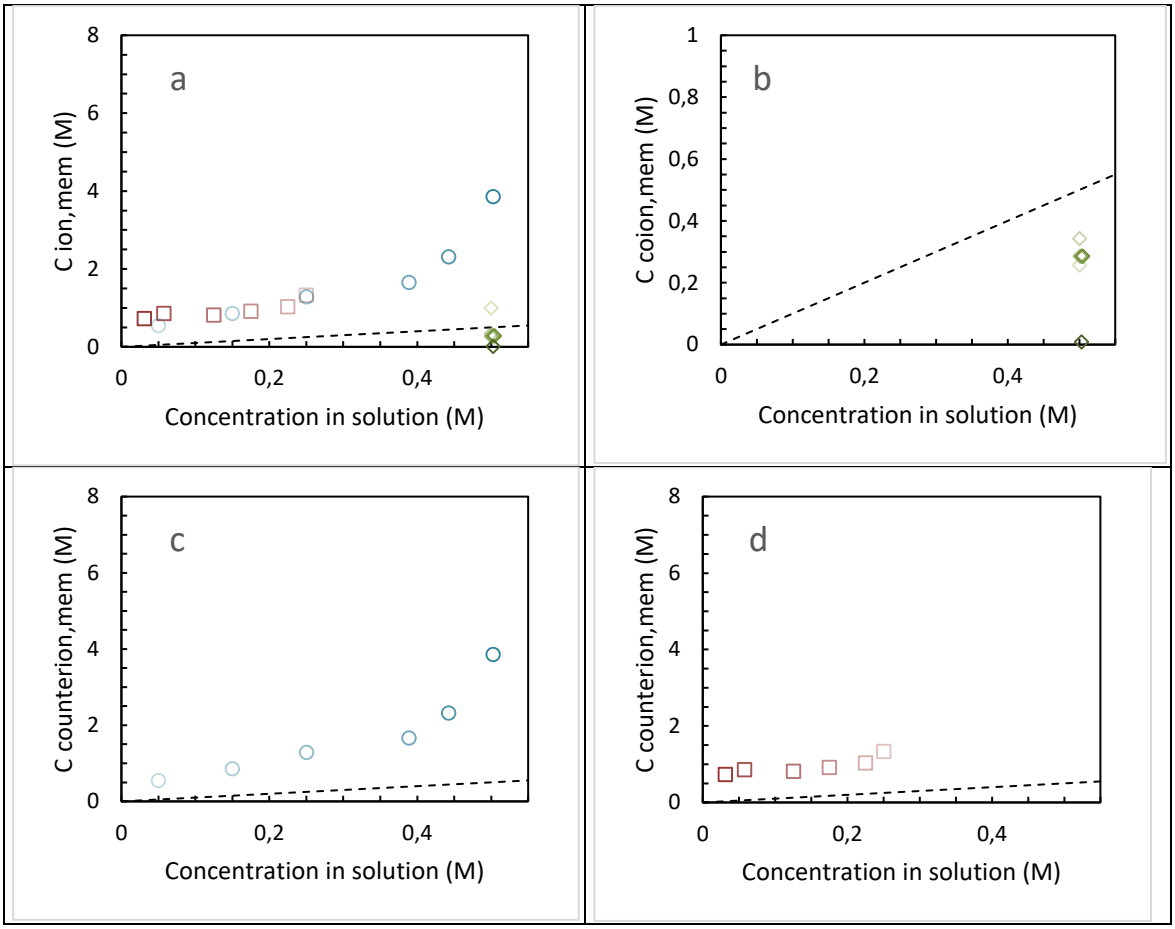

Figure 4.11. Ion concentration in CEM membrane as function of external concentration for NaCl and $MgCl_{2...}$ a) Concentration of Co ions and counter ions, b) Concentration of co ions in membrane as function of external concentration., c) concentration of Na^+ in membrane as function of external solution , d) concentration of bivalent counter ion (Mg^{+2}) in membrane as function of external concentration

Figure 4.12 shows results for AMX membranes with mixture of NaCl and $MgCl_{2...}$

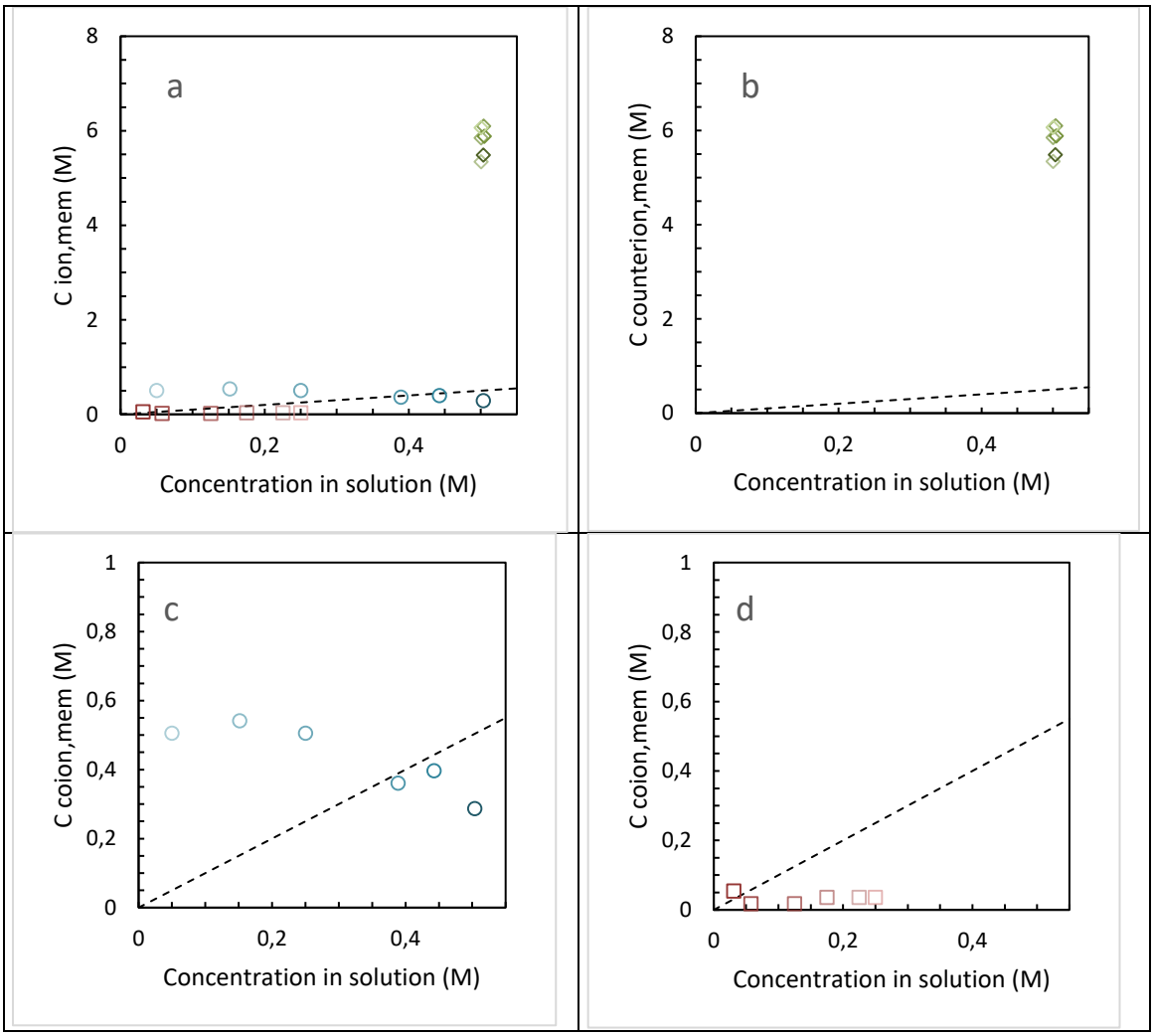

Figure 4.12. Ion concentration in AMX membrane as function of external concentration for NaCl and $MgCl_2$. a) Concentration of Co ions and counter ions, b) Concentration of counter ion Cl^- in membrane as function of external concentration., c) concentration of co ion Na^+ in membrane as function of external solution, d) concentration of bivalent co ion Mg^{+2} in membrane as function of external concentration

Figure 4.13 shows results for Fujifilm AEM membranes with mixture of NaCl and $MgCl_2$.

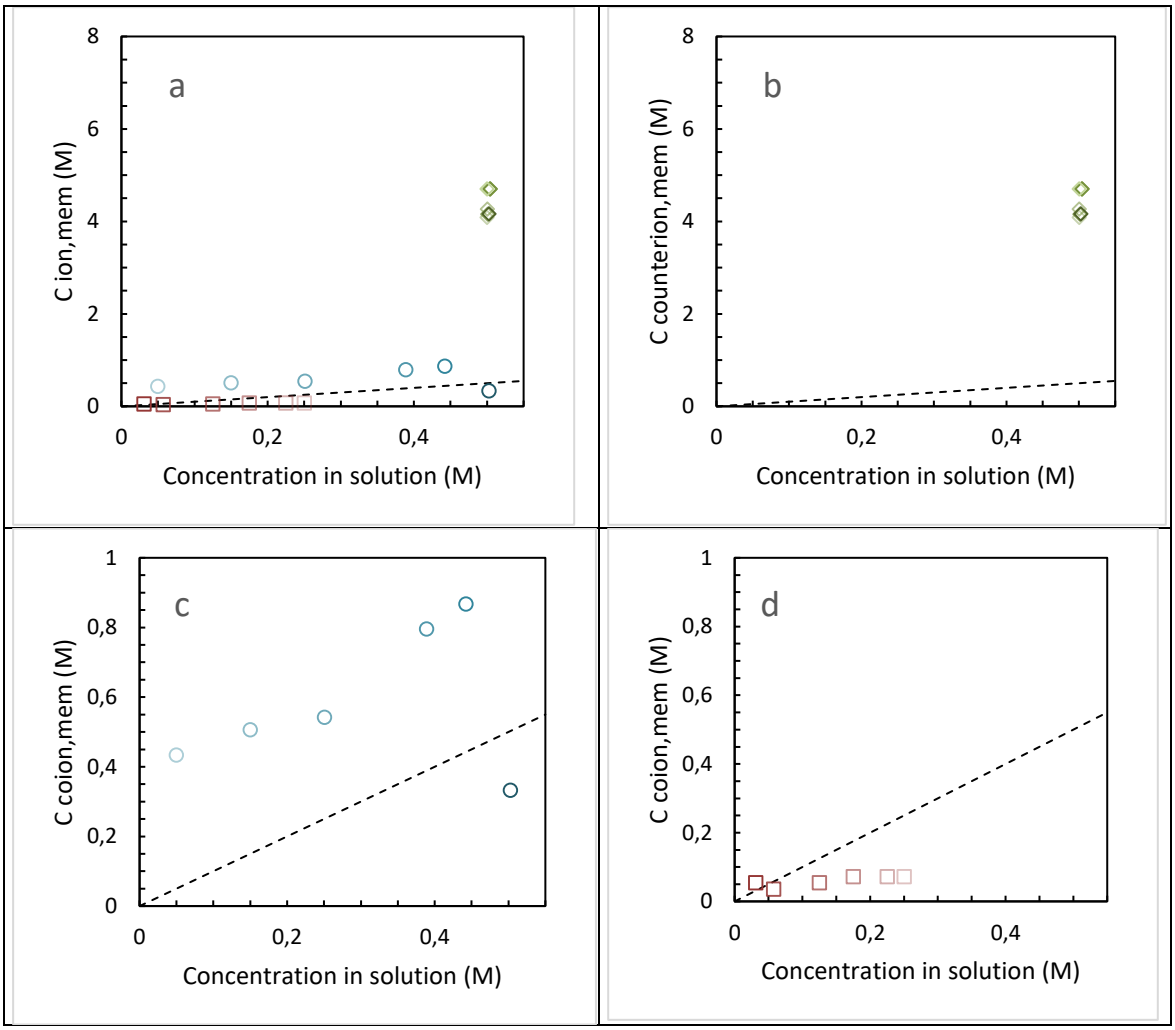

Figure 4.13 . Ion concentration in AEM membrane as function of external concentration for NaCl and $MgCl_2$. a) Concentration of Co ions and counter ions, b) Concentration of counter ion Cl^- in membrane as function of external concentration., c) concentration of co ion Na^+ in membrane as function of external solution, d) concentration of bivalent co ion Mg^{+2} in membrane as function of external concentration

The opposite effect is observed in anion exchange membranes, where Na^+ and Mg^{+2} act as co ions in the membrane. From Figures 4.12 and 4.13 it appears that although the increase in Mg^{+2} ions in the solution reduces the sorption of Na^+, in all the experiments with different solutions Na^+ concentration was always higher by a factor of more than 2.

4.4.4 Effect of Calcium ions

This section presents the effect of Ca^{+2} ions by performing tests with NaCl and $CaCl_2$ with 4 different membranes. Figures 4.14 to 4.17 review the effect observed of ions sorption in the membrane, in the presence of Ca^{+2} ions in the external bulk solution. In this section,

blue circles (○) represent Na^{+} ions, gray rhombs (◊) symbolize Cl^{-} ions and green triangles (Δ) denote Mg^{+2} ions.

Solutions with the highest NaCl concentration (e.g. Solution 1 with only 0.5 M NaCl) are depicted in stronger colors, and in order to distinguish the mixtures investigated, the transparence of the color increases along the reduction of NaCl concentration from solution 1 to 7. Table 4-4. **Correspondence of symbols in the figures with the solutions given in Table 4.2**Can be used to interpret the figures presented in this section.

Table 4-5. Correspondence of symbols in the figures with the solutions given in Table 4 - 2

Solution	**1**	**2**	**3**	**4**	**5**	**6**	**7**	**8**
Na^{+}	○	○	○	○	○	○	○	
Ca^{+2}		Δ	Δ	Δ	Δ	Δ	Δ	Δ
Cl^{-}	◊	◊	◊	◊	◊	◊	◊	◊

Figure 4.14 shows results for CMX membranes in solutions of NaCl and $CaCl_2$. From figures 4.14a and 4.15a it is possible to notice that Ca^{+2} ions have higher concentration inside the cation exchange membranes in comparison with Mg^{+2} ions in the same concentration ranges and ratios. Nonetheless, in low concentration ranges, Na^{+} ion sorption capacity of cation exchange membranes seem to be less affected by Ca^{+2} ions than for Mg^{+2} ions.

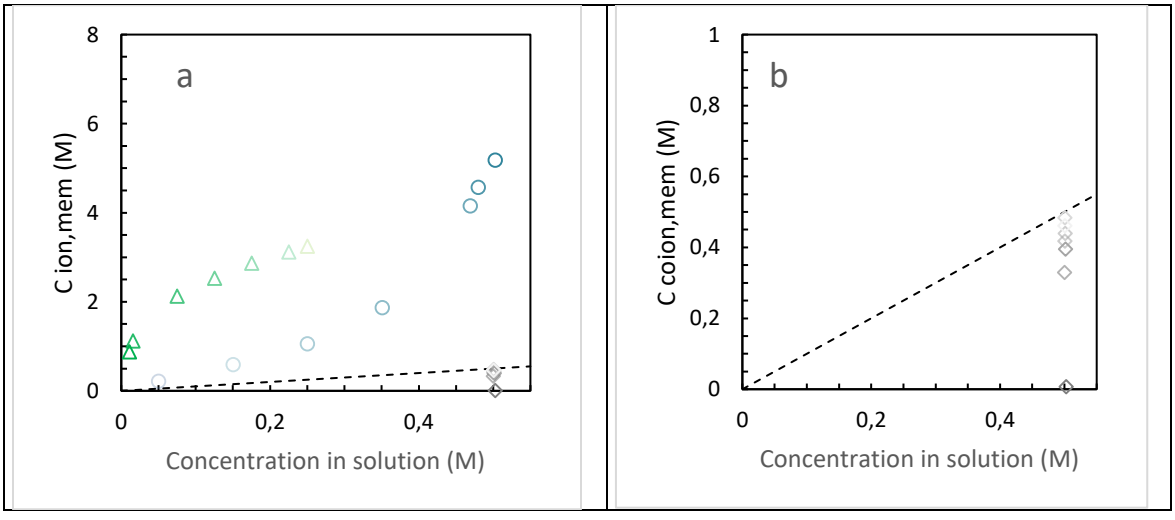

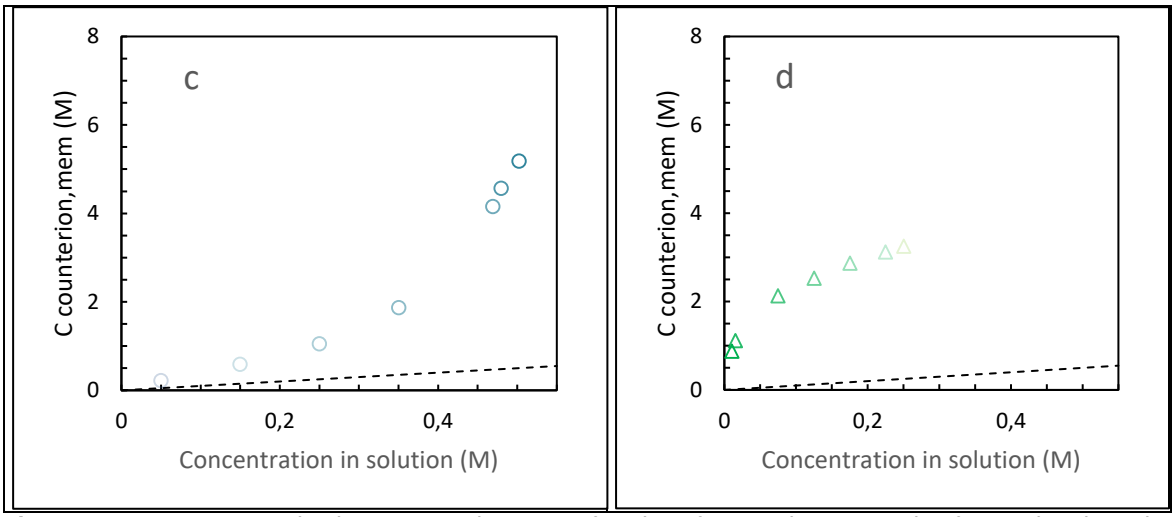

Figure 4.14. Ion concentration in CMX membranes as function of external concentration for NaCl and CaCl2. a) Concentration of Co-ions and counter-ions, b) Concentration of co-ions in membrane as function of external concentration., c) concentration of Na^{+} in membrane as function of external solution , d) concentration of bivalent counter-ion Ca^{+2} in membrane as function of external concentration

Figure 4.15 shows results for Fujifilm CEM membranes in solutions of NaCl and $CaCl_2$. In general it can be observed that Fujifilm membranes have less sorption capacity than Neosepta membranes.

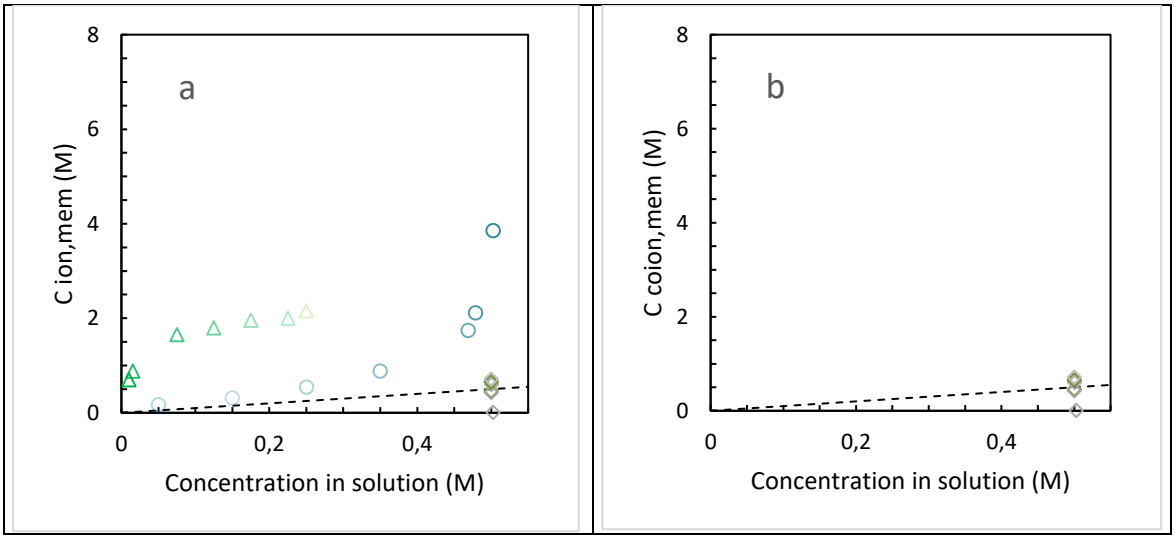

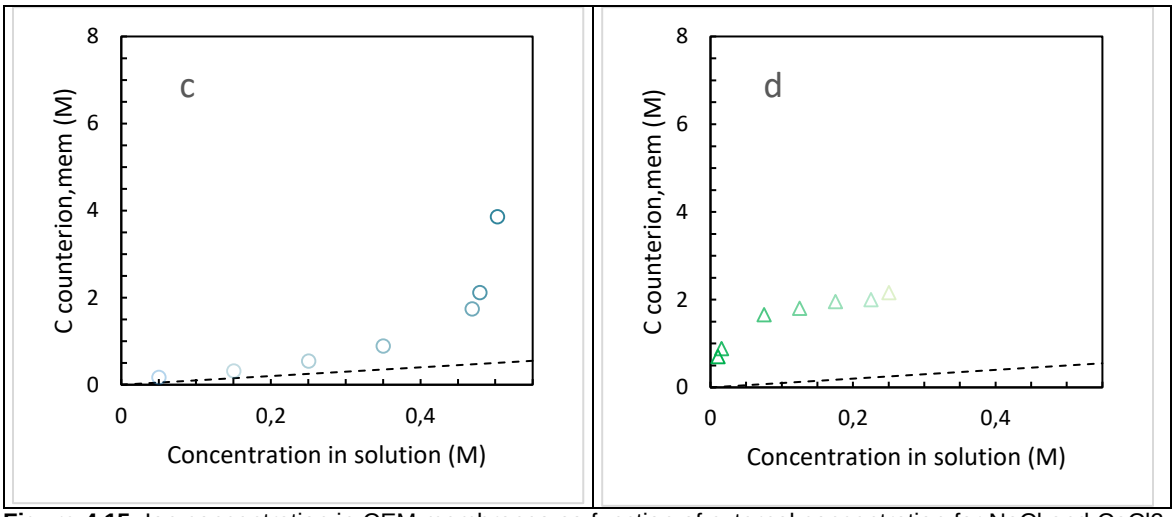

Figure 4.15. Ion concentration in CEM membranes as function of external concentration for NaCl and CaCl2. a) Concentration of Co-ions and counter-ions, b) Concentration of co-ion Cl^- in membrane as function of external concentration., c) concentration of counter ion Na^+ in membrane as function of external solution , d) concentration of bivalent counter-ion Ca^{+2} in membrane as function of external concentration.

Figure 4.16 shows results for AMX membranes in solutions of NaCl and $CaCl_2$.

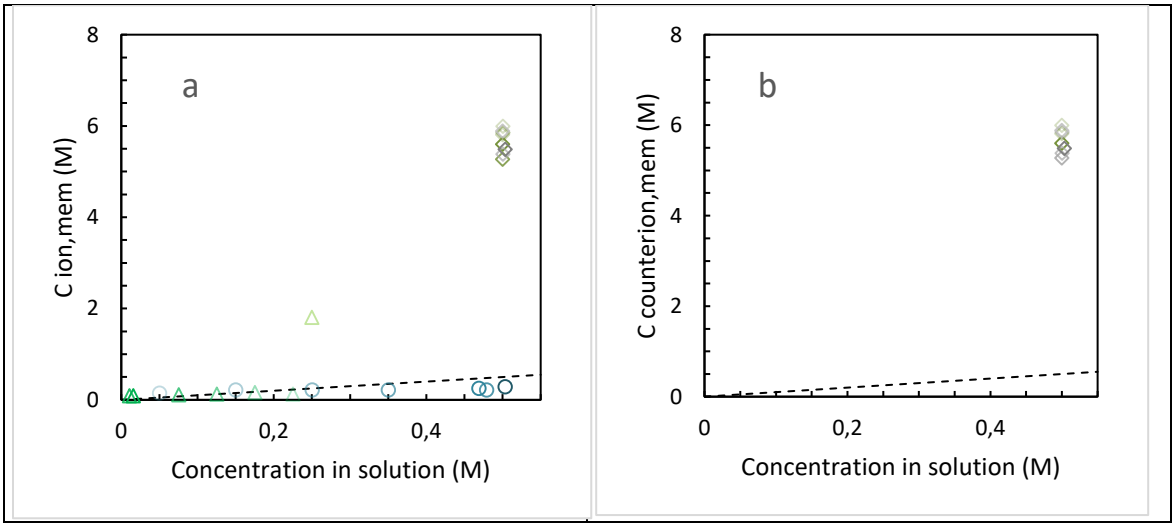

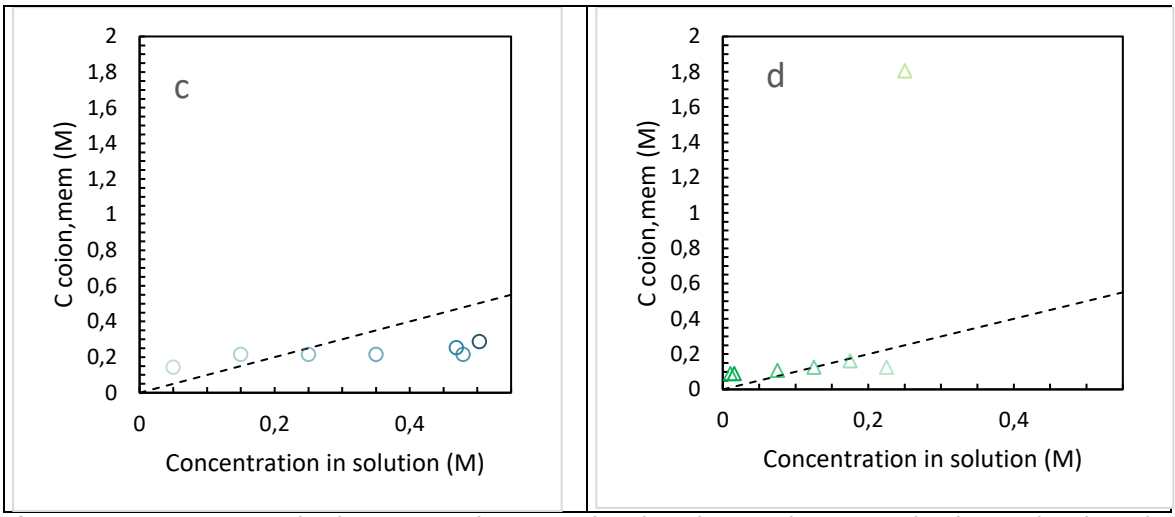

Figure 4.16. Ion concentration in AMX membranes as function of external concentration for NaCl and CaCl2. a) Concentration of Co-ions and counter-ions, b) Concentration of counter ion in membrane as function of external concentration., c) concentration of co ion Na^{+} in membrane as function of external solution , d) concentration of bivalent co ion Ca^{+2} in membrane as function of external concentration

Figure 4.17 shows results for AEM membranes in solutions of NaCl and $CaCl_2$.For anion exchange membranes it can be observed that repulsion of Ca^{+2} ions is not as stronger as the one found for Mg^{+2} ions, and co ion concentration is very similar for Na^{+} and Ca^{+2}.

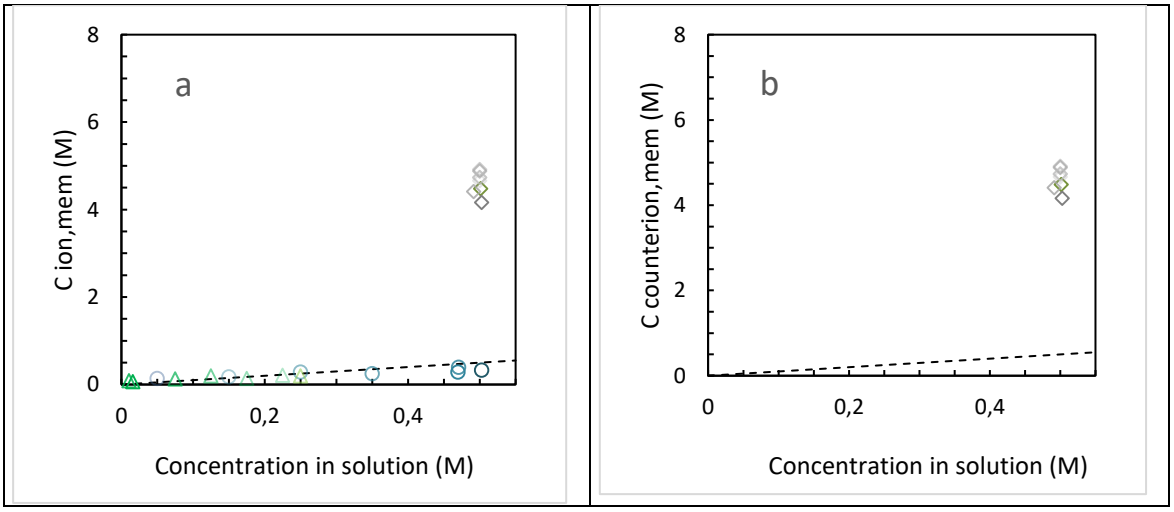

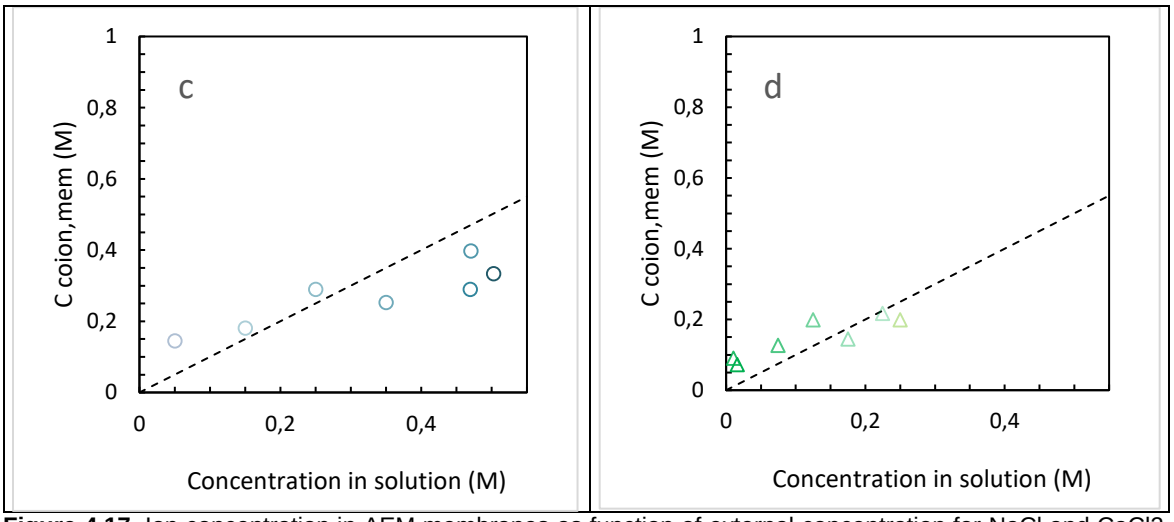

Figure 4.17. Ion concentration in AEM membranes as function of external concentration for NaCl and CaCl2. a) Concentration of Co-ions and counter-ions, b) Concentration of counter ion in membrane as function of external concentration., c) concentration of co ion Na^{+} in membrane as function of external solution , d) concentration of bivalent co ion Ca^{+2} in membrane as function of external concentration

Apparently more Cl^{-} ions are absorbed in anion exchange membranes when solution is les concentrated in NaCl. Unfortunately it is not possible to confirm this with confidence because the range of variability of Cl^{-} ions is too high. It is possible to asseverate that a more accurate technique is necessary for performing this kind of analysis.

4.4.5 Ion sorption with artificial seawater

Finally figures 4.18 to 4.20 show results of ion sorption tests using artificial seawater for all the investigated membranes. Artificial seawater was prepared using NaCl, Na_2SO_4, $CaCl_2$ and $MgCl_2$ according to the ion composition reported in Table 4.3. For all the cations, a trend may be seen in general, while for Cl and SO_4 ions it is not that obvious. This might be because absorption spectroscopy is a very accurate technique and it is very different from the techniques used for measuring Cl- and SO_4^{2-} ions. It may also be seen that in these mixtures, Na+ ion concentration inside the membrane is higher than Mg^{2+} or Ca^{2+} ions, and less comparable than the cases seen before of mixtures of two salts.

Figure 4.18 shows results of ion sorption in membranes for salinity conditions similar to Wadden Sea. From Figure 4.18a a marked increase in sorption capacity of CMX membranes compared to CEM membranes is observed. This effect is repeatedly observed in Figures 4.19 and 4.20, where CMX membranes double the ion exchange sorption capacity of Fujifilm membranes.

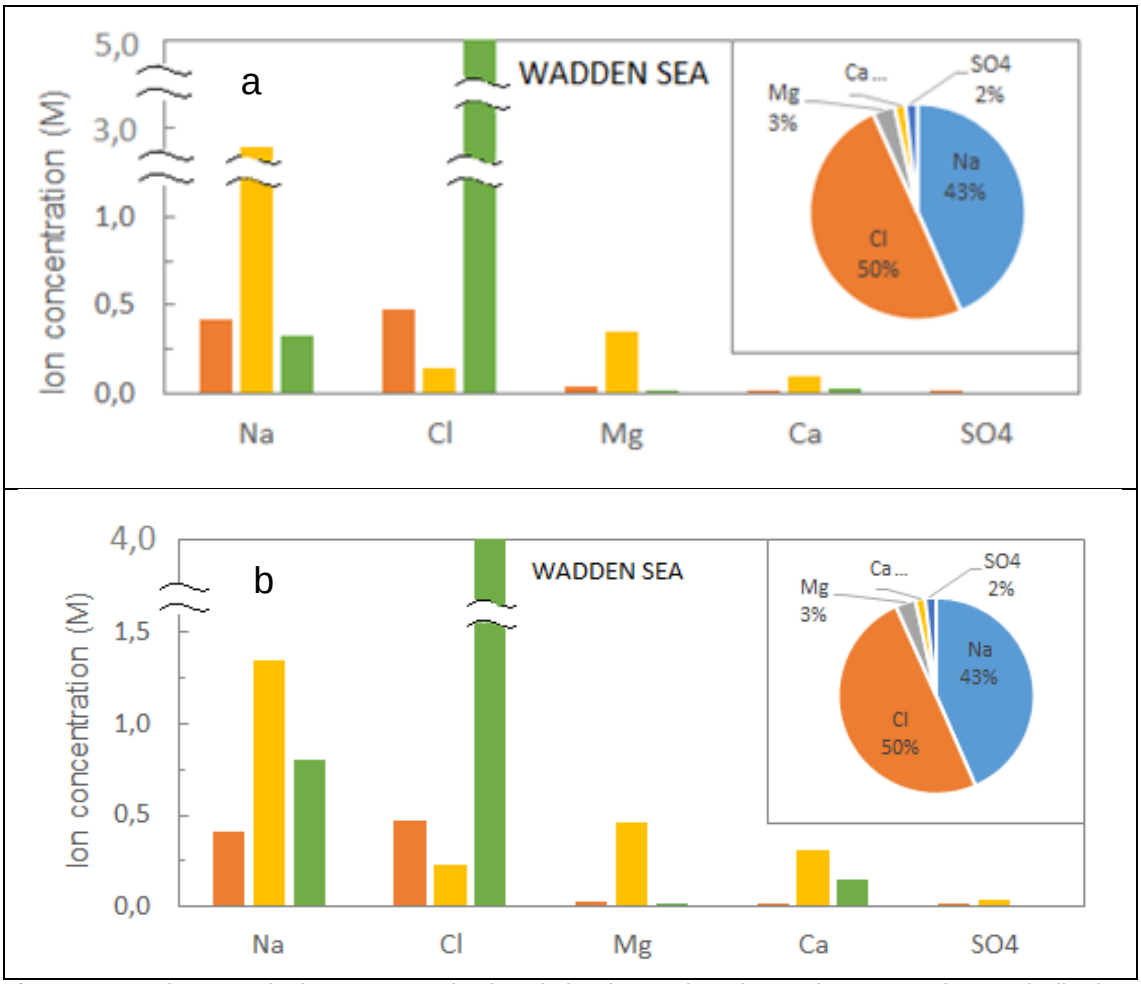

Figure 4.18. Histogram for ion concentration in solution (orange), cation exchange membranes (yellow) and anion Exchange membranes (green) in conditions similar to the Wadden Sea. 18a) Results for Neosepta membranes (CMX and AMX). 18b) Results for Fujifilm membranes (CEM and AEM)

Figure 4.19 shows results of ion sorption in membranes for salinity conditions similar to Mediterranean Sea. A remarkable advantage of Wadden sea is that the presence of Mg^{+2} ions is lower compared to Mediterranean and Caribbean sea, which have both 6% Mg^{+2} ions in solution. This fact is reflected in the values for ion sorption of Mg^{+2} in cation exchange membranes, which is higher for Mediterranean and Caribbean Sea than for the Wadden Sea.

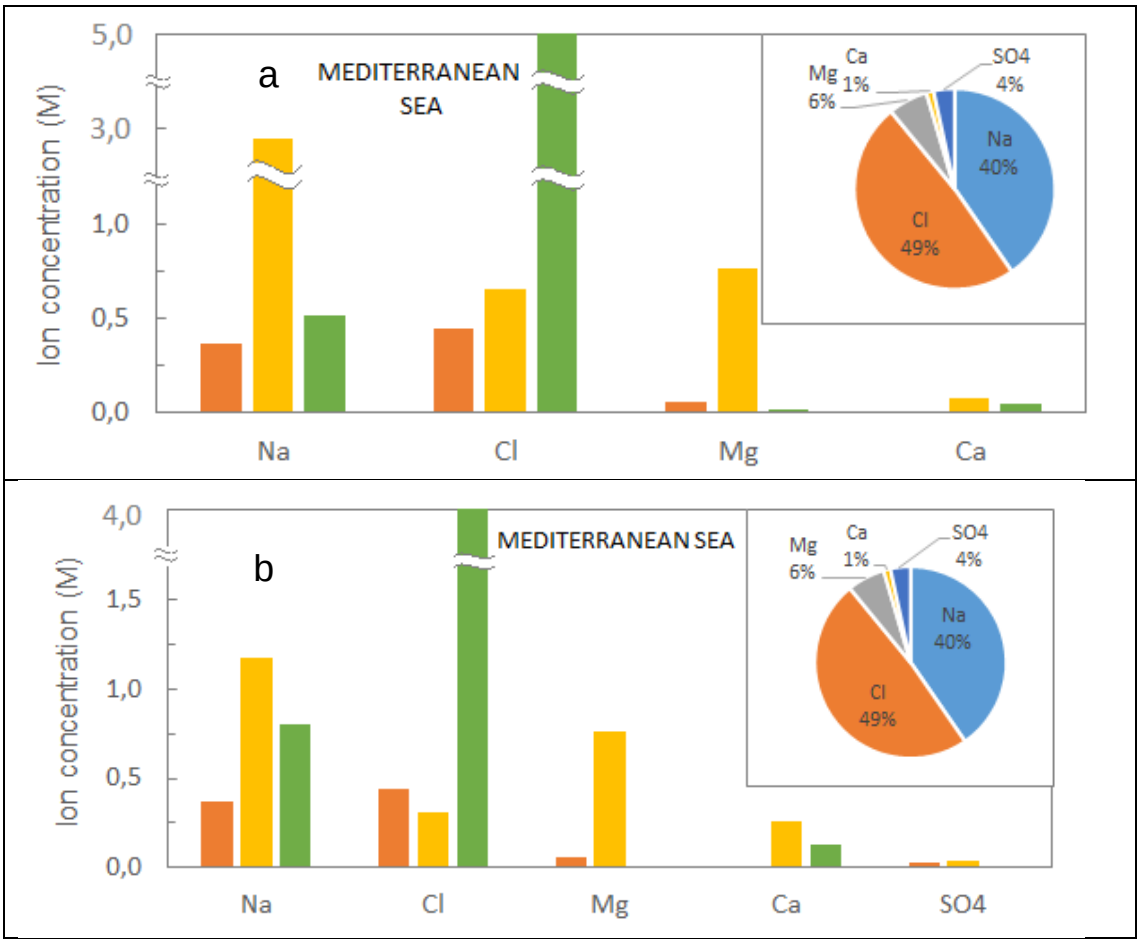

Figure 4.19. Histogram for ion concentration in solution (orange), cation exchange membranes (yellow) and anion Exchange membranes (green) in conditions similar to the Mediterranean Sea. 19 a) Results for Neosepta membranes (CMX and AMX). 19b) Results for Fujifilm membranes (CEM and AEM).

Figure 4.20 shows results of ion sorption in membranes for salinity conditions similar to Caribbean Sea.

In general, only small differences between the tests may be noticed, this leads to conclude that ion sorption inside cation and anion exchange membranes is not highly affected by the different ion concentrations that might be found in different seas. However, it is important to remind that artificial solutions were prepared keeping total normality of the solution constant, which means concentration in solutions is not real salinity found in seawater.

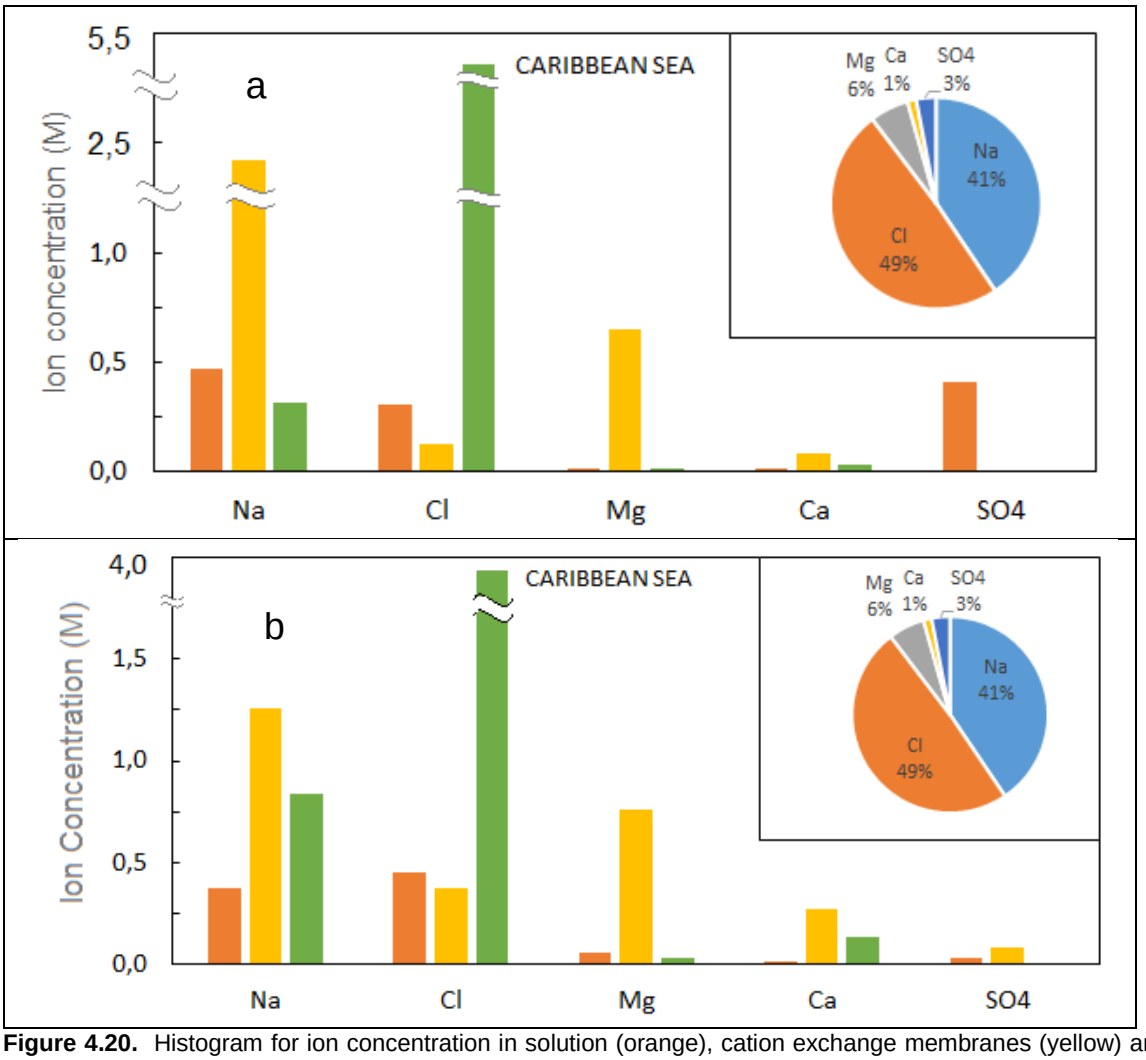

Figure 4.20. Histogram for ion concentration in solution (orange), cation exchange membranes (yellow) and anion Exchange membranes (green) in conditions similar to the Caribbean Sea. 19a) Results for Neosepta membranes (CMX and AMX). 19b) Results for Fujifilm membranes (CEM and AEM).

4.5 Conclusions

The aim of this work has been to investigate the effects of bivalent ions concentration in solution, on the ion sorption capacity of different membranes. The experimental campaign has shown that bivalent ions present in solution have a major effect in monovalent ion sorption capacity of the membranes. In very small concentration ranges of bivalent ions (like the ones found in real seawater) Na^+ sorption capacity of membranes can be reduced by almost half. Furthermore, it was found that differences in ion concentration between the different seas studied using artificial seawater are very small to have an observable effect in ion concentration inside the membranes.

4.5.1 Recommendations

Membranes should be cut with a die in order to ensure exactly the same area in all the experiments performed. In addition, it is necessary to repeat the experiments with more accurate measuring techniques like ion chromatography for anions.

4.5.2 Outlook

Future work should be focused on theoretical modelling of ion equilibrium. It is necessary to determine which factors affect ion sorption of bivalent ions and specifically why is membrane sorption capacity affected by some ions (like Mg^{+2}) more than others (like Ca^{+2}), in small concentrations like the ones found in real seawater.

A. Appendix 1: Derivation of dynamical model from mol balance

This section presents the derivation of the dynamical model starting from the mole balances presented in Chapter 2.Figure 2.2 shows a scheme that explains salt and water transport through the compartments with length L, width b, and thickness δ.

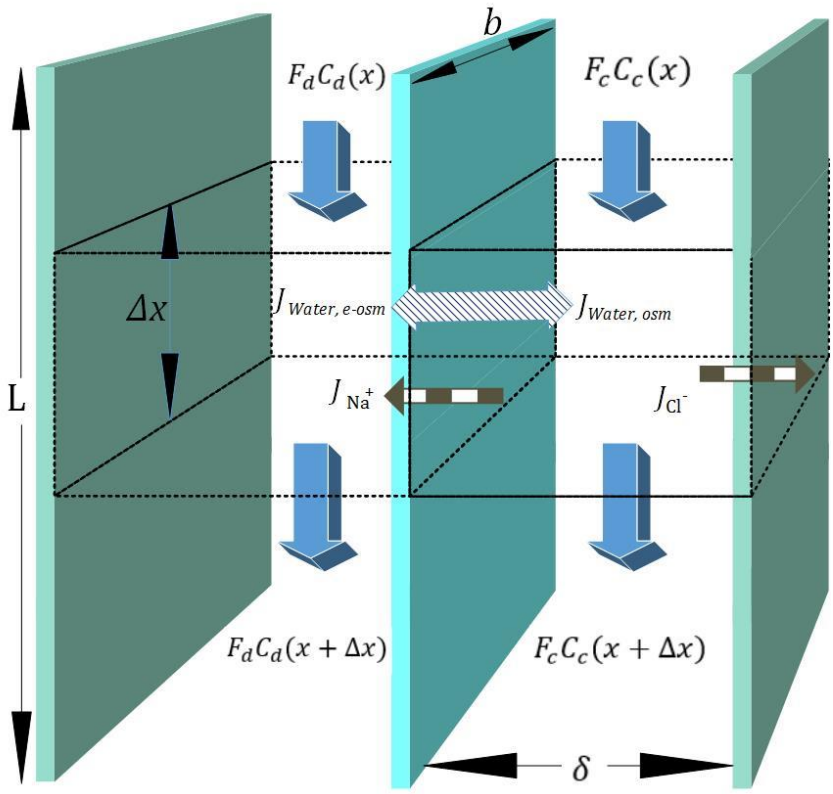

Figure 4.21. Mass balance for concentrated and diluted compartments. Source: The authors

Convective flow is defined in the *x* direction. In the length differentials, transport of ions occurs from the concentrated to the diluted compartments through the membranes due to a salt concentration gradient. Water passes in the same direction as salt due to electro

osmotic drag. In the opposite direction an osmotic effect is presented and the non-ideal behavior of membranes causes water transport in the undesired direction.

A mole balance within the length differential, in concentrated and diluted compartments leads to Eq. (A.1) and Eq. (A.2) respectively

$$\frac{(b\ \delta\ \Delta x)\ dC_c(x)}{dt} = F_c C_c(x) - (\ F_c + b\ \Delta x\ T_w) C_c(x + \Delta x) - b\ \Delta x\ T_{NaCl}(x) \tag{A.1}$$

$$\frac{(b\ \delta\ \Delta x)\ dC_d(x)}{dt} = F_d C_d(x) - (\ F_d + b\ \Delta x\ T_w) C_d(x + \Delta x) - b\ \Delta x\ T_{NaCl}(x) \tag{A.2}$$

Dividing Eq. (A.1) and (A.2) by F_c and F_d respectively leads to

$$\frac{(b\ \delta\ \Delta x)}{F_c}\frac{dC_c(x)}{dt} = C_c(x) - \left(1 + \frac{b\ \Delta x\ T_w}{F_c}\right) C_c(x + \Delta x) - \frac{b\ \Delta x}{F_c}\ T_{NaCl}(x) \tag{A.3}$$

$$\frac{(b\ \delta\ \Delta x)}{F_d}\frac{dC_d(x)}{dt} = C_d(x) - \left(1 + \frac{b\ \Delta x\ T_w}{F_d}\right) C_d(x + \Delta x) - \frac{b\ \Delta x}{F_d}\ T_{NaCl}(x) \tag{A.4}$$

Rearrengin Eq. (A.3) and (A.4)

$$\frac{(b\ \delta\ \Delta x)}{F_c}\frac{dC_c(x)}{dt} = C_c(x) - C_c(x + \Delta x) + \frac{b\ \Delta x\ T_w}{F_c} C_c(x + \Delta x) - \frac{b\ \Delta x}{F_c}\ T_{NaCl}(x) \tag{A.5}$$

$$\frac{(b\ \delta\ \Delta x)}{F_d}\frac{dC_d(x)}{dt} = C_d(x) - C_d(x + \Delta x) + \frac{b\ \Delta x\ T_w}{F_d} C_d(x + \Delta x) - \frac{b\ \Delta x}{F_d}\ T_{NaCl}(x) \tag{A.6}$$

Taking the limit when Δx tends to cero and dividng by Δx each of the factors in Eqs. (A.5) and (A.6) leads to the dynamical model. Procedure is going to be demonstrated for Eq. (A.5) and derivation for (A.6) is straightforward

$$\lim_{\Delta x \to 0} \frac{(b\ \delta\ \Delta x)}{F_c \Delta x}\frac{dC_c(x)}{dt} = \frac{(b\ \delta\ )}{F_c}\frac{dC_c(x)}{dt} \tag{A.7}$$

$$\lim_{\Delta x \to 0} \frac{C_c(x) - C_c(x + \Delta x)}{\Delta x} = \frac{dC_c(x)}{dx} \tag{A.8}$$

$$\lim_{\Delta x \to 0} \frac{b\,\Delta x\,T_w}{F_c \Delta x} C_c(x + \Delta x) = \frac{b\,T_w}{F_c} C_c(x) \tag{A.9}$$

$$\lim_{\Delta x \to 0} \frac{b\,\Delta x}{F_c \Delta x}\, T_{NaCl}(x) = \frac{b}{F_c}\, T_{NaCl}(x) \tag{A.10}$$

After applying limits, partial differential equations showed in Chapter 2 are obtained

$$\frac{dC_{NaCl}(x)}{dt} = \frac{F_c}{b\,\delta}\frac{\partial C_c(x)}{\partial x} - \frac{1}{\delta}\, T_w C_c(x) - \frac{1}{\delta}\, T_{NaCl}(x) \tag{A.11}$$

$$\frac{dC_{NaCl}(x)}{dt} = \frac{F_d}{b\,\delta}\frac{\partial C_d(x)}{\partial x} - \frac{1}{\delta} T_w C_d(x) - \frac{1}{\delta} T_{NaCl}(x) \tag{A.12}$$

5. Bibliography

[1] The World Bank, “Energy & Mining | Data,” 2013. [Online]. Available: http://data.worldbank.org/topic/energy-and-mining.

[2] International Bank for Reconstruction and Development, World Bank, and International Energy Agency (IEA), “Progress toward sustainable energy 2015,” Washington DC, 2015.

[3] M. I. Hoffert, K. Caldeira, A. K. Jain, E. F. Haites, L. D. D. Harvey, S. D. Potter, M. E. Schlesinger, S. H. Schneider, R. G. Watts, T. M. L. Wigley, and D. J. Wuebbles, “Energy implications of future stabilization of atmospheric CO2 content,” *Nature*, vol. 395, pp. 881–884, 1998.

[4] United Nations, *UNITED NATIONS FRAMEWORK CONVENTION ON CLIMATE CHANGE*. 1992, p. 33.

[5] Statkraft and ICTPOL, “The Salinity Power project,” pp. 1–12, 2004.

[6] R. E. Pattle, “Production of Electric Power by mixing Fresh and Salt Water in the Hydroelectric Pile,” *Nature*, vol. 174, no. 4431. pp. 660–660, 1954.

[7] J. Kuleszo, C. Kroeze, J. Post, and B. M. Fekete, “The potential of blue energy for reducing emissions of CO_2 and non-CO_2 greenhouse gases,” *J. Integr. Environ. Sci.*, vol. 7, no. sup1, pp. 89–96, Aug. 2010.

[8] J. W. Post, “Blue Energy: electricity production from salinity gradients by reverse electgrodialysis,” 2009.

[9] P. Stenzel and H. Wagner, “Osmotic power plants: Potential analysis and site criteria,” *3rd Int. Conf. Ocean Energy, …*, pp. 1–5, 2010.

[10] O. A. Alvarez-Silva, A. F. Osorio, and C. Winter, “Practical global salinity gradient energy potential,” *Renew. Sustain. Energy Rev.*, vol. 60, pp. 1387–1395, 2016.

[11] J. D. Restrepo and B. Kjerfve, “Water Discharge and Sediment Load from the Western Slopes of the Colombian Andes with Focus on Rio San Juan,” *J. Geol.*, vol. 108, no. 1, pp. 17–33, Jan. 2000.

[12] O. Alvarez-Silva and A. F. Osorio, “Salinity gradient energy potential in Colombia considering site specific constraints,” *Renew. Energy*, vol. 74, pp. 737–748, 2015.

[13] O. Alvarez-Silva, “Salinity Gradient Energy Harnessing at River Mouths,” 2014.

[14] J. W. Post, J. Veerman, H. V. M. Hamelers, G. J. W. Euverink, S. J. Metz, K. Nymeijer, and C. J. N. Buisman, “Salinity-gradient power: Evaluation of pressure-retarded osmosis and reverse electrodialysis,” *J. Memb. Sci.*, vol. 288, no. 1–2, pp. 218–230, Feb. 2007.

[15] S. Loeb and R. S. Norman, “Osmotic Power Plants,” *Science (80-.).*, vol. 189, no.

4203, 1975.

[16] N. Y. Yip, D. Brogioli, H. V. M. Hamelers, and K. Nijmeijer, “Salinity Gradients for Sustainable Energy: Primer, Progress, and Prospects,” *Environ. Sci. Technol.*, p. acs.est.6b03448, 2016.

[17] G. Z. Ramon, B. J. Feinberg, and E. M. V. Hoek, “Membrane-based production of salinity-gradient power,” *Energy Environ. Sci.*, vol. 4, no. 11, p. 4423, 2011.

[18] J. Maisonneuve, C. B. Laflamme, and P. Pillay, “Experimental investigation of pressure retarded osmosis for renewable energy conversion: Towards increased net power,” *Appl. Energy*, vol. 164, no. January, pp. 425–435, 2016.

[19] S. Chou, R. Wang, L. Shi, Q. She, C. Tang, and A. G. Fane, “Thin-film composite hollow fiber membranes for pressure retarded osmosis (PRO) process with high power density,” *J. Memb. Sci.*, vol. 389, pp. 25–33, 2012.

[20] D. a. Vermaas, M. Saakes, and K. Nijmeijer, “Doubled power density from salinity gradients at reduced intermembrane distance,” *Environ. Sci. Technol.*, vol. 45, no. 16, pp. 7089–7095, 2011.

[21] D. a. Vermaas, E. Guler, M. Saakes, and K. Nijmeijer, “Theoretical power density from salinity gradients using reverse electrodialysis,” *Energy Procedia*, vol. 20, pp. 170–184, 2012.

[22] D. Brogioli, “Extracting renewable energy from a salinity difference using a capacitor,” *Phys. Rev. Lett.*, vol. 103, no. 5, pp. 31–34, 2009.

[23] R. A. Rica, R. Ziano, D. Salerno, F. Mantegazza, M. Z. Bazant, and D. Brogioli, “Electro-diffusion of ions in porous electrodes for capacitive extraction of renewable energy from salinity differences,” *Electrochim. Acta*, vol. 92, pp. 304–314, 2013.

[24] G. R. Iglesias, M. M. Fernández, S. Ahualli, M. L. Jiménez, O. P. Kozynchenko, and A. V. Delgado, “Materials selection for optimum energy production by double layer expansion methods,” *J. Power Sources*, vol. 261, pp. 371–377, 2014.

[25] R. a. Rica, D. Brogioli, R. Ziano, D. Salerno, and F. Mantegazza, “Ions transport and adsorption mechanisms in porous electrodes during capacitive-mixing double layer expansion (CDLE),” *J. Phys. Chem. C*, vol. 116, pp. 16934–16938, 2012.

[26] D. Brogioli, R. Zhao, and P. M. Biesheuvel, “A prototype cell for extracting energy froma water salinity difference bymeans of double layer expansion in nanoporous carbon electrodes,” *R. Soc. chemestry*, no. 8, pp. 1166–1169, 2010.

[27] D. a. Vermaas, S. Bajracharya, B. B. Sales, M. Saakes, B. Hamelers, and K. Nijmeijer, “Clean energy generation using capacitive electrodes in reverse electrodialysis,” *Energy Environ. Sci.*, vol. 6, p. 643, 2013.

[28] D. A. Vermaas, J. Veerman, and M. Saakes, “REVERSE ELECTRODIALYSIS ENERGY GENERATING SYSTEM USING CAPACITIVE ELECTRODES,” 2015.

[29] M. Tedesco, C. Scalici, D. Vaccari, A. Cipollina, A. Tamburini, and G. Micale,

"Performance of the first reverse electrodialysis pilot plant for power production from saline waters and concentrated brines," *J. Memb. Sci.*, vol. 500, pp. 33–45, 2016.

[30] M. Tedesco, A. Cipollina, A. Tamburini, and G. Micale, "Towards 1 kW power production in a reverse electrodialysis pilot plant with saline waters and concentrated brines," *J. Memb. Sci.*, vol. 500, pp. 33–45, 2016.

[31] R. A. Tufa, E. Curcio, E. Brauns, W. Van Baak, E. Fontananova, and G. Di, "Membrane Distillation and Reverse Electrodialysis for Near-Zero Liquid Discharge and low energy seawater desalination," *J. Memb. Sci.*, 2015.

[32] R. Long, B. Li, Z. Liu, and W. Liu, "Hybrid membrane distillation-reverse electrodialysis electricity generation system to harvest low-grade thermal energy," *J. Memb. Sci.*, no. August, pp. 1–8, 2016.

[33] R. A. Tufa, E. Rugiero, D. Chanda, J. Hn??t, W. van Baak, J. Veerman, E. Fontananova, G. Di Profio, E. Drioli, K. Bouzek, and E. Curcio, "Salinity gradient power-reverse electrodialysis and alkaline polymer electrolyte water electrolysis for hydrogen production," *J. Memb. Sci.*, vol. 514, pp. 155–164, 2016.

[34] a. D'Angelo, a. Galia, and O. Scialdone, "Cathodic abatement of Cr(VI) in water by microbial reverse-electrodialysis cells," *J. Electroanal. Chem.*, no. Vi, 2015.

[35] X. Luo, X. Cao, Y. Mo, K. Xiao, X. Zhang, P. Liang, and X. Huang, "Power generation by coupling reverse electrodialysis and ammonium bicarbonate: Implication for recovery of waste heat," *Electrochem. commun.*, vol. 19, no. 1, pp. 25–28, 2012.

[36] R. S. Kingsbury, K. Chu, and O. Coronell, "Energy storage by reversible electrodialysis: The concentration battery," *J. Memb. Sci.*, vol. 495, pp. 502–516, 2015.

[37] P. Dlugolecki, K. Nymeijer, S. Metz, and M. Wessling, "Current status of ion exchange membranes for power generation from salinity gradients," *J. Memb. Sci.*, vol. 319, no. 1–2, pp. 214–222, Jul. 2008.

[38] J. Veerman, M. Saakes, S. J. Metz, and G. J. Harmsen, "Reverse electrodialysis: A validated process model for design and optimization," *Chem. Eng. J.*, vol. 166, pp. 256–268, 2011.

[39] D. a Vermaas, "Energy generation from mixing salt water and fresh water," Twentee, 2013.

[40] R. Banan Sadeghian, O. Pantchenko, D. Tate, and A. Shakouri, "Miniaturized concentration cells for small-scale energy harvesting based on reverse electrodialysis," *Appl. Phys. Lett.*, vol. 99, no. 17, pp. 99–101, 2011.

[41] S. Pawlowski, V. Geraldes, J. G. Crespo, and S. Velizarov, "Computational fluid dynamics (CFD) assisted analysis of profiled membranes performance in reverse electrodialysis," *J. Memb. Sci.*, vol. 502, pp. 179–190, 2016.

[42] D. A. Vermaas, M. Saakes, and K. Nijmeijer, “Power generation using profiled membranes in reverse electrodialysis,” *J. Memb. Sci.*, vol. 385, pp. 234–242, 2011.

[43] E. Güler, R. Elizen, M. Saakes, and K. Nijmeijer, “Micro-structured membranes for electricity generation by reverse electrodialysis,” *J. Memb. Sci.*, vol. 458, pp. 136–148, May 2014.

[44] P. Długołęcki, J. Dąbrowska, K. Nijmeijer, and M. Wessling, “Ion conductive spacers for increased power generation in reverse electrodialysis,” *J. Memb. Sci.*, vol. 347, no. 1, pp. 101–107, 2010.

[45] E. Korngold, L. Aronov, and O. Kedem, “Novel ion-exchange spacer for improving electrodialysis. I. Reacted spacer,” *J. Memb. Sci.*, vol. 138, no. 2, pp. 165–170, 1998.

[46] B. Zhang, H. Gao, and Y. Chen, “Enhanced Ionic Conductivity and Power Generation Using Ion-Exchange Resin Beads in a Reverse-Electrodialysis Stack,” *Environ. Sci. Technol.*, vol. 49, no. 24, pp. 14717–14724, 2015.

[47] S. Mikhaylin and L. Bazinet, “Fouling on ion-exchange membranes: Classification, characterization and strategies of prevention and control,” *Adv. Colloid Interface Sci.*, vol. 229, pp. 34–56, 2015.

[48] D. A. Vermaas, D. Kunteng, J. Veerman, M. Saakes, and K. Nijmeijer, “Periodic feedwater reversal and air sparging as antifouling strategies in reverse electrodialysis.,” *Environ. Sci. Technol.*, vol. 48, no. 5, pp. 3065–73, Jan. 2014.

[49] S. Mulyati, R. Takagi, A. Fujii, Y. Ohmukai, T. Maruyama, and H. Matsuyama, “Improvement of the antifouling potential of an anion exchange membrane by surface modification with a polyelectrolyte for an electrodialysis process,” *J. Memb. Sci.*, vol. 417–418, pp. 137–143, 2012.

[50] E. Güler, W. van Baak, M. Saakes, and K. Nijmeijer, “Monovalent-ion-selective membranes for reverse electrodialysis,” *J. Memb. Sci.*, vol. 455, pp. 254–270, 2014.

[51] A. P. Straub, A. Deshmukh, and M. Elimelech, “Pressure-retarded osmosis for power generation from salinity gradients: is it viable?,” *Energy Environ. Sci.*, vol. 9, no. 1, pp. 31–48, 2016.

[52] T. Höpner and J. Windelberg, “Elements of environmental impact studies on coastal desalination plants,” *Desalination*, vol. 108, pp. 11–18, 1997.

[53] T. Höpner and S. Lattemann, “Chemical impacts from seawater desalination plants — a case study of the northern Red Sea,” *Desalination*, vol. 152, pp. 133–140, 2003.

[54] T. Bleninger and G. H. Jirka, “Modelling and environmentally sound management of brine discharges from desalination plants,” *Desalination*, vol. 221, no. 1–3, pp. 585–597, 2008.

[55] A. Osorio, P. Agudelo, L. Otero, and J. Correa, “Las energias del mar,” *propiedad*

pública, 2013. .

[56] M. Tedesco, A. Cipollina, A. Tamburini, I. D. L. Bogle, and G. Micale, “A simulation tool for analysis and design of reverse electrodialysis using concentrated brines,” *Chem. Eng. Res. Des.*, vol. 93, no. JANUARY, pp. 441–456, 2015.

[57] J. Veerman, *reverse electro- dialysis*. .

[58] M. L. Jiménez, M. M. Fernández, S. Ahualli, G. Iglesias, and a. V. Delgado, “Predictions of the maximum energy extracted from salinity exchange inside porous electrodes,” *J. Colloid Interface Sci.*, vol. 402, pp. 340–349, 2013.

[59] Z. Jia, B. Wang, S. Song, and Y. Fan, “Blue energy: Current technologies for sustainable power generation from water salinity gradient,” *Renew. Sustain. Energy Rev.*, vol. 31, pp. 91–100, 2014.

[60] Y. Cui, X. Y. Liu, and T. S. Chung, “Enhanced osmotic energy generation from salinity gradients by modifying thin film composite membranes,” *Chem. Eng. J.*, vol. 242, pp. 195–203, 2014.

[61] J. Veerman, *reverse electro-dialysis. Design and optimization by modeling and experimentation*. 2010.

[62] H. Alvarez, R. Lamanna, P. Vega, and S. Revollar, “Metodología para la Obtención de Modelos Semifísicos de Base Fenomenológica Aplicada a una Sulfitadora de Jugo de Caña de Azúcar,” *Rev. Iberoam. Automática e Informática Ind. RIAI*, vol. 6, no. 3, pp. 10–20, Jul. 2009.

[63] J. Veerman, M. Saakes, S. J. Metz, and G. J. Harmsen, “Reverse electrodialysis: Performance of a stack with 50 cells on the mixing of sea and river water,” *J. Memb. Sci.*, vol. 327, pp. 136–144, 2009.

[64] J. Veerman, R. M. de Jong, M. Saakes, S. J. Metz, and G. J. Harmsen, “Reverse electrodialysis: Comparison of six commercial membrane pairs on the thermodynamic efficiency and power density,” *J. Memb. Sci.*, vol. 343, no. 1, pp. 7–15, 2009.

[65] K. S. Pitzer and G. Mayorga, “Thermodynamics of electrolytes. II. Activity and osmotic coefficients for strong electrolytes with one or both ions univalent,” *J. Phys. Chem.*, vol. 77, no. 19, pp. 2300–2308, 1973.

[66] M. C. Gilstrap, “Renewable electricity generation from salinity gradients using reverse electrodialysis,” no. August, p. 37, 2013.

[67] R. Audinos, “Electrodialyse inverse. Etude de l’energie electrique obtenue a partir de deux solutions de salinites differentes,” *J. Power Sources*, vol. 10, no. 3, pp. 203–217, 1983.

[68] J. W. Post, H. V. M. Hamelers, and C. J. N. Buisman, “Energy recovery from controlled mixing salt and fresh water with a reverse electrodialysis system,” *Environ. Sci. Technol.*, vol. 42, no. 15, pp. 5785–5790, 2008.

[69] A. H. Avci, P. Sarkar, R. A. Tufa, D. Messana, P. Argurio, G. Di Profio, E. Curcio, P. Argurio, E. Fontananova, and G. Di Profio, “Effect of Mg 2+ ions on energy generation by reverse electrodialysis,” *J. Memb. Sci.*, 2016.

[70] J. W. Post, H. V. M. Hamelers, and C. J. N. Buisman, “Influence of multivalent ions on power production from mixing salt and fresh water with a reverse electrodialysis system,” *J. Memb. Sci.*, vol. 330, no. 1–2, pp. 65–72, 2009.

[71] D. a. Vermaas, J. Veerman, M. Saakes, and K. Nijmeijer, “Influence of multivalent ions on renewable energy generation in reverse electrodialysis,” *Energy Environ. Sci.*, vol. 7, no. 4, pp. 1434–1445, 2014.

[72] G. M. Geise, A. J. Curtis, M. C. Hatzell, M. A. Hickner, and B. E. Logan, “Salt concentration differences alter membrane resistance in reverse electrodialysis stacks,” *Environ. Sci. {&} Technol. Lett.*, vol. 1, pp. 36–39, 2014.

[73] O. Scialdone, C. Guarisco, S. Grispo, a. D. Angelo, and a. Galia, “Investigation of electrode material – Redox couple systems for reverse electrodialysis processes. Part I: Iron redox couples,” *J. Electroanal. Chem.*, vol. 681, pp. 66–75, Aug. 2012.

[74] J. Veerman, M. Saakes, S. J. Metz, and G. J. Harmsen, “Reverse electrodialysis: Evaluation of suitable electrode systems,” *J. Appl. Electrochem.*, vol. 40, no. 8, pp. 1461–1474, 2010.

[75] O. Scialdone, a. Albanese, a. D’Angelo, a. Galia, and C. Guarisco, “Investigation of electrode material – redox couple systems for reverse electrodialysis processes. Part II: Experiments in a stack with 10–50 cell pairs,” *J. Electroanal. Chem.*, vol. 704, pp. 1–9, Sep. 2013.

[76] J. O. M. Bockris and A. K. N. Reddy, *Modern Electrochemistry 2B*, 2nd ed. 2000.

[77] B. E. Conway, *Electrochemical Supercapacitors*. 1999.

[78] Z. Stević and M. Rajčić-Vujasinović, “Construction and characterisation of double layer capacitors,” *ACTA Phys. Pol.*, vol. 117, no. 1, pp. 228–233, 2009.

[79] L. Zhang, F. Zhang, X. Yang, G. Long, Y. Wu, T. Zhang, K. Leng, Y. Huang, Y. Ma, A. Yu, and Y. Chen, “Porous 3D graphene-based bulk materials with exceptional high surface area and excellent conductivity for supercapacitors,” *Sci. Rep.*, vol. 3, pp. 356–361, Mar. 2013.

[80] J. Liu, F. Mirri, M. Notarianni, M. Pasquali, and N. Motta, “High performance all-carbon thin film supercapacitors,” *J. Power Sources*, vol. 274, pp. 823–830, 2014.

[81] M. Notarianni, J. Liu, F. Mirri, M. Pasquali, and N. Motta, “Graphene-based supercapacitor with carbon nanotube film as highly efficient current collector,” *Nanotechnology*, vol. 25, p. 435405, 2014.

[82] T. Xu, W. Yang, and B. He, “Partition equilibrium between charged membrane and single electrolyte aqueous solution,” *Chinese Journal of Chemical Engineering*, vol. 9, no. 3. pp. 326–330, 2001.

[83] R. A. Tufa, E. Curcio, W. Van Baak, J. Veerman, S. Grasman, and E. Fontananova, “Potential of brackish water and brine for energy generation by salinity gradient power-reverse electrodialysis (SGP-RE),” *RSC Adv.*, vol. 4, pp. 42617–42623, 2014.

[84] C. Casademont, M. A. Farias, G. Pourcelly, and L. Bazinet, “Impact of electrodialytic parameters on cation migration kinetics and fouling nature of ion-exchange membranes during treatment of solutions with different magnesium/calcium ratios,” *J. Memb. Sci.*, vol. 325, no. 2, pp. 570–579, 2008.

[85] S. Pawlowski, “Experimental and modeling studies on reverse electrodialysis for sustainable power generation,” 2015.

[86] A. Chapotot, G. Pourcelly, and C. Gavach, “Transport competition between monovalent and divalent cations through cation-exchange membranes. Exchange isotherms and kinetic concepts,” *J. Memb. Sci.*, vol. 96, no. 3, pp. 167–181, Dec. 1994.

[87] J. Kamcev, M. Galizia, F. M. Benedetti, E.-S. Jang, D. R. Paul, B. Freeman, and G. S. Manning, “Partitioning of Mobile Ions Between Ion Exchange Polymers and Aqueous Salt Solutions: Importance of Counter-ion Condensation,” *Phys. Chem. Chem. Phys.*, vol. 18, no. 8, pp. 6021–6031, Feb. 2016.

[88] J. . Wijmans and R. . Baker, “the solution-diffusionmodel: a riview,” *J. Memb. Sci.*, vol. 107, no. 1–2, pp. 1–21, 1995.

[89] a. H. Galama, J. W. Post, M. a. Cohen Stuart, and P. M. Biesheuvel, “Validity of the Boltzmann equation to describe Donnan equilibrium at the membrane-solution interface,” *J. Memb. Sci.*, vol. 442, pp. 131–139, 2013.

[90] F. G. Donnan, “Theory of membrane equilibria and membrane potentials in the presence of non-dialysing electrolytes . A contribution to physical-chemical physiology,” vol. 100, pp. 45–55, 1995.

[91] K. Konttury and J. A. Manzanares, *Ionic Transport Processes In Electrochemistry and Membrane Science*. 2008.

[92] M. M. Smith, J. M.; Van Ness, H. C.; Abbott, *Introducción a la Termodinámica en Ingeniería Química*. 1997.

[93] E. Fontananova, W. Zhang, I. Nicotera, C. Simari, W. van Baak, G. Di Profio, E. Curcio, and E. Drioli, “Probing membrane and interface properties in concentrated electrolyte solutions,” *J. Memb. Sci.*, vol. 459, pp. 177–189, 2014.